LULEÅ TEKNISKA UNIVERSITET

1998:331

MASTER'S THESIS

Free vibration analysis of rocket nozzles using energy methods

Bäcklund, Jesper

Civilingenjörsprogrammet

1998:331 • ISSN: 1402-1617 • ISRN: LTU-EX--98/331--SE

PREFACE

As a final part of the Master of Science programme in Mechanical Engineering at the Luleå University of Technology, one performs a large project, a master thesis. This report is the results of a 20-week-long project that has been performed at the Space Propulsion Division at Volvo Aero Corporation in Trollhättan, Sweden. The project started in the beginning of August and ended in the middle of December 1998.

I would like to take this opportunity to thank all people that have given me support during the project, especially my supervisor Thomas Gustafsson at Volvo Aero Corporation and my examinator Lars-Erik Lindgren at Luleå University of Technology.

Trollhättan, December 1998

.....

Jesper Bäcklund

ABSTRACT

The vibration characteristics of stiffened thin shells are studied numerically within the context of the Donnell-Mushtari theory. Different stiffener spacing and dimensions are considered in the formulations. The natural frequencies of a clamped-free ring-stiffened truncated conical shell are calculated by the use of the Rayleigh-Ritz method and compared with ANSYS. The conical shell model is extended to approximate shells of revolution with small curvature and a study of the Vulcain 2NE with different stiffener arrangements, using the developed method, has been performed. This is done to gain understanding of how different frequency regions are effected by variation of stiffener dimensions and numbers. From the study, it can be concluded that the membrane frequencies are fairly insensitive of different stiffener arrangements and more than fifteen stiffeners have little influence on the bending frequencies. The stiffener height has the largest impact on the frequencies when the shell is stiffened by many stiffeners.

LIST OF SYMBOLS

Nomenclature

A	cross-sectional area
C	stretching rigidity
D	bending rigidity
E	modulus of elasticy
G	shear modulus
H	height of shell
I	moment of inertia
J	torsional constant
L	meridional length of shell, arc length
M	moment resultant
N	force resultant
P	number of rings
R	radius of curvature
R_1, R_2	mean radius of shell at the small end and at the large end respectively
S	distance between equally spaced stiffeners
S_r	distance of r:th ring from cone apex in meridoinal direction
T	kinetic energy
U	strain energy
V	volume
a	typical dimension of shell or acceleration
b	width of rings
c	distance from shell middle surface to stiffener centroid
h	thickness of thin shell wall or height of rings
e	total strains
f	resonans frequency
g	acceleration of gravity
i	radius of gyration
m	number of meridional half-waves
n	number of circumferential waves
s	distance from cone apex along meridian to a point on shell middle surface
s_1, s_2	distance along meridion from cone apex to small base and large base respectively
t	time

u, v, w	displacement of a point on shell middle surface in s, θ, z directions, respectively
z	distance of a point in shell wall or in stiffeners from middle surface in direction normal to middle surface

Greek symbols

α	cone apex angle
ε	membrane strain
κ	bending strain
ν	Poisson's ratio
θ	angular distance in circumferential direction
ρ	mass density
σ	stress
ω	circular frequency
ω_0	fundamental frequency

Subscripts

c	cone
r	ring
s, θ, sθ	refer to meridional and circumferential directions and shear, respectively

Abbreviations

ESA	European Space Agency
ISP	Specific impulse
NE	Nozzle Extension
SP	Sveriges Forsknings- och Provningsinstitut
TEG	Turbine Exhaust Gases
VAC	Volvo Aero Corporation

TABLE OF CONTENTS

1 Introduction

Volvo Aero Corporation (VAC) began its engagement in space propulsion in 1974 by producting technology development and manufacturing of combustion chambers and nozzles for the Viking engines on Ariane 1-4. Since then VAC has delivered over 900 nozzles and is today the world-leading commercial supplier of nozzles. In later engine programs, i.e. Vulcain for Ariane 5, VAC has expanded the role in development to design and manufacturing of nozzles as well as turbine components. The Ariane program is maintained by the European Space Agency (ESA) and was adopted in Brussels on July, 1973. The first flight, Ariane 1, took place on December 24, 1979. When the mass of the satellites increased, Ariane 2 and Ariane 3 took over in 1984. In 1988, it was time for the new and more powerful Ariane 4 to take over. The 100th flight with a European launcher took place in November 1997. In 1985, the Ariane 5 program started. Ariane 5 is Europe's newest launcher, with an overall height of about 50 meters and a total weight of about 750 tonnes. The next generation of Ariane 5, Ariane 5 Evolution, is already under development which will be able to carry even bigger satellites into orbit. The first flight is planned for the middle of 2001.

Propulsion for the main cryogenic stage of the Ariane 5 launcher, is provided by a single Vulcain engine. Cryogenic propulsion provides very high performance, but requires extensive expertise in low-temperature systems. The propellants used in the Vulcain engine are liquid oxygen (-182°C) and liquid hydrogen (-253°C). They are fed under pressure from tanks and injected under high pressure into a thrust chamber. The high pressure is supplied by two independent turbopumps, whose turbines are driven by hot gas from a single gas generator. In the thrust chamber the propellants react to form hot gasses, which in turn are accelerated and ejected at a high velocity through a supersonic nozzle, thereby imparting momentum to the system. The nozzle itself is composed of up to 1800 meters of thin-walled spiral-joined tubes, in which liquid hydrogen flow to cool the entire nozzle.

Rocket extension nozzles can be seen as modern applications of the thin shell as a construction element. One of the oldest application is the egg. The thin shell provides excellent strength-to-weight ratio and appears as a load-carrying element in virtual every item of modern industrial equipment. Optimisation with respect to weight has lead to extremely thin-walled nozzles in certain applications. In these applications, the shell is subjected to dynamic loading which may cause excessive vibration or fatigue damage unless an adequate vibration study is performed at the design stage. Most of the loads for these nozzles contains of vibrations. These vibrations have their origin from the engine, boosters and also from pressure variations in the flame. Another type of loading that is critical to the nozzle is buckling. One of the common means for achieving high strength-to-weight ratio is to stiffen the shell by longitudinal (stringer) and circumferential (ring) stiffeners. The design problem becomes one of finding the skin thickness of the shell, the sizes of the stiffeners and the number of rings and stringer while satisfying all the specified design requirements.

The purpose of this report is to gain understanding of what governs the free vibration characteristics of stiffened shells. To accomplish this, a survey of literature on thin shell theory and stiffened shell theory is conducted. There exist a large amount of literature dealing with the thin shell theory, both static and dynamic analysis, excellent examples are written by Kraus [1] and Soedel [2]. Studies of the free vibration characteristics of cylindrical and truncated conical shells made of isotropic and orthotropic materials have been referenced by Leissa in his monograph [3]. A detailed analysis on the basics of solid mechanics and energy methods is written by Shames and Dym [4]. The free vibration of truncated conical shells has been studied to a lesser extent than that of

cylindrical shells because of the greater mathematical complexity involved in characterising their geometry and dynamic behaviour. Even fewer studies concerning stiffened conical shells exists. Greenwelge and Muster [5] and Mecitogly [6] analysed conical shells with stringers and rings using an ”equivalent orthotropic” shell model and they compared the frequencies with experimental results. Rao and Reddy [7] studied the optimum design of stiffened conical shells with natural frequencies and buckling strength constraints. Yamada and Kaneko [8] calculated natural frequencies of truncated conical shells under various different boundary conditions. Soedel [9] investigated similitude requirements for vibrating thin shells.

In this report, the vibration characteristics of a stiffened truncated conical shell are studied numerically. The governing equations are based upon the Donnell-Mushtari theory. Different stiffener spacing and dimensions are considered in the formulations. The natural frequencies of a clamped-free ring-stiffened conical shell are calculated by the use of the Rayleigh-Ritz method and compared with ANSYS [10] to quantify the accuracy of the developed method. Thanks to the development of packages for manipulating functions, such as Mathematica [11], it is no longer hard to manage the cumbersome integration of displacement functions. Of course, the finite element method may be another powerful solution method for the combined structures. However, the preparation of input into the solution still takes much time and post-process to interpret the solution is also difficult. The commercial FEM package ANSYS calculates the natural frequencies rather easily. Nevertheless, to identify the mode shapes corresponding to certain frequencies, the solution must be extracted for each mode shape and classified one by one, which can be very tiresome work. If an analytic solution for a structure is given, it yields accurate natural frequencies and mode shapes very fast and easily.

2 Thin shell theory

A thin shell is a three-dimensional body which is bounded by two closely spaced curved surfaces. As such, it can be considered as the materialisation of a curved surface, just as the beam and the flat plate can be considered as the materialisation of a line and a flat surface. A shell has three fundamental identifying features: its reference surface, its thickness and its edges. Of these, the reference surface is the most significant, because it defines the shape of the shell and because the behaviour of the shell is governed by behaviour of its reference surface. Once the shell's reference surface has been selected, the shell can be described completely. Thus, the thickness of the shell at a given point is determined as the distance between its bounding surfaces as measured along a normal to the reference surface that passes through the point. The thickness does not need be uniform, although constant thickness results in governing equations which are easier to solve.

A large number of differing sets of equations have been derived by various academicians, all purporting to describe the motion of a given shell. This state of affairs is in contrast with the thin plate theory, wherein a single fourth order differential equation of motion is universally agreed upon. One of the most commonly used theories in shell vibrations is the Donnell-Mushtari theory. In the following chapters, the basis of the general thin shell is explained and also where the Donnell-Mushtari theory is specific.

2.1 Historical development of vibration analysis

Vibration analysis has its beginnings with Galileo Galilei (1564-1642), who solved by geometrical means the dependence of the natural frequency of a simple pendulum on the pendulum length. He proceeded to make experimental observations on the vibration behaviour of string and plates, but could not offer any analytical treatment.

The foundation for a more precise treatment of the vibration of continuous systems was laid by Robert Hooke (1635-1703) when he established the basic law of elasticity, by Newton (1642-1727) when he established that force was equal to mass times acceleration and by Leibnitz (1646-1716) when he established differential calculus. The latter paved the way for Jean Le Rond d'Alembert (1717-1785), who derived in 1747 the partial differential equation, which today is referred to as the wave equation and who found the wave travel solution. He was assisted in this by his friends Daniel Bernoulli (1700-1782) and Leonhard Euler (1707-1783), but did not give them due credit. It is still a controversial subject to decide who did actually what, especially since the participants were not too bashful to insult each other and claim credit right and left. However, it is almost a rule in the history of science that people who are credited with an achievement do not completely deserve it. Progress moves in small steps and it is often the person who publishes at the right developmental step and at the right time who gets the public acclaim.

The equation for the transverse vibration of flexible thin beams was derived in 1735 by Daniel Bernoulli, and the first solutions for simply supported ends, clamped ends and free ends were found by Euler and published in 1744. In the field of membrane vibrations, in 1766, Euler published equations for a rectangular membrane that were incorrect for the general case. Work on plate vibration analysis went on in parallel. German experimentalist Chladni demonstrated the beautiful node lines of vibrating plates at the courts of Europe and at a presentation before emperor Napoleon, Chladni caused the latter to transfer money to the French Academy of Sciences for a prize to the person who could best explain the vibration behaviour of plates. The prize was

won, after several attempts, by a woman, Sophie Germaine (1776-1831) in 1815. She gave an almost correct form of the plate equation, but the errors are the reason that her name is not associated today with the equation, despite the brilliance in her approach. Thus, we find the equation first stated in its modern form by Lagrange in 1811.

What is even more interesting is that in 1821, Sophie Germaine published a very simplified equation of the vibration of a cylindrical shell. Unfortunately, again it contained mistakes. In 1874, Aron derived a set of five equations, but because of his reluctance to employ simplifications the equations are complicated. The simplifications that are logical extensions of the beam and plate equations for both transverse and in-plane motion were introduced by Love (1863-1940) in 1888. Love's equations brought the basic development of the theory of vibration of continuous structures, which have a thickness that is much less than any length or surface dimensions to a satisfying end.

2.2 Love's first approximation

The basic equations which Love derived is based on the following assumptions:

1. The shell is thin
2. The deflection of the shell is small
3. The transverse normal stress is negligible
4. Normals to the undeformed middle surface remain straight and normal to the deformed middle surface and suffer no extension.

These four assumptions taken together give rise to what Love called his "first approximation" shell theory. These approximations are almost universally accepted by others in the derivation of the thin shell theory.

The first assumption defines what is meant by a thin shell and sets the stage for the entire theory. Although no precise definition of thinness is available, it will be convenient at various places in the subsequent derivation of shell theories to neglect the ratio of the thickness to the radius of curvature of the reference surface in comparison with unity, $z / R << 1$. As a rule of thumb, however, it is suggested that the resulting theory is only applied to shells whose thickness is everywhere less than one tenth of the smallest radius of curvature of the reference surface.

The second assumption permits one to refer all calculations to the original configuration of the shell and, together with Hooke's law, ensures that the resulting theory will be a linear, elastic one.

The two remaining assumptions deal with the constitutive equations of thin elastic shells and represent the most significant features of the first approximation and reduce the general constitutive law to a two-dimensional constitutive law of thin shells.

2.3 Fundamental relationships

Three different sets of relationships forms the basis of solid mechanics. Equilibrium equations are obtained from a balance of the forces acting on some fundamental element of the medium considered and connects between external forces on a body and the stresses that form to maintain static equilibrium. Compability equations are obtained from a strictly geometrical consideration of the process of deformation and describe how different parts in a body are connected during deformation until fracture occurs. Equilibrium and compability equations are linear at small deformations and they

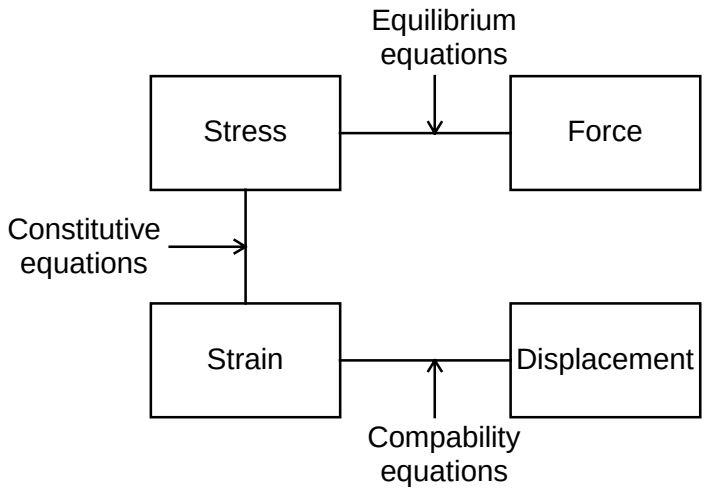

Figure 2.1 The three fundamental relationships of solid mechanics

are material independent. The relationship between stress and strain in a material is described in the constitutive equations. All three sets of equations form a chain according to figure 3.1. The compability and the equilibrium equations are specific for the Donnell-Mushtari theory.

2.3.1 Compability equations

From the well-known compability equations, or strain-displacement equations, of the three dimensional theory of elasticity in orthogonal curvilinear co-ordinates, various types of simplifications have been made. Depending on where and how the simplification that z / R is much smaller than unity is introduced, different relationships are obtained. The equations contain six generalised components of strain which are given explicitly in terms of the three displacement components. See Appendix 1 for the Donnell-Mushtari version.

2.3.2 Constitutive equations

Hooke's law will be assumed as the constitutive law. This will limit all shells considered to be made from materials which are linearly elastic. As mentioned earlier, Love's approximations reduce the general three dimensional constitutive law to a two dimensional one. The equations express the three principal stresses in terms of the six generalised components of strain. See Appendix 1 for details.

2.3.3 Equilibrium equations

Again, depending on where and how the simplification that z / R is much smaller than unity is introduced, different relationships are obtained. However, these equations are not used in the free vibration analysis that follows and they are not included in Appendix 1.

3 Free vibration of shells

Time-dependent vibratory motions are set up in a shell whenever it is disturbed from a position of stable equilibrium. These motions are classified as ”free” vibrations, if they occur in the absence of external loads, or they are referred to as ”forced” vibrations if they are set up by time-dependent external loads. A knowledge of the free-vibration characteristics of thin shells is important to our general understanding of the behaviour of a shell and to the industrial application of shell structures. The natural frequencies of shell structures must be known, in order to avoid the destructive effect of resonans with nearby rotating or oscillating equipment and they are also the foundation of forced response calculations. The frequency is defined as one over the periodic time of the motion.

3.1 Modes and frequencies

An ideal pendulum, consisting of a massless rod, pivoted at one end and with a mass attached to the other end, oscillates with one frequency. This is due to the fact that the system only has one degree of freedom, which can be interpreted as the system only is allowed to move in one direction. A shell on the other hand, is composed of an infinite number of mass particles and as a consequence it has an infinite number of degrees of freedom. Its response to a disturbance may thus be analysed into an infinite number of periodic motions, which are referred to as its normal modes of free vibration. Each of these normal modes has an associated natural frequency of free vibration. The lowest natural frequency is often refereed to as the fundamental frequency. A normal mode can be thought of as the shape that the shell deforms according to and it can be divided into meridional and circumferential waves. The points or lines with zero-displacement on these waves are sometimes called node-points or node-lines and the nodal pattern of a cylindrical shell is shown in figure 3.1. The number of waves

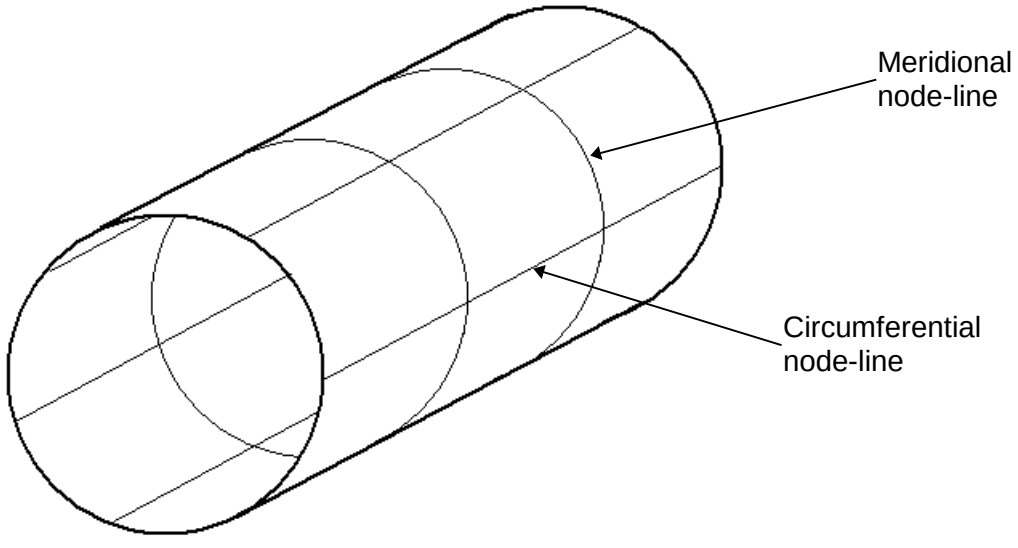

Figure 3.1 Nodal pattern of a cylindrical shell

distributed around the circumference are denoted by *n* and the number of meridional half-waves are denoted by *m*. Every normal mode can then be described by the numbers *m* and *n*. In figure 3.1, two meridional node-lines are shown, allowing three meridional half-waves to be present, m = 3. If one considers the case of a vibrating

cylinder, it is possible to simplify the characteristics of the vibration by replacing the cylinder with a beam and a ring. The beam corresponds to the meridional vibration of the cylinder and the ring corresponds to the circumferential vibration of the cylinder.

3.1.1 Beam vibration

The transverse vibration of a beam is dependent upon the boundary conditions. Each different set of boundary conditions will results in different vibration mode shapes. Examples of beam vibration mode shapes are shown in figure 3.2 and examples with

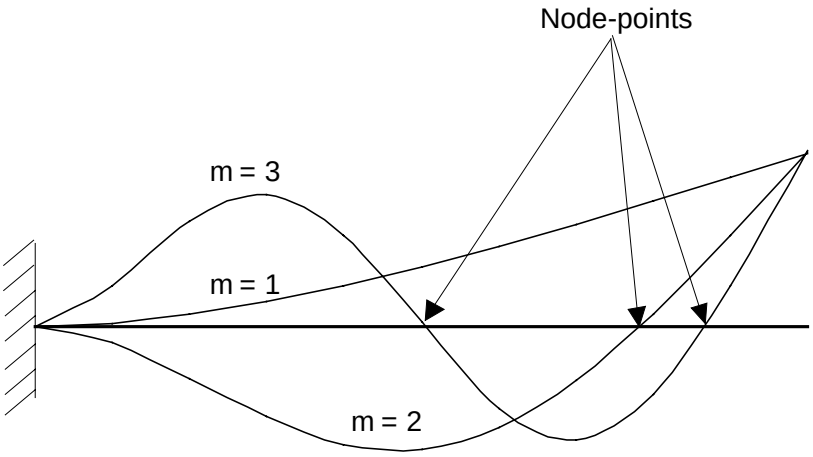

Figure 3.2 Clamped - free beam vibration mode shapes (m = 1, m = 2, m = 3)

other boundary conditions are given in Appendix 2. Points with zero displacement are marked as node-points and will coincide with the meridional node-lines in figure 3.1. Since the first meridional mode, m = 1, consists of only one half-wave, no node-points are present in figure 3.2. The more general shell, with one small and one large end, will also have meridional modes that resemble that of a beam which has the same boundary conditions as the shell, but the displacement will be more concentrated to the large end.

3.1.2 Ring vibration

The vibration of a circular ring in its plane of curvature, resembles the circumferential vibration modes of any shell with any combination of boundary condition. The mode shape of a ring is shown in figure 3.3 and is sometimes called the breathing mode of the ring. More examples of ring mode shapes are given in Appendix 2.

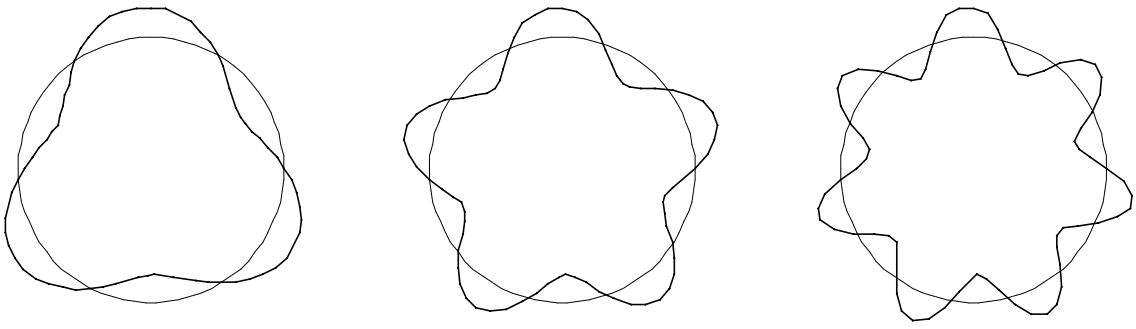

Figure 3.3 Circular ring vibration mode shapes (n = 3, n = 5, n = 7)

3.1.3 Shell vibration

So, by combining the modes of a circular ring with the modes of a beam, the vibration modes of a shell can be obtained. The circumferential modes are not dependent on the boundary conditions, whereas the meridional modes are. An example of a conical shell vibration mode shape is found in figure 3.4 and more are given in Appendix 3. The

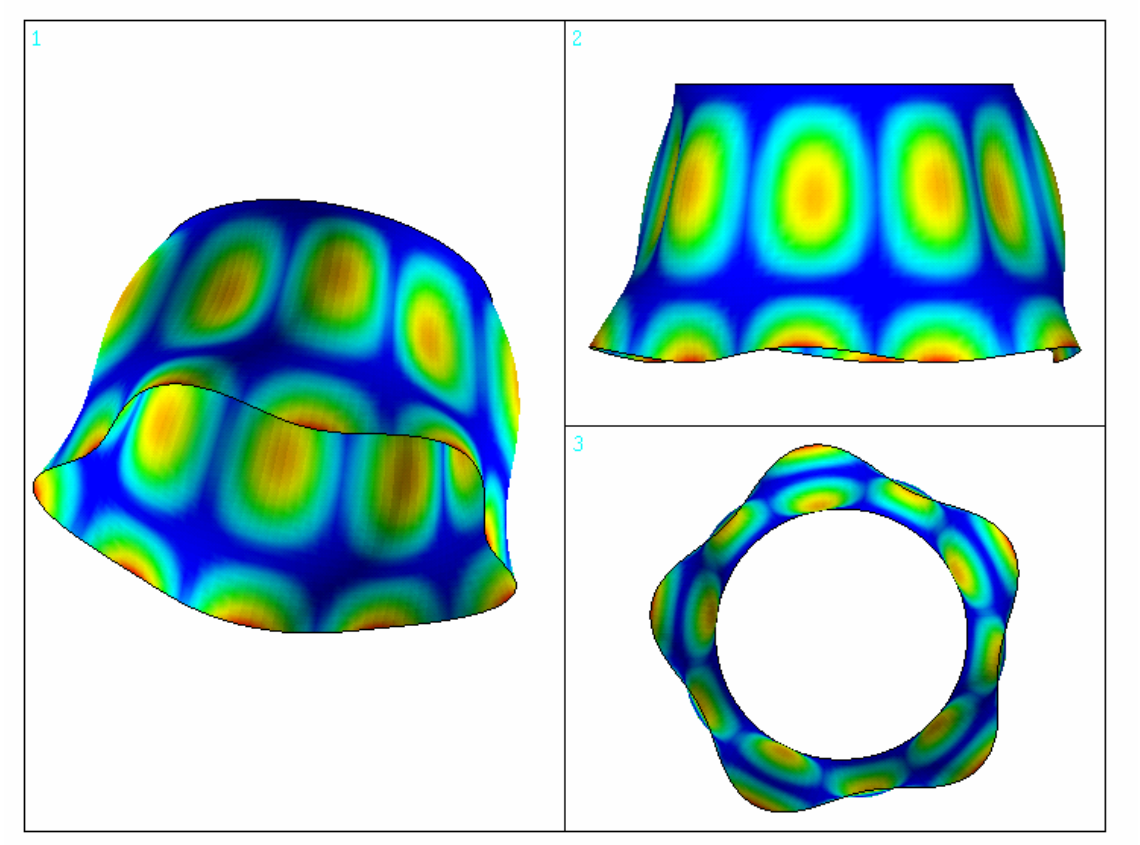

Figure 3.4 Clamped - free conical shell vibration mode shape (m = 2, n = 5)

colours represent absolute values of displacement. The smaller end is clamped and the larger end is free. One meridional node line is present in figure 3.4 and consequently *m* will be equal to two. By looking at the bottom right view, on can detect five waves distributed around the circumference, n = 5, and there exist ten circumferential nodal lines. So, it is possible to classify the mode shape of a shell by counting the number of waves that are distributed around the circumference and in the meridional direction of the shell, or by counting the number of node-lines that also are distributed in meridional and circumferential direction.

3.2 Bending and membrane energy

The results from beam and plate vibrations show that the natural frequencies increase as the shape of the displacement pattern becomes more complicated, which means that the lowest frequency always occurs for the least complicated displacement pattern. However, this is not the case for shell vibration, where the lowest frequency can occur for very complicated displacement patterns. This can be explained from a consideration of the strain energy associated with bending and stretching of the reference surface. Shells especially exhibit certain effects that are not present in beams or even in plates and they cannot be approximated as vibrating beams or plates.

It is seen in figure 3.5 that at the low circumferential wave number, the bending strain energy is low and the stretching or membrane strain energy is high, while at the higher circumferential wave numbers, the relative contribution from the two types of strain energy is reversed. Figure 3.5 also shows that the bending strain energy is insensitive to the number of meridional waves while the membrane energy is strongly dependent on the number of such waves.

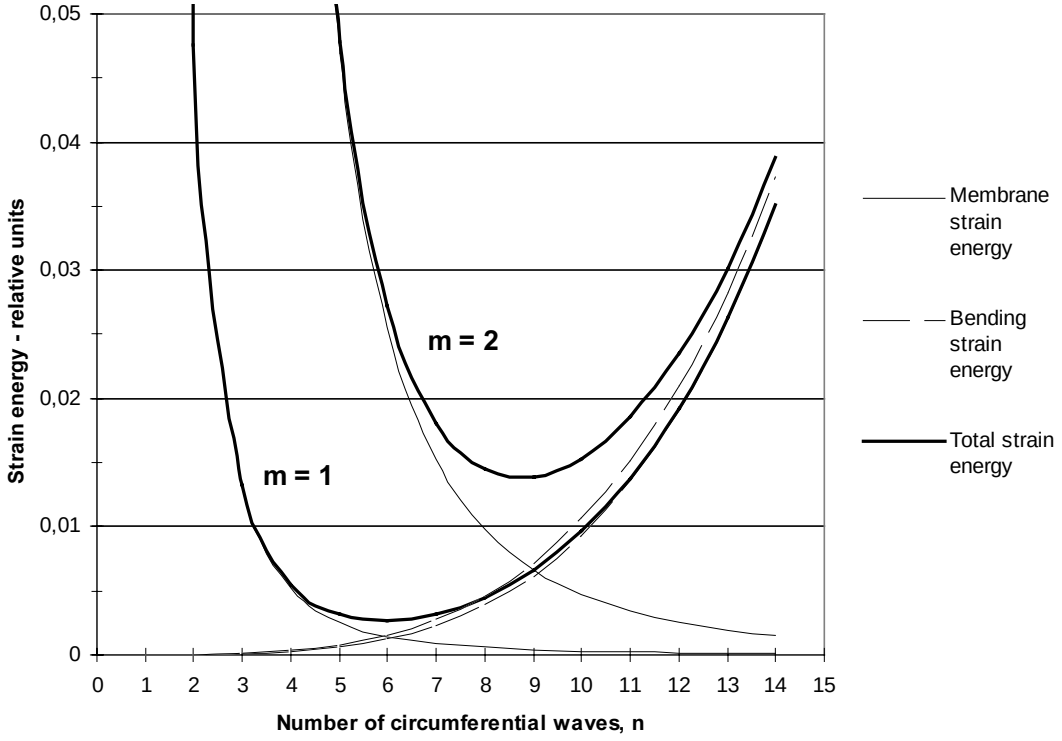

Figure 3.5 Strain energy contributions for a typical freely vibrating circular cylindrical shell [1]

A common approximation in static analysis of shells is to assume that the bending stiffness can be neglected, but this will lead to the fact that high circumferential waves cannot be properly calculated in the dynamic analysis. It is however possible to introduce two separate approximations, membrane and bending, which will give good results in respective area where the approximation is valid, but the lowest frequency is dependent upon both bending and membrane effects and can not be calculated using either approximation.

The infinite number of normal modes can be grouped by the numbers *m* and *n*. By plotting the frequency versus the circumferential wave number, the lowest frequency

for every value of *m* will be visualised, different curves are obtained for different values of *m*. By looking at figure 3.6 it becomes obvious that the lowest frequency does not occur at the lowest circumferential wave-number. In this case the lowest frequency occurs for a circumferential wave number of six. As expected the lowest frequency second meridional mode occurs for a higher circumferential wave number. The lowest frequency is almost always associated with the first meridional half wave. The curves can be split into two parts. One with negative slope, where membrane strains dominate and one with positive slope, where bending strains dominate as expected from the strain energy consideration.

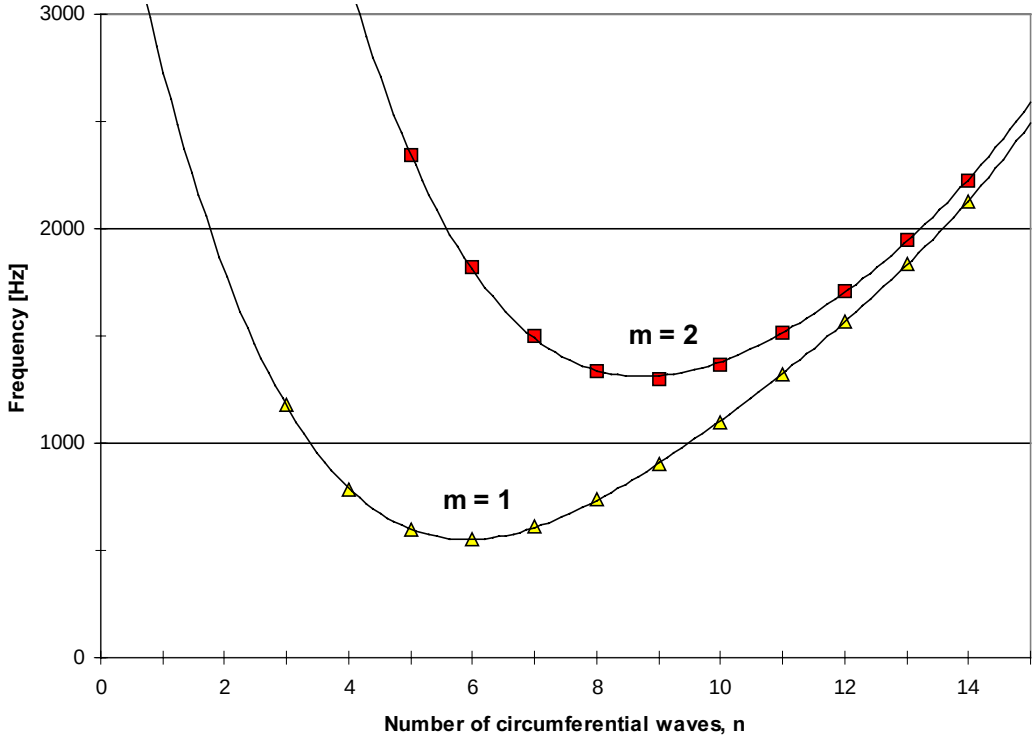

Figure 3.6 Natural frequencies for a freely vibrating circular cylindrical shell with clamped ends [1]

4 Stiffened conical shell theory

Two approaches are commonly used to analyse stiffened shells. In the first approach, the stiffener is assumed to be smeared over the whole shell to yield a single equivalent orthotropic shell. A stiffener is considered as a discrete element in the second approach. The stiffener causes a kind of structural inhomogenity. When the stiffening spacing is too large or if the wavelength of vibration is much smaller than the stiffener spacing, the stiffener has to be modelled as a discrete element. On the other hand, if the wavelength of the vibration is long enough relative the stiffener spacing, the equivalent orthotropic theory can be used. The structural inhomogeneous shell is changed to a homogeneous orthotropic shell. Due to the relative ease in the formulation and solution of the equivalent orthotropic shell equations, this representation is mostly used in the vibration and buckling analysis of stiffened shells.

4.1 Energy formulations

Consider a thin truncated conical shell of the geometry and co-ordinates shown in figure 4.1. It can be dived into three parts: a conical shell, ring stiffeners and stringer stiffeners. For each of these parts the strain and kinetic energy can be stated. However, in this report only the case with ring-stiffened shells will be considered, but the implementation of stringers is however rather easy.

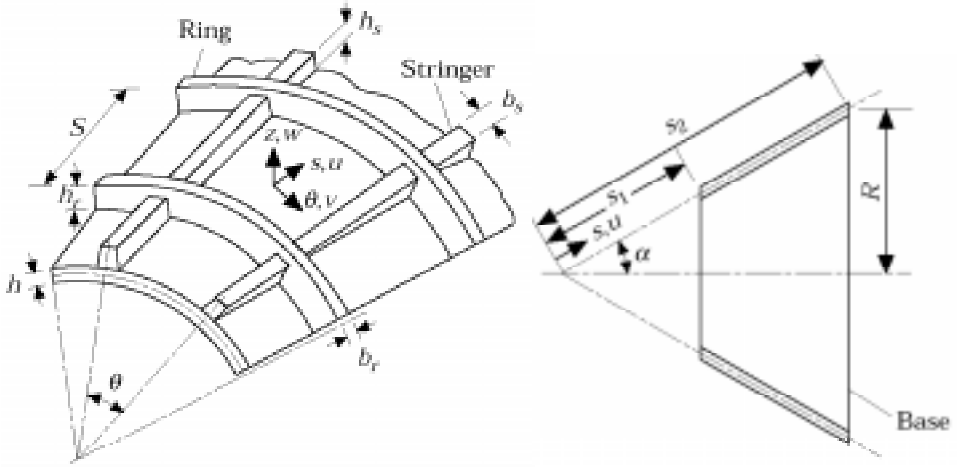

Figure 4.1 Geometry and co-ordinates used for stiffened conical shell

In an ideal elastic body, there will be no heat produced during deformation and the only form of energy that will exist is potential and kinetic energy. In the absence of external loads, the potential energy will consist of only strain energy. The strain energy stored in one infinitesimal element that is acted on by the stresses σ_{ij} is:

$$dU = \tfrac{1}{2}(\sigma_s e_s + \sigma_\theta e_\theta + \sigma_{s\theta} e_{s\theta})dV \qquad (4.1)$$

The total strains $(e_s, e_\theta, e_{s\theta})$ at a distance z from the middle surface are obtained simply by adding the membrane strains (independent of z) and the bending strains (proportional to z). The membrane strains $(\varepsilon_s, \varepsilon_\theta, \varepsilon_{s\theta})$ and bending strains $(\kappa_s, \kappa_\theta, \kappa_{s\theta})$ are given in Appendix 1, according to the Donnell-Mushtari theory.

The kinetic energy in one infinitesimal element, neglecting rotatory inertia, is given by:

$$dT = \tfrac{1}{2}\rho(\dot{u}^2 + \dot{v}^2 + \dot{w}^2)dV \qquad (4.2)$$

The task is to express the energies in the same unknowns, namely in terms of the displacements *u, v, w*. This can be done by the use of the constitutive equations and the compability equations in the general expression for the strain energy, equation 4.1 of a elastic body and integrating over the shells middle surface. The kinetic energy is already stated in terms of the displacements.

4.1.1 Strain energies

The strain energy, U_c, of a thin, linear elastic, homogeneous conical shell is then given by equation 4.3.

$$U_c = \tfrac{1}{2}\int_{s_1}^{s_2}\int_0^{2\pi}\begin{Bmatrix} C\left[\varepsilon_s^2 + \varepsilon_\theta^2 + 2\nu_c\varepsilon_s\varepsilon_\theta + \tfrac{1}{2}(1-\nu_c)\varepsilon_{s\theta}^2\right] + \\ D\left[\kappa_s^2 + \kappa_\theta^2 + 2\nu_c\kappa_s\kappa_\theta + 2(1-\nu_c)\kappa_{s\theta}^2\right] \end{Bmatrix} sSin\alpha d\theta ds \qquad (4.3)$$

To make the expression as simple as possible, the compability equations have not been used to replace the strains by the wanted displacements. The integral over the shells middle surface can be divided into different parts, to allow the shell to be made by different plate thickness and materials. Instead of integrating directly over the whole meridional direction from s_1 to s_2, a third position indicating a stepwise change in shell thickness can be introduced and the integral will be evaluated first between s_1 to s_{12} and then between s_{12} to s_2. Different plates are joined by having the same middle surface according to figure 4.2.

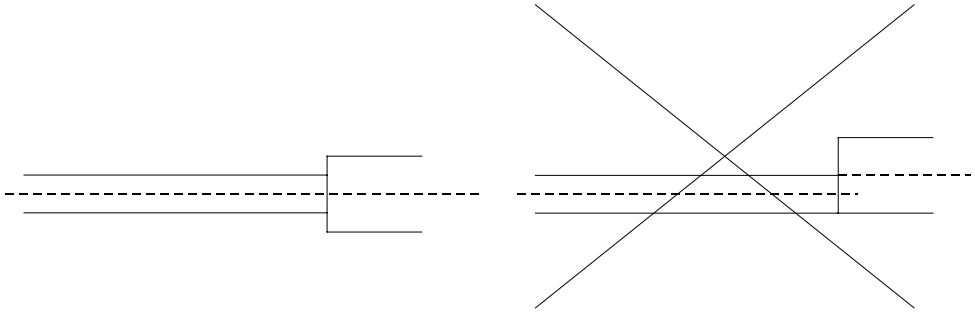

Figure 4.2 How different plates are joined in the energy formulations

The stretching rigidity, *C*, and the bending rigidity, *D*, are given by equation 4.4, where *h* is the thickness of the shell and *E, G* and *ν* denote the modulus of elasticity, the modulus of shear and the Poisson ratio, respectively. α is the cone apex angle and *s* is the distance from the cone apex to a point on shell middle surface.

$$C = \frac{Eh}{1-\nu^2}, D = \frac{Eh^3}{12(1-\nu^2)} \qquad (4.4)$$

The derivation of the stiffeners' strain energy is complicated by the need to express the displacements of the stiffeners in terms of the displacements of the middle surface of the shell. The derivation is made under the following assumptions:

1. The stiffeners are prismatic and have a symmetrical cross-section.
2. The material of the stiffeners is linear elastic, homogeneous and isotropic.
3. The stiffeners are concentrated along the curvilinear co-ordinates.
4. The normal strains vary linearly in the stiffener as in the shell.

5. The stiffness of the stiffener in in-plane direction, perpendicular to their co-ordinates equal to zero - as a result of this assumption, the shear membrane force, N_{s_θ}, is carried entirely by the shell.
6. Lateral bending of the stiffeners is neglected.
7. Crippling is negligible.
8. The stiffeners carry torsional moment on account of their torsional rigidity.

Now, the stiffened conical shell is approximated by smearing the effect of the stiffeners over the shell surface. The smearing process is achieved by dividing the strain energy of a stiffener by the stiffener spacing, *S*. The strain energy of the rings, U_r, is given by equation 4.5.

$$U_r = \tfrac{1}{2}\int_{s_1}^{s_2}\int_0^{2\pi}\left\{E_r A_r / S\left[\varepsilon_\theta^2 - 2c_r\varepsilon_\theta\kappa_\theta + (i_r^2 + c_r^2)\kappa_\theta^2\right] + (G_r J_r / S)\kappa_{s\theta}^2\right\} s\,Sin\alpha\, d\theta\, ds \qquad (4.5)$$

The cross sectional area of the stiffener is denoted by *A*, and *J, c* and *i* are the torsional constant, the distance to the centriod of a stiffener from the shell middle surface and the radius of gyration respectively and they are expressed in terms of the width *b* and height *h* of the stiffener according to equation 4.6. The ring stiffeners have a rectangular cross-section and the height must be greater than or equal to the width.

$$J = \frac{h_r b_r^{\,3}}{3}\left(1 - 0.63\left(\frac{b_r}{h_r}\right) + 0.052\left(\frac{b_r}{h_r}\right)^5\right)$$
$$c = \frac{h + h_r}{2} \qquad (4.6)$$
$$i = \frac{h_r}{\sqrt{12}}$$
$$A = b_r h_r$$

This assumes that the stiffeners are close together with equal spacing between rings On the other hand, in [5], the general case is considered for which the shell may have any number of stiffeners that are not necessarily closely or equally spaced. Here the effect of the stiffeners are considered to be concentrated at the respective stiffener location S_r and the strain energy is given by:

$$U_r = \tfrac{1}{2}\sum_{r=1}^{P}\left\{\int_0^{2\pi}\left\{E_r A_r\left[\varepsilon_\theta^2 - 2c_r\varepsilon_\theta\kappa_\theta + (i_r^2 + c_r^2)\kappa_\theta^2\right] + G_r J_r \kappa_{s\theta}^2\right\} S_r\, Sin\alpha\, d\theta\right\}_r \qquad (4.7)$$

The total strain energy of a ring stiffened conical shell is then given by adding equations 4.3 and 4.7:

$$U = U_c + U_r \qquad (4.8)$$

4.1.2 Kinetic energies

If the rotary inertia term is neglected, the kinetic energy of a conical shell can be written as:

$$T_c = \tfrac{1}{2}\int_{s_1}^{s_2}\int_0^{2\pi}\left\{\rho_c h(\dot{u}^2 + \dot{v}^2 + \dot{w}^2)\right\} s\,Sin\alpha\, d\theta\, ds \qquad (4.9)$$

where ρ is the density and the dot indicates a time derivative. Again, different plate thicknesses and materials can be used by dividing the integral into different parts. Although the rotary inertia of the shell is negligible, the rotary inertia of the stiffeners can substantially effect the natural frequencies of stiffened shells. This effect is on the other hand more dominant for higher frequencies and is considered to be negligible for the lower frequencies. The kinetic energy for rings can be written as:

$$T_r = \tfrac{1}{2}\int_{s_1}^{s_2}\int_0^{2\pi}\left\{\rho_r A_r / S(\dot{u}^2 + \dot{v}^2 + \dot{w}^2)\right\} s Sin\alpha d\theta ds \qquad (4.10)$$

Again, for the general case of a reinforced shell, the kinetic energy is:

$$T_r = \tfrac{1}{2}\sum_{r=1}^{P}\left\{\int_0^{2\pi}\left\{\rho_r A_r(\dot{u}^2 + \dot{v}^2 + \dot{w}^2)\right\} S_r Sin\alpha d\theta\right\}_r \qquad (4.11)$$

The total kinetic energy of a ring stiffened conical shell is then given by adding equations 4.9 and 4.11:

$$T = T_c + T_r \qquad (4.12)$$

4.2 Solution method

From the energy formulations, it is possible by the use of, for instance, Hamilton's principal to derive the governing differential equation. This can be quite tedious, but it has only to be done once and then the governing differential equation can be solved with appropriate methods. But, compared to the large number of possible shell configurations, very few exact solutions are possible. The approximate solution methods can roughly be divided into two categories. In the first category, a minimisation of energy approach is used, like for instance, the Rayleigh-Ritz or the Galerkin method. In the second category the finite difference and the finite element method are found.

The Rayleigh-Ritz method is used in this report. This method of solution can be justified by the fact that it is easy to include the effect of the stiffeners. The Rayleigh-Ritz method equates maximum strain energy to maximum kinetic energy. The first step requires a displacement vector to be assumed for the mode shape of the shell. This assumed mode shape must satisfy the natural boundary conditions and must contain a linear condition of arbitrary constants. From the assumed mode shapes, the maximum strain and kinetic energies of the shell are obtained and by diffenrenting the difference between kinetic and potential energy with respect to the arbitrary constant, a set of linear equations is obtained. The problem of finding the natural frequencies is now reduced to an eigenvalue problem.

4.2.1 Boundary conditions

In the case of circular cylindrical shells, 136 combinations of "simple" boundary conditions exist. However, because for conical shells there is symmetry with respect to the axial mid-plane, there exist 256 distinct types of problems. The nine most used types arise when each end is either clamped, pinned or free. More details on the different boundary conditions are found in Appendix 1. For a stiffened, clamped-free conical shell, the solution must satisfy the natural boundary conditions

$$u = v = w = \partial w/\partial s = 0, \qquad (4.13)$$

at $s = s_1$ and the static boundary condition:

$$N_s = M_s = S_{s_\theta} = V_s = 0, \qquad (4.14)$$

at $s = s_2$. However, using the Rayleigh-Ritz method, it is enough if the natural boundary conditions are fulfilled and the arbitrary constants are then used to fulfil the static boundary condition as good as possible.

4.2.2 Mode shape assumption

The displacement assumptions for *u, v, w* can be expected to have some sort of orthogonal, since the mode shapes are orthogonal. They are often written in the following form:

$$\begin{aligned} u &= \Sigma A_i \cdot f_i(s) \cdot \sin(n\theta) \cdot \cos(\omega t) \\ v &= \Sigma B_i \cdot g_i(s) \cdot \cos(n\theta) \cdot \cos(\omega t) \\ w &= \Sigma C_i \cdot h_i(s) \cdot \sin(n\theta) \cdot \cos(\omega t) \end{aligned} \qquad (4.15)$$

The terms A_i, B_i, and C_i represent arbitrary constants, *f, g* and *h* are referred to as displacement functions. The $\sin(n\theta)$ and $\cos(n\theta)$ terms are used to include the variation in circumferential direction and it is possible to uncouple the θ-dependence. Time enters the displacement assumptions with the $\cos(\omega t)$ term, where *t* represents time and ω is the circular frequency.

Different ways to select the displacement functions *f, g, h* are possible. One way is to select the displacement of a beam, with the same boundary condition. The advantage with that is that the higher mode shapes are already built in and only a few terms in the sum are needed. One disadvantage of selecting beam functions is that only *w* can easily be replaced with the corresponding beam function. Other displacements are more difficult to select. Some tests with beam functions were conducted, but the results were not satisfying in the membrane area. In other papers [3] the beam functions are used successfully in the case of cylindrical shell. However, for the conical shell the displacements are more concentrated at the larger radius and a term that shifts the displacement towards the large radius is needed. Depending on if membrane or bending effects dominate, different ways are needed to shift the displacements. This can be accomplished by introducing a variety of shifting functions, but the amount of terms needed are unfortunately increased.

Another way to select the displacement functions is to use polynomials and in order to satisfy the natural boundary conditions the displacement functions are written as:

$$\begin{aligned} u &= (s - s_1) \cdot \Sigma A_i \cdot s^{a \cdot i} \cdot \sin(n\theta) \cdot \cos(\omega t) \\ v &= (s - s_1) \cdot \Sigma B_i \cdot s^{b \cdot i} \cdot \cos(n\theta) \cdot \cos(\omega t) \\ w &= (s - s_1)^2 \cdot \Sigma C_i \cdot s^{c \cdot i} \cdot \sin(n\theta) \cdot \cos(\omega t) \end{aligned} \qquad (4.16)$$

At first the coefficients were selected as follows: $(A_1 + A_2 \cdot s + A_3 \cdot s^2)$, $(B_1 + B_2 \cdot s + B_3 \cdot s^2)$, $(C_1 + C_2 \cdot s + C_3 \cdot s^2)$, but the results at low *n* were not at all satisfying. After modifying the assumption according to equation 4.17, the results were satisfying for all values of *n*.

$$\begin{aligned} u &= (s - s_1) \cdot (A_1 \cdot s^{-2} + A_2 \cdot s^{-1} + A_3) \cdot \sin(n\theta) \cdot \cos(\omega t) \\ v &= (s - s_1) \cdot (B_1 \cdot s^{-2} + B_2 \cdot s^{-1} + B_3) \cdot \cos(n\theta) \cdot \cos(\omega t) \\ w &= (s - s_1)^2 \cdot (C_1 \cdot s^{-3} + C_2 \cdot s^{-2} + C_3 \cdot s^{-1}) \cdot \sin(n\theta) \cdot \cos(\omega t) \end{aligned} \qquad (4.17)$$

These polynomials are capable of allowing different mode shapes at membrane and bending areas. The disadvantage of choosing polynomials is that only frequencies for

one meridional mode shape, corresponding to the lowest frequencies and often m = 1, can be calculated.

4.2.3 Mathematica

The assumed displacements are substituted into the expressions of the strain and kinetic energy. This leads to the fact that they can be expressed as:

$$U = U_{max} \cdot \cos^2(\omega t) \qquad (4.18)$$
$$T = T_{max} \cdot \sin^2(\omega t)$$

For a conservative system, the maximum kinetic energy must be the same as the maximum strain energy, but because of the simplifications that are made in the assumptions of the displacement functions, this will not necessarily be true. The arbitrary set of independent constants, $A_1, A_2, ..., A_N$, will be chosen such that the difference between kinetic and strain energy is as small as possible:

$$\partial(T_{max} - U_{max})/ \partial A_i = 0 \ , \ i = 1, 2 ,..., N \qquad (4.19)$$

This leads to a set of linear equations, which can be written according to equation 4.20 where P_{ij} and Q_{ij} are elements that are obtained from equation 4.19.

$$\left[\begin{bmatrix} P_{11} & P_{21} & P_{N1} \\ P_{12} & P_{22} & P_{N2} \\ P_{1N} & P_{1N} & P_{NN} \end{bmatrix} + \omega^2 \begin{bmatrix} Q_{11} & Q_{21} & Q_{N1} \\ Q_{12} & Q_{22} & Q_{N2} \\ Q_{1N} & Q_{1N} & Q_{NN} \end{bmatrix}\right] \cdot \begin{bmatrix} A_1 \\ A_2 \\ A_N \end{bmatrix} = 0 \qquad (4.20)$$

The problem of finding the natural frequencies is now reduced to an eigenvalue problem. Implementation in Mathematica is rather straight forward and the program is listed in Appendix 4. To improve on the computation speed, the energy integrals are first symbolically integrated in the circumferential direction and the obtained results are substituted into the expressions. The remaining meridional integration is done numerically for every value of *n*.

4.3 Comparison of results

To verify that the developed theory has sufficient accuracy, comparison with ANSYS and tabulated values are made.

4.3.1 Model data

Three modal analyses with increasingly finer mesh were carried out in ANSYS, using 8-node structural shell element SHELL93, with six degrees of freedom at each node. To model the clamped - free boundary, the nodes at the smaller radius are first rotated according to a cylindrical co-ordinate system and then the translations *x, y* and *z* and rotation about *y* are set equal to zero. The first calculation used 16 elements in circumferential direction and 8 elements in meridional direction. See Appendix 5 for input-file to ANSYS. The model has properties according to table 4.1 and is defined according to figure 4.3.

Table 4.1 Model properties used in calculations

α [°]	R_1 [m]	R_2 [m]	L [m]	h [m]	E [GPa]	ρ [kg /m^3]	ν
30	0.25	1	1.5	0.01	208	7850	0.3

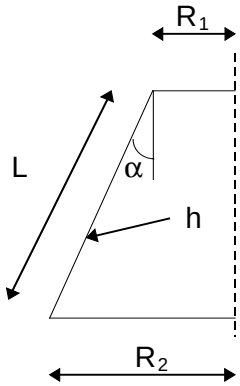

Figure 4.3 Geometry used in calculations

4.3.2 Results

The results from the three ANSYS calculations, the developed theory and [8] are shown in table 4.2 and the results indicate that a relatively fine mesh is required in ANSYS to be able to calculate very high circumferential modes, but a relative coarse mesh is only needed to calculate the lower circumferential modes. When the mesh becomes coarse, very large errors occur. As a rule of thumb, it should be suggested that the number of elements in the circumferential direction should be at least four times as large as the number of the highest circumferential mode that is calculated, but using a 4-node shell element like SHELL63 the number of elements must be doubled.

Table 4.2 Frequencies in Hertz with different mesh-sizes and methods (m = 1)

n	ANSYS 16x8	ANSYS 32x16	ANSYS 64x32	[8]	Theory
0	194,6	194,7	194,7	194,6	
1	101,5	101,5	101,5	101,5	103,8
2	46,8	46,8	46,8	47,2	48,9
3	39,3	39,2	39,1	40,3	41,7
4	57,4	57,1	57,1	58,4	60,0
5	83,5	82,7	82,7	84,0	86,0
6	115,0	113,2	113,3	114,7	118,4
7	151,3	148,6	148,9	150,5	157,5
8	178,2	189,8	189,9	191,6	202,7
9	266,4	236,1	236,1	238,1	253,7

A graphical representation of the ANSYS calculation with the finest mesh and the theory can be found in figure 4.4. The lowest frequency occurs for a circumferential wave number of three and it appears as if the theory calculates the lowest frequencies with small errors. At least, the theory is capable of predicting the large scale behaviour

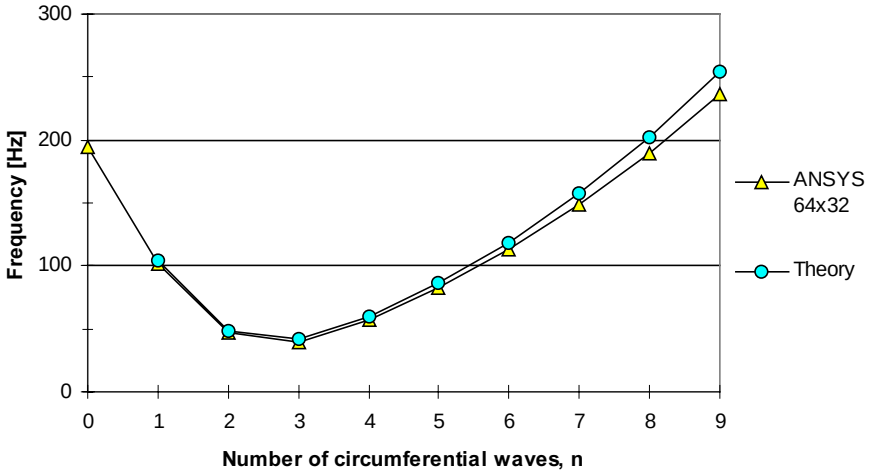

Figure 4.4 Frequencies from table 4.2 grouped by wave-numbers (m = 1)

of the shell. By plotting the residuals between the theory and [8], normalised by [8], it shows that the theory only has a relative error of about three percent in the interesting area where *n* is smaller than six. This can be considered to be accurate enough for most purposes. However, it is not clear exactly how the results in [8] are obtained or what theory the calculations are based on, so the result that ANSYS is three percent wrong in the lowest frequency could have other explanations.

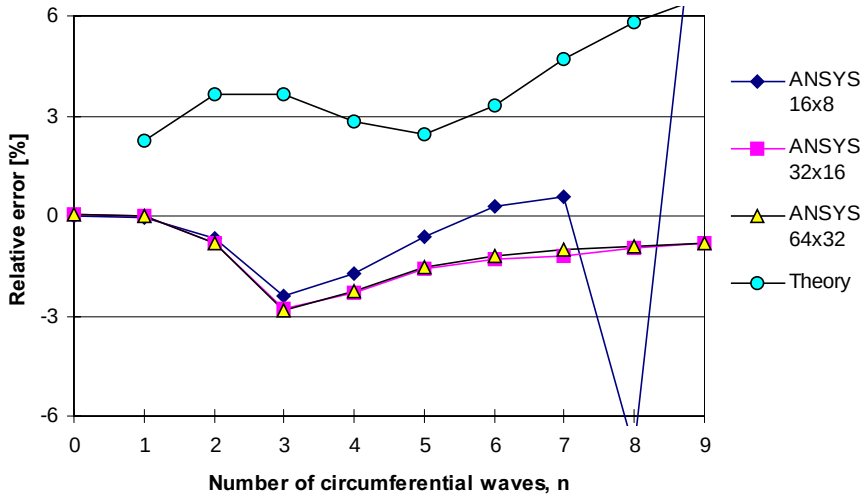

Figure 4.5 Residuals between theory, ANSYS and [8], normated by [8]

5 Similitude theory

In the case of large shells of complicated geometry, vibration analysts have been turning to the use of models. The accepted way of doing this is to scale shell and model faithfully in every respect, shape, thickness and all, and to employ the classical scaling law, first derived by Newton. This law, however, sometimes proves to be too restrictive, since it is not always convenient, for instance, to scale the thickness of the shell in proportion with typical surface dimensions.

5.1 Free vibrations

By substituting non-dimensional expressions into the equations of motion, it is possible to obtain similitude condition for the free vibrations of shells according to table 5.1, where *a* is a typical dimension of the shell and *h* is the thickness of the shell.

Table 5.1 True similitude conditions

	Shells
Thickness scaling	$\frac{h_2}{h_1} = \frac{a_2}{a_1}$
Poisson's ratio	$\nu_2 = \nu_1$
Natural frequency	$\omega_{n2} = \omega_{n1} \frac{a_1}{a_2} \left(\frac{\rho_1 E_2}{\rho_2 E_1} \right)^{½}$

The equation of motion can be divided into two areas, where membrane respectively bending resistance dominate. This leads to the fact that separate similitude relationships can be derived according to table 5.2. The membrane frequencies are not dependent on the thickness of the shell, but the bending frequencies are directly proportional to the shell thickness and approximately inversely proportional to the square of the radius of the shell.

Table 5.2 Approximate similitude conditions

	Shells	
	Dominant membrane	Dominant bending
Thickness scaling	$\frac{h_2}{h_1} = arbitrary$	$\frac{h_2}{h_1} = arbitrary$
Poisson's ratio	$\nu_2 = \nu_1$	$\nu_2 = \nu_1$
Natural frequency	$\omega_{n2} = \omega_{n1} \frac{a_1}{a_2} \left(\frac{\rho_1 E_2}{\rho_2 E_1} \right)^{½}$	$\omega_{n2} = \omega_{n1} \frac{h_2}{h_1} \left(\frac{a_1}{a_2} \right)^2 \left(\frac{\rho_1 E_2}{\rho_2 E_1} \right)^{½}$

To test that the approximate similitude conditions hold, a model with properties according to table 5.3, was scaled down four times in length and two times in thickness and the material properties were also changed according to table 5.4.

Table 5.3 Model properties

α [°]	R_1 [m]	R_2 [m]	L [m]	h [mm]	E [GPa]	ρ [kg /m^3]	ν
9.6	0.75	1	1.5	5	208	7850	0.3

Table 5.4 Subscale model properties

α [°]	R_1 [m]	R_2 [m]	L [m]	h [mm]	E [GPa]	ρ [kg /m^3]	ν
9.6	0.1875	0.25	0.375	2.5	150	2200	0.3

Using Mathematica, the natural frequencies for the real-scale model and for the subscale model were calculated. Using the model properties in table 5.3 and 5.4, scale factors can then be calculated with equations in table 5.2. By multiplicating the frequencies from the real-scale model with the scale factors from equation 5.1, the membrane and the bending approximations can then be obtained according to table 5.5

Membrane frequencies: $\omega_{n2} = 6.4\ \omega_{n1}$
Bending frequencies: $\omega_{n2} = 12.8\ \omega_{n1}$ *(5.1)*

Table 5.5 Results from similitude calculation in Hertz (m = 1)

n	Real model	Subscale model	Membrane approximation	Bending approximation
1	269	1724	1723	3447
2	142	915	913	1825
3	82	547	528	1057
4	56	435	357	714
5	49	497	314	629
6	55	659	355	710
7	71	874	452	905
8	89	1126	573	1146
9	111	1411	714	1427

The results from the calculations show that the respective approximate scaling law shows good agreement at the section where each law is supposed to be valid. The membrane approximation is valid up to n = 3 and the bending approximation is valid from n = 6. In order to be able to use the approximate similitude conditions, one has to know if the frequency is dominated by membrane or bending energy. A list of frequencies can not be used unless the mode shape of each frequency is known.

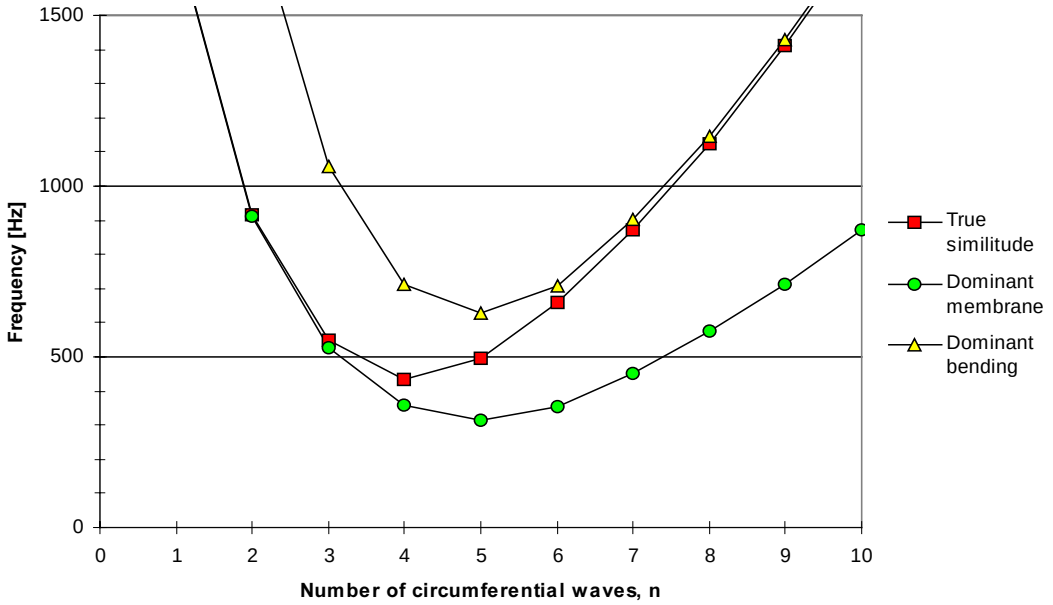

Figure 5.1 Results from approximate similitude conditions (m = 1)

6 Subscale nozzle experiment

VAC has performed a subscale nozzle vibration test at ”Sveriges Forsknings- och Provningsinstitut” (SP). The aim of the experiment was to gain understanding of design considerations of upper stage nozzles and to learn more about the physical behaviour regarding vibrations. For this purpose, a subscale nozzle (see figure 6.1) was designed.

6.1 Experimental set-up

To imitate the stiffness properties of a real nozzle, the skirt was manufactured with decreasing sheet thickness axially and inlet and outlet stiffeners were added. The contour of the nozzle is identical to the second cone of Viking 5. The two stiffeners were mounted to the skirt by 60 bolts each. Three supports were bolted to the inlet stiffener with two bolts each and attached to the base plate with two bolts. Three tri-accelerometers were mounted on the outlet stiffener and one on the inlet stiffener. Also three strain gauges were mounted on the skirt. All measurements from the vibration and strain gauges were recorded on tape, but not all data have been extracted and analysed. No data from the strain gauges have been extracted and not all accelerations. The test was divided into two load cases: sinusoidal vibration testing and random vibration testing. More details about the test hardware and test procedures are found in [12].

Figure 6.1 Subscale nozzle in test rig

6.1.1 Results from resonans investigation

From the sinusoidal vibration testing, a resonans investigation was also performed with a constant acceleration of 2g in both horizontal and vertical direction, with a sweep rate of two minutes per octave. From the resonans investigation, the acceleration versus the frequency was plotted, see figure 6.2. The peaks in the plot indicate resonans and consequently a natural frequency should be present at that frequency. By comparing

data between different gauges, it is possible to arrive at a table with possible frequencies, but it is hard to draw any conclusions about the vibration characteristics because of the lack of corresponding mode shapes.

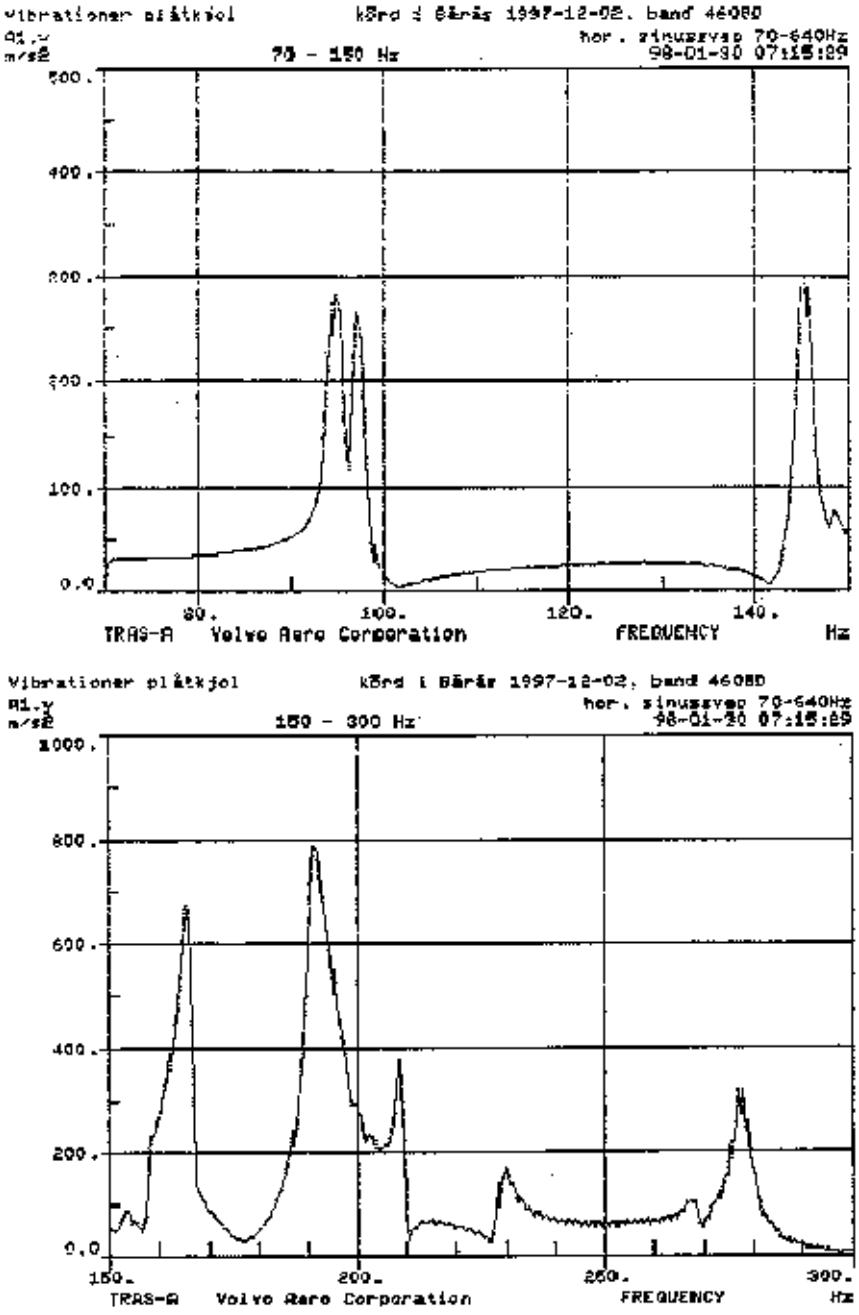

Figure 6.2 Forced response of subscale nozzle in experiment [13]

6.2 ANSYS model of subscale nozzle

It would be of great interest if the ANSYS calculations could be used to verify the structure properties. By arriving at the same natural frequencies as in the experiment, any dynamic loading would then be possible to calculate in ANSYS for the actual structure. The ANSYS model of the subscale nozzle can be divided into four parts: skirt, inlet stiffener, outlet stiffener and base support. A total of 12 576 elements with 240 elements in circumferential direction, 8-node structural shell element SHELL93,

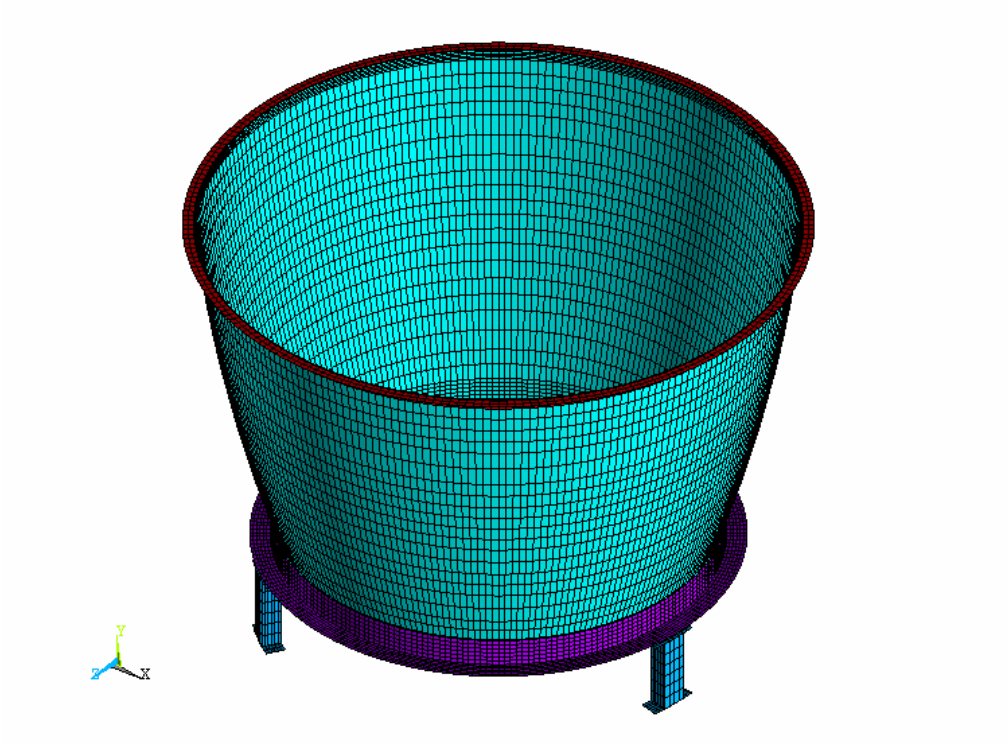

Figure 6.3 ANSYS model of the subscale nozzle

are used. The material properties are evaluated at a temperature of 293 K. The nodes at the same position as the bolts are coupled together in all degrees of freedom. Nodes at the bottom of the supports are clamped.

6.2.1 Natural frequencies from ANSYS calculation

From the modal analysis in ANSYS a list of frequencies is obtained. By individually examining each mode and classifying it according to its wave-numbers *m* and *n*, it is possible to plot the frequencies as a function of the wave-numbers, as seen in figure 6.4. Because of the more complex structure with supports, some of the mode shapes involves motion of the supports and cannot be classified by their wave-numbers *m* and *n*. These mode shapes are referred to as *non-classified* and are only indicated in what region they are most likely to appear in. The m = 1 curve changes slope at n = 5. This is because the shell changes meridional mode shape from clamped - free to something similar to clamped - clamped.

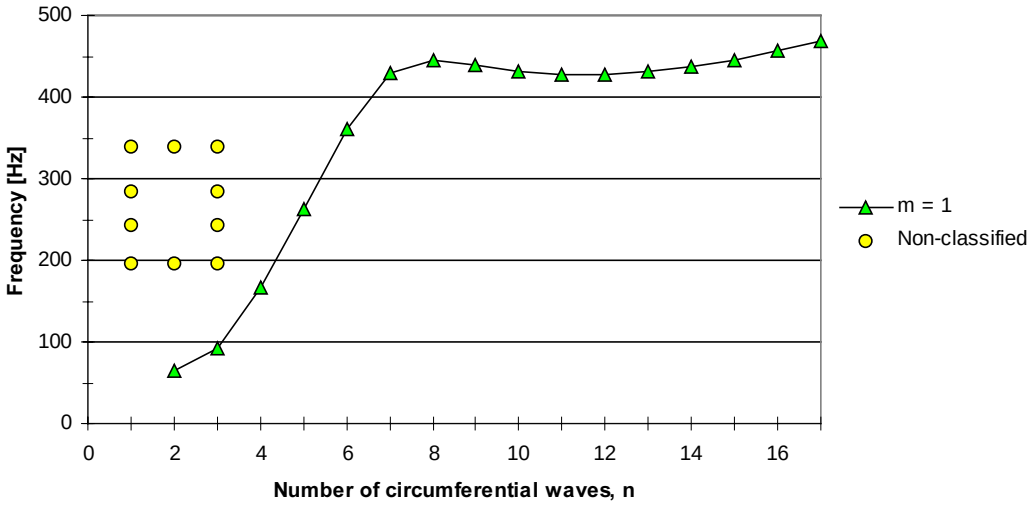

Figure 6.4 Natural frequencies from subscale nozzle, grouped by wave-numbers

An example of a mode shape is shown in figure 6.5 and more examples are given in Appendix 6. Even if some of the frequencies obtained from the modal analysis are close to the experimental values it is still hard to be sure if the model behaves as the experiment and a simulation of the test procedure is needed.

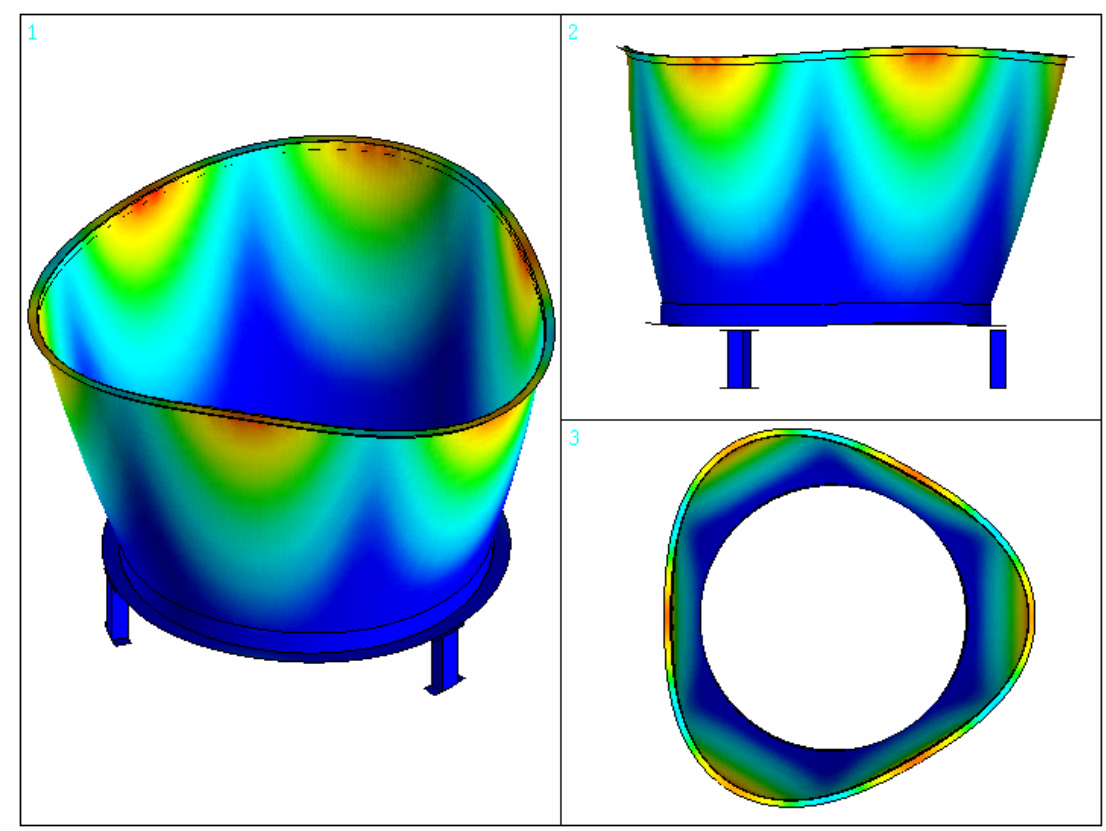

Figure 6.5 Subscale nozzle mode shape (m = 1, n = 3, f = 92.2 Hz)

6.2.2 Forced response from ANSYS calculation

To compere data from the experiment, a simulation of the 2g horizontal acceleration of nozzle is done in ANSYS using harmonic response analysis. This is a technique used to determine the steady-state response of a linear structure to loads that vary sinusoidal (harmonically) with time. ANSYS has three different solutions methods: full method, reduced method and mode superposition method. The latter is used in this analysis due to its superior computationally speed. Mode superposition method is a method of using the natural frequencies and mode shapes from the modal analysis to characterise the dynamic response of a structure to a transient or steady harmonic excitations. Harmonically varying element loads (such as pressures, temperatures or accelerations) have to be specified in the modal analysis even if the loads are ignored in the modal analysis, but a load vector will be written and later used when the modes are superpositioned. The mesh and boundary conditions are the same as in the modal analysis, but an acceleration vector is introduced in the horizontal x-direction. It is recommended that the number of modes extracted from the modal analysis should cover about 50 percent more than the frequency range of the harmonic loads. The previous modal analysis gave frequencies up to 470 Hz, which is enough for a harmonic load up to 300 Hz. A damping-ratio of 0.5 percent is used to avoid infinite displacements at the resonans-frequencies.

The harmonic response is extracted for two frequency ranges, 50 – 150 Hz and 150 – 300 Hz, and the displacement of the nodes at the same position as the acceleration gauges is used to calculate the accelerations. This can be done by the use of equation 6.1 and 6.2 and a response curve is shown in figure 6.6.

$$u = A\cos(\omega t) \qquad (6.1)$$

$$a = \ddot{u} = -\omega^2 u \qquad (6.2)$$

By comparing figure 6.2 and 6.6, the appearance in the 150 - 300 Hz range is fairly similar. In the 70 - 150 Hz range, the experiment has peaks at 95 Hz and 145 Hz, but the ANSYS calculations have either. However, the experimental equipment did also have a resonans frequency at 100 Hz and this could explain why a peak at 95 Hz is present. The model response is however close enough to the experimental response, so the model can be used to calculate other properties that could not be measured.

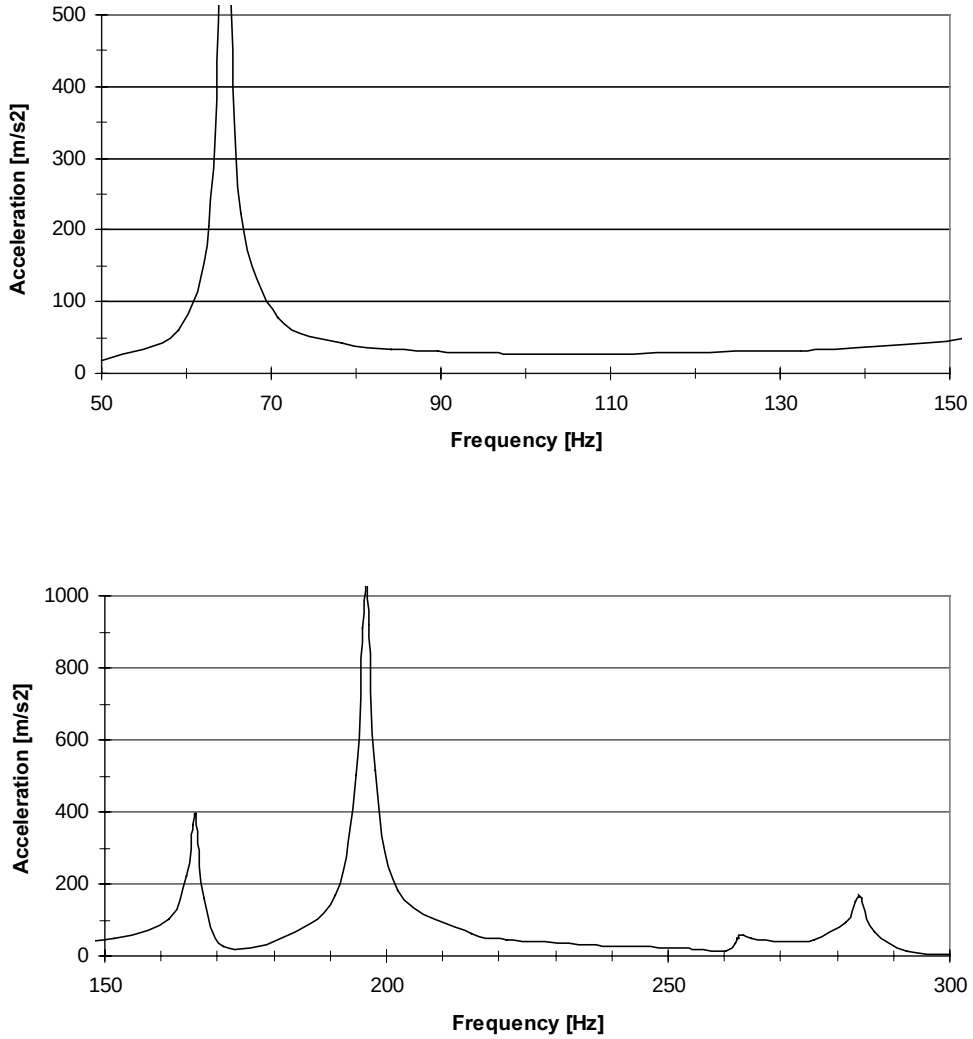

Figure 6.6 Forced response of subscale nozzle in ANSYS

7 Shells with curvature

To make the expansion in the nozzle as efficient as possible, the shape of the nozzle is crucial. This is why the nozzles have a slight curvature. It would be of great interest if a conical shell model could be used to predict the performance of a shell with slight curvature.

7.1 Approximation of Vulcain 2 NE skirt

It is possible to select the parameters that describe the conical shell in many different ways. One could select the same radius and height or the same height and the same arc length. However, the fundamental identifying feature of a shell is its reference surface and maintaining the same surface area and arc length would seem reasonably. The parameters L_c and R_c are then chosen such that the conical shell will have the same surface area and the same arc length as the shell with curvature.

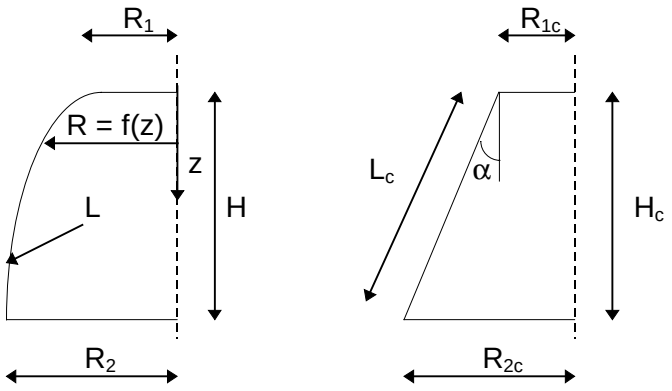

Figure 7.1 Parameters used to describe shells

The contour used for the Vulcain 2 NE skirt is given in equation 7.1, where *z* is varied between *a* (top) and *b* (bottom) and the coefficients *A, B, C* and *D* are given in [14].

$$R = f(z) = A + Bz + Cz^2 + Dz^3 \qquad (7.1)$$

This is the cold delivery contour and it is far from valid at the operating temperature of about 1200 K.

The smaller radius are selected to be the same in both cases and subsequently:

$$R_1 = R_{1c} \qquad (7.2)$$

The arc length of the shell is given by equation 7.3, which directly gives L_c in terms of the contour according to equation 7.2.

$$L = L_C = \int_a^b \sqrt{1 + f'(z)^2}\, dz \qquad (7.3)$$

The surface area for a truncated cone is given by:

$$A_c = \pi (R_1 + R_2) L_c \qquad (7.4)$$

The surface area for the shell with curvature is given by:

$$A = \int_a^b 2\pi \cdot f(z)\sqrt{1+f'(z)^2}\,dz \tag{7.5}$$

Equation 7.4 equal to equation 7.5 gives:

$$R_{2c} = \frac{1}{\pi L_c}\int_a^b 2\pi \cdot f(z)\sqrt{1+f'(z)^2}\,dz - R_1 \tag{7.6}$$

The apex angle α can then be calculated as:

$$\alpha = \sin^{-1}\frac{R_{2c}-R_{1c}}{L_c} \tag{7.7}$$

Using Mathematica and equations 7.1, 7.2, 7.3, 7.6 and 7.7 the conical shell approximation can be calculated according to table 7.1.

Table 7.1 Cone approximation of Vulcain 2 NE skirt

α [°]	R_1 [m]	R_2 [m]	L [m]	h [mm]
13.83	0.7975	1.113	1.319	1.6

Using simple trigonometry the height of the conical shell can be calculated.

7.2 Comparison with ANSYS

To verify that the conical shell approximation captures the behaviour of the shell with curvature, two calculations with ANSYS are made for comparison. The calculations are made on the Vulcain 2 NE skirt contour without stiffeners, to reduce the influence of other parameters on the results. The material used for the shell is Haynes 230 and the properties at 300 K are given in table 7.2. Shell element SHELL93 with all displacement constrained and rotation about y constrained at the upper radius is used. A total of 1664 elements with 64 elements distributed around the circumference are used.

Table 7.2 Material data for Haynes 230 at 300K

E [GPa]	ρ [kg /m^3]	ν
210	8970	0.3

The Mathematica calculations used data from table 7.1.

7.2.1 Results

Figure 7.2 show that the conical shell approximation captures the large scale behaviour of both shells. The relative errors at the lowest frequencies are rather large. By adding stiffness to the model by increasing the plate thickness five times, the membrane frequencies remain almost constant and the bending frequencies increase a lot. The lowest frequency is moved from a high circumferential mode, to a much lower circumferential mode. Also the number of low frequencies, less than 100 Hz, are substantially reduced from more than 13 to 5.

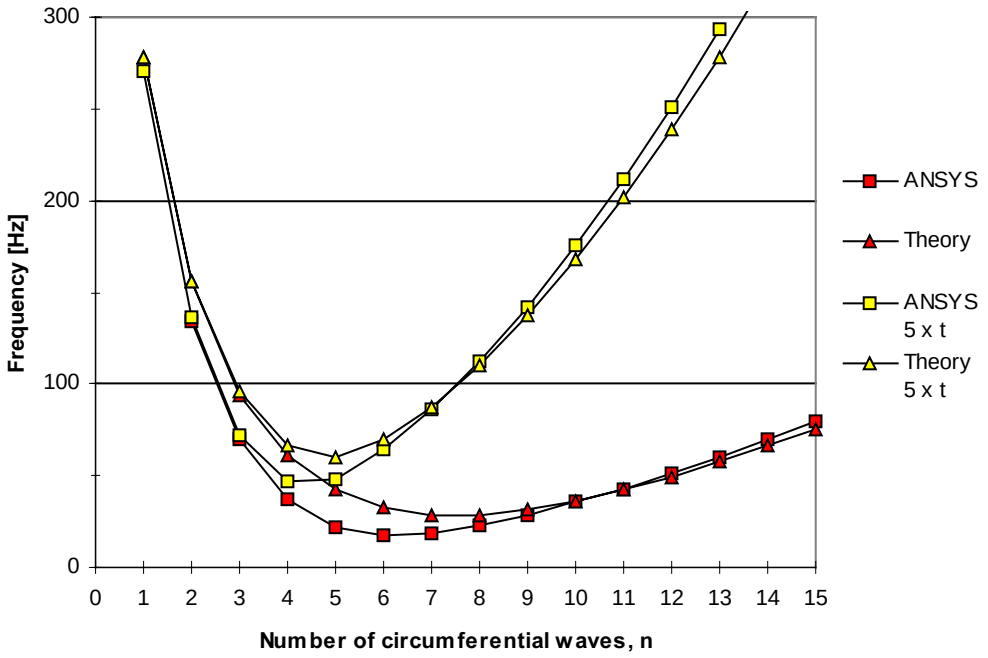

Figure 7.2 Natural frequencies of the Vulcain 2 NE skirt without stiffeners and with two different plate thicknesses (m = 1)

Some calculations with small variations of the length and the radius of the cone approximation, indicate that the quotient ω/ω_0 is not so dependent on the approximation, but the relative errors are much more sensitive to the approximation.

8 Vulcain 2 NE Skirt

In 1996, VAC won a contract from ESA for the evolution of the Vulcain engine. To increase the payload performance of Ariane 5, a seven year development program was started. The Vulcain 2 engine is a part of the ESA program Ariane 5 Evolution. It will be an upgraded version of the main engine of the evolved Ariane 5, developed to boost launcher payload to 7.4 tons in geostationary transfer orbit. The major differences between the Vulcain and Vulcain 2 engines are increases in thrust and ISP. This is done by increasing combustion chamber mixture ratio and pressure, as well as nozzle expansion ratio. The nozzle needs to be redesigned to incorporate the filmcooling of dumped hydrogen as well as turbine exhaust gases. The nozzle also needs to utilise a special wall reinforcement concept to enable the increased outlet area ratio.
The nozzle extension (see figure 8.1) can roughly be divided into three major parts: the

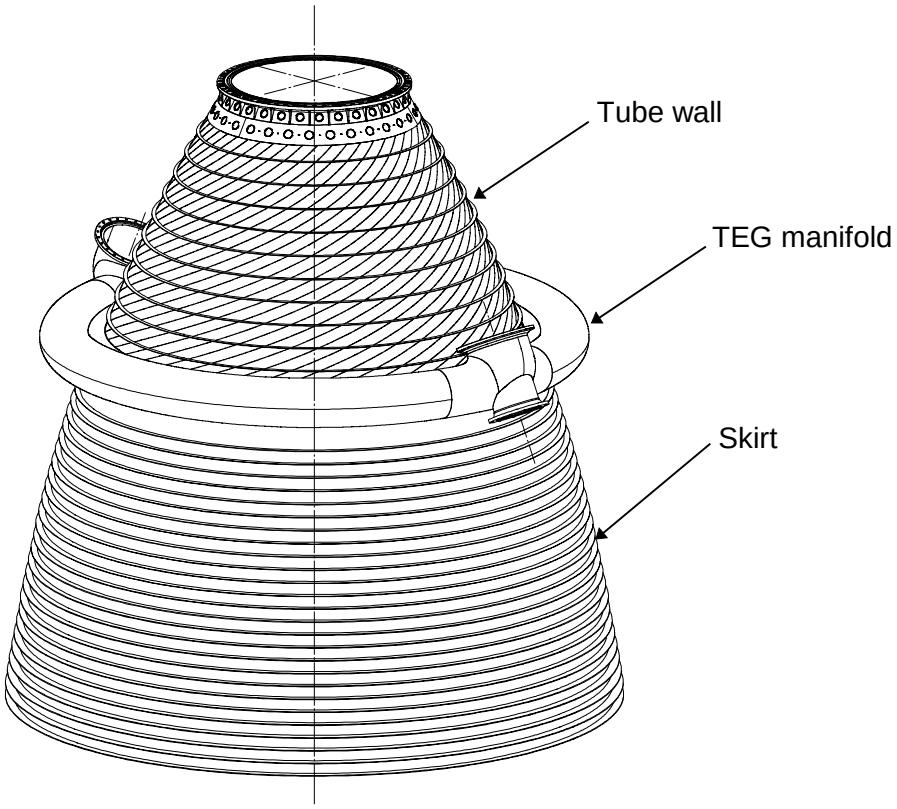

Figure 8.1 Major parts of the Vulcain 2 NE

skirt, the tube wall and the TEG (Turbine Exhaust Gases) manifold. The tube wall, which is located in the upper part of the nozzle extension, is made of thin-walled tubes (6x4 mm) welded side-by-side. This part of the nozzle is cooled by liquid hydrogen, which flows though the tubes. The lower part of the nozzle extension, the skirt, is cooled by film cooling. The medium used for the film cooling is exhausts from the turbines for the oxygen and hydrogen fuel pumps. The film is injected by the TEG injector, to which the skirt is welded. Calculations will only concern the skirt.

8.1 Comparison between ANSYS and Theory

Using the method to approximate a shell with curvature derived in the previous chapter, comparison with the Vulcain 2 NE skirt is made. In its design, the skirt is stiffened with 22 rings with varying dimensions and spacing. All calculations are made using the cold contour of the skirt and all material properties are those of Haynes 230 at 300 K.

8.1.1 ANSYS model of Vulcain 2 NE skirt

An existing model of the Vulcain 2 NE skirt was used to make a modal analyse in ANSYS. Only boundary conditions had to be implemented into the model. All nodes at the smaller radius were first rotated according to a cylindrical co-ordinate system and then restrained in *x, y, z* and rotation about *y*. This is to simulate a clamped end. Since the TEG manifold is very stiff in comparison with the skirt, the clamped end condition can in some sense be justified. The model uses 11 760 elements, with 80 elements distributed around the circumference, and is shown in figure 8.2. As many modes as possible were extracted from the analysis, to get as much information about the vibration characteristics as possible.

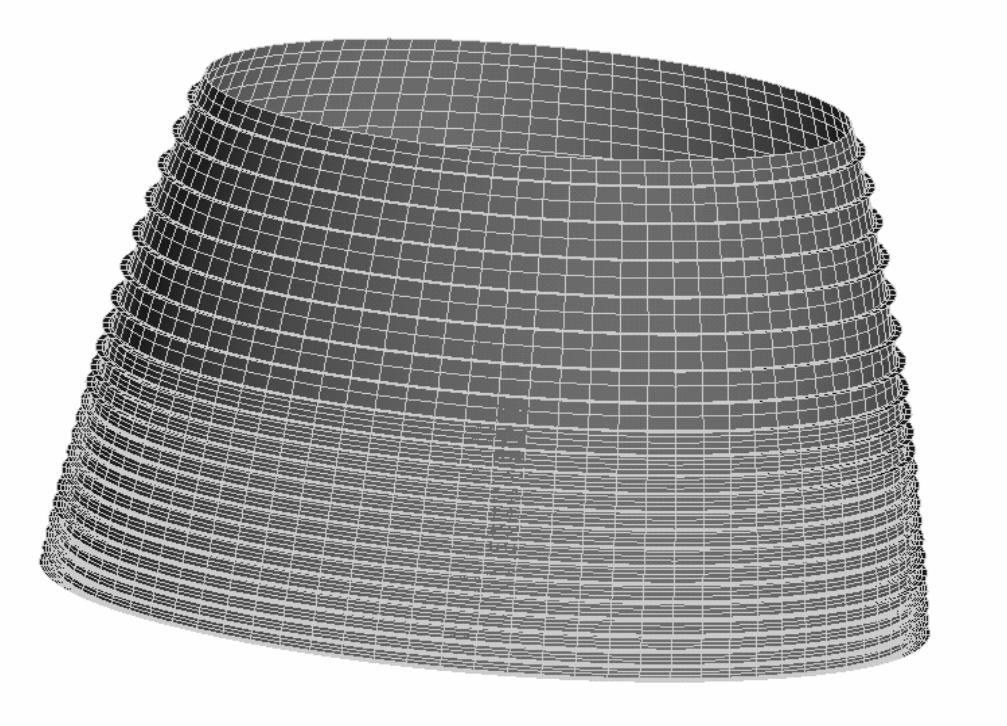

Figure 8.2 ANSYS model of the Vulcain 2 NE skirt

8.1.2 Mathematica model of Vulcain 2 NE skirt

The skirt contour is modelled using the approximation derived in the previous chapter. Three different vectors containing information about the stiffener location, height and thickness are needed to fully describe the stiffening of the skirt. The stiffeners are placed at the same arc-length position as in the real model.

8.1.3 Results from Vulcain 2 NE skirt calculations

As a result of the modal analyse in ANSYS, a list of frequencies is obtained. By individually examining each mode and classifying it according to its wave-numbers m and n, it is possible to plot the frequencies as a function of the wave-numbers as seen in figure 8.3. As expected the first meridional mode, m = 1, has the lowest values and the other two are found higher up. It is also expected that the frequencies converge for high circumferential wave numbers, independent of *m*. The theory is only capable of calculating frequencies for the meridional mode that has the lowest frequencies, but the agreement for the first meridional mode is very good. The theory is only about 13 percent too high at the lowest frequency and is capable of capturing the large scale behaviour of the shell.

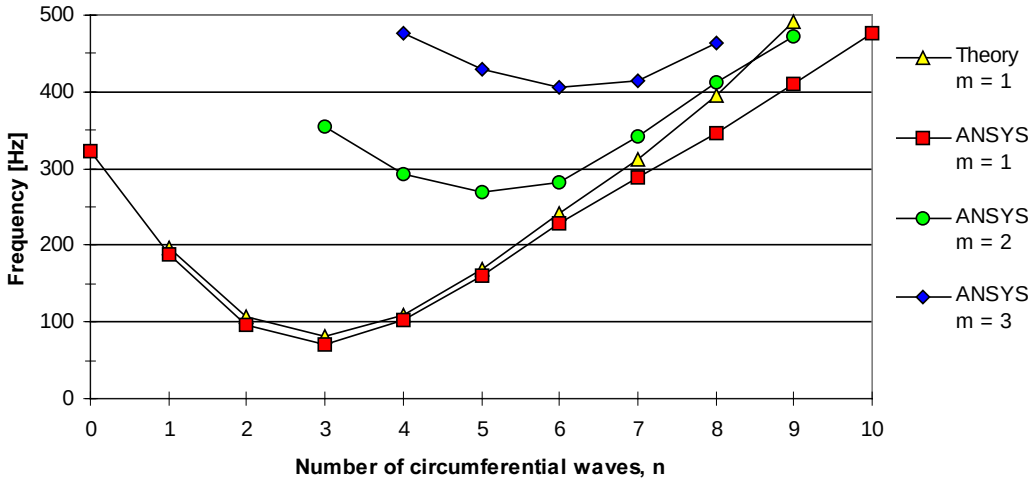

Figure 8.3 Natural frequencies from Vulcain 2 NE skirt, grouped by wave-numbers

The ANSYS m = 1 curve, tends to bend downwards at higher circumferential wave numbers. This can be explained by examining figure A7.4 where it appears that the shell changes meridional mode shape, from clamped - free to clamped - clamped. An example of a mode shape is found in figure 8.4 and more mode shapes are also found in Appendix 7. The calculations in ANSYS took about 11 hours and the calculations using Mathematica took under two minutes.

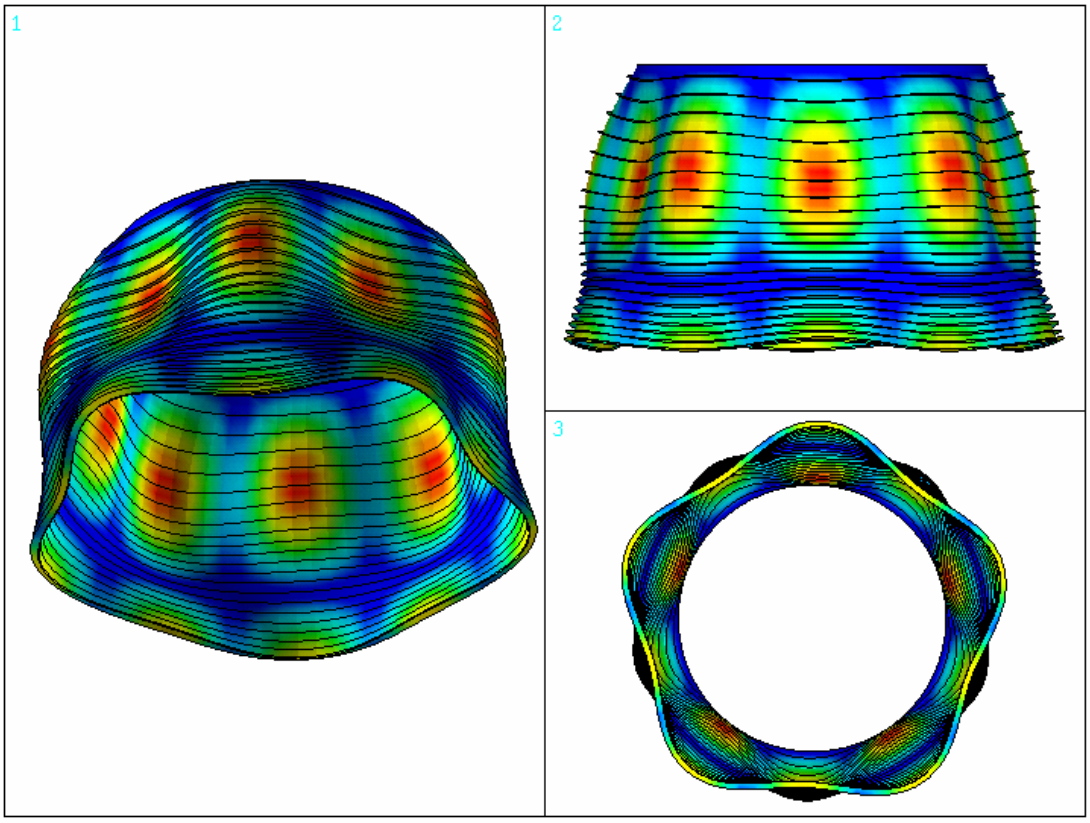

Figure 8.4 Vulcain 2 NE skirt mode shape (m = 2, n = 5, f = 268.8 Hz)

8.2 Variation of stiffener dimensions and numbers

The full model comparison between ANSYS and the theory shows that the theory is very capable of capturing the large scale behaviour of stiffened shells with curvature. It is then possible to use the theory in order to get some understanding of how the dimensions and the number of the stiffeners effect the fundamental frequency, membrane and bending frequencies. As a measure of how the membrane frequencies and the bending frequencies are effected, the improvement of a specific frequency from a membrane or bending mode is calculated. Only frequencies from the first meridional mode are considered and for the membrane case the first circumferential mode in considered whereas for the bending case the sixth circumferential mode is considered.

8.2.1 Variation levels

A model with the same contour as the Vulcain 2 NE skirt is used, but with equally spaced and sized rings. Height, width and number of stiffeners are varied. The width is chosen to be 2.39 or 3.18 mm. The height is chosen to be 15, 25 or 35 mm and the number of rings is varied from 2 to 25. So, the fundamental frequency improvement, the membrane frequency improvement and the bending frequency improvement are calculated for every combination of *b, h* and number of rings.

8.2.2 Results from calculations with varying stiffener properties

According to figure 8.5, the rings with the largest height give the largest fundamental frequency improvement. The improvement is large up to 5-10 rings and adding more rings can even decrease the fundamental frequency improvement. Also with many rings, the smaller width gives larger frequency improvement than the larger width.

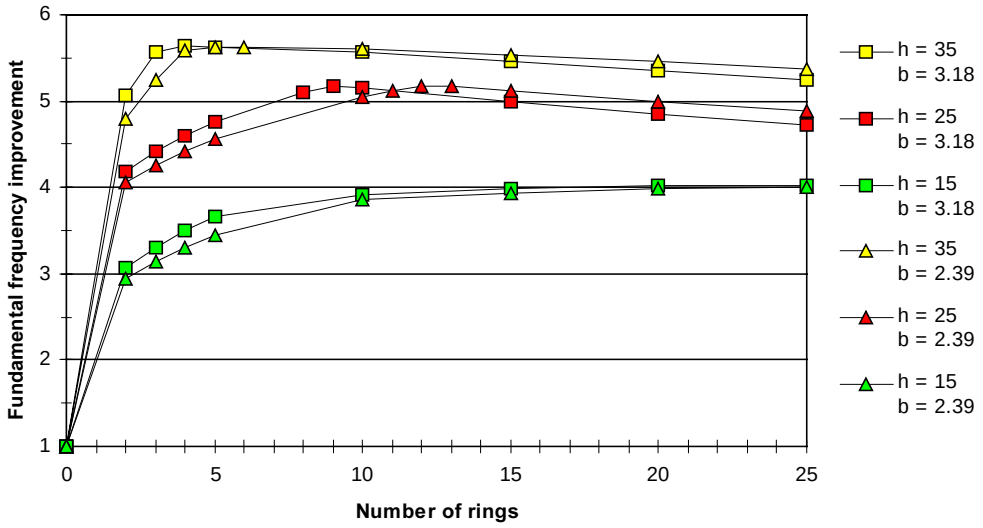

Figure 8.5 Fundamental frequency improvement of the Vulcain 2 NE skirt conical shell approximation with varying ring dimensions and numbers

The bending frequency improvement is more sensitive to variation in stiffener dimensions and numbers. Increase in stiffener height has the greatest impact on the bending frequency improvement and this is not at all strange since the bending rigidity is proportional to the cube of *h*. When the shell is stiffened with more than 10 rings, the bending improvement slows down, but it never starts to decay. The absolute value of the bending frequency improvement should be taken with some carefulness, since it is only a measure of the frequent improvement of a specific frequency.

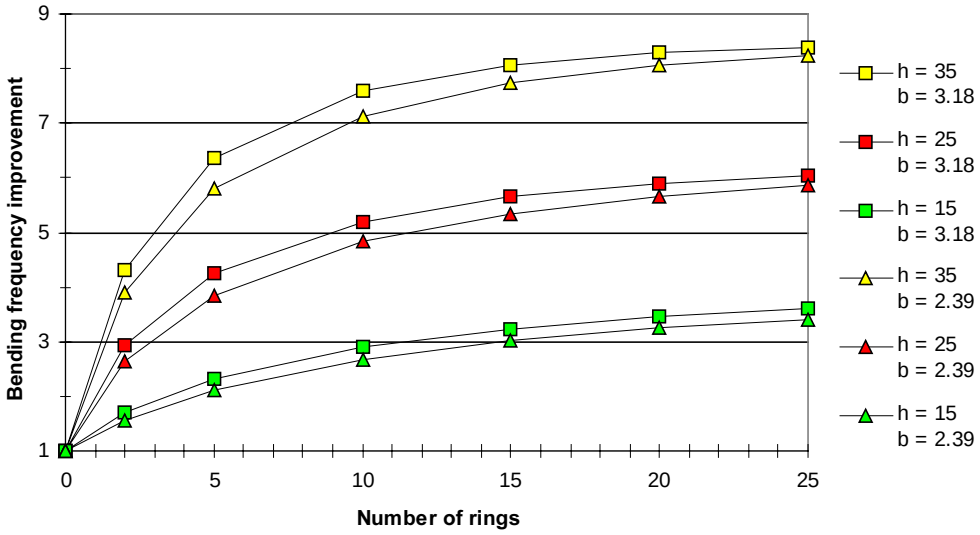

Figure 8.6 Bending frequency improvement of the Vulcain 2 NE skirt conical shell approximation with varying ring dimensions and numbers

The membrane frequencies are not very sensitive to the number of stiffeners or the dimensions of them. At most, a 30 percent decrease in frequency is observed for the worst case with the largest stiffeners and with 25 rings.

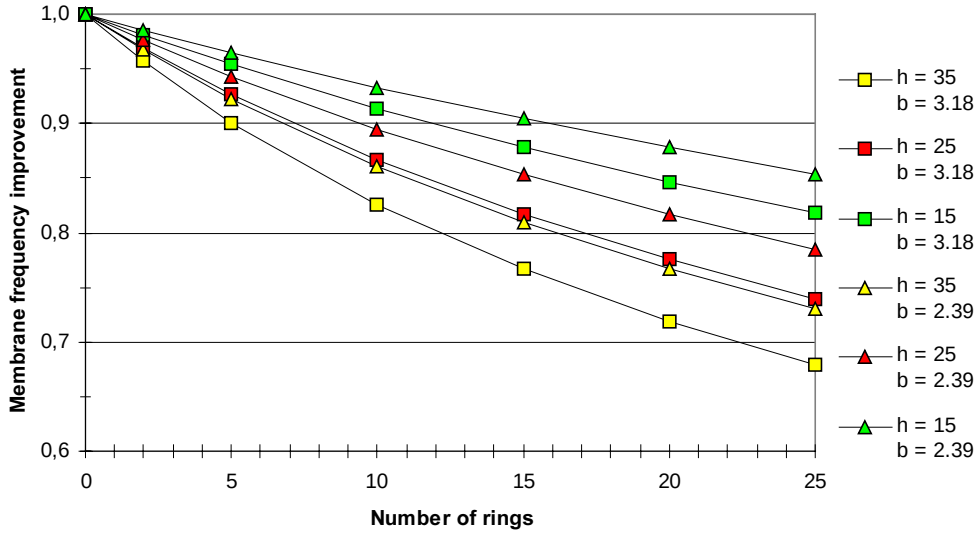

Figure 8.7 Membrane frequency improvement of the Vulcain 2 NE skirt conical shell approximation with varying ring dimensions and numbers

8.3 Distribution of stiffener height

In the previous examinations, the stiffeners were all of the same dimension. Because of the fact that the shell undergoes much more deformation at the large end, it seems reasonable to increase the height of the rings at the free end. By doing this, a large amount of weight can be saved.

8.3.1 Calculation of ring-height distribution

A curve, $h_r = As^m + B$, is used to describe the distribution of ring-height along the shell and *m* is the grade number, where m = 1 represent a linear distribution. The constants *A* and *B* are selected by choosing a height on the first and last stiffener. See figure 8.8

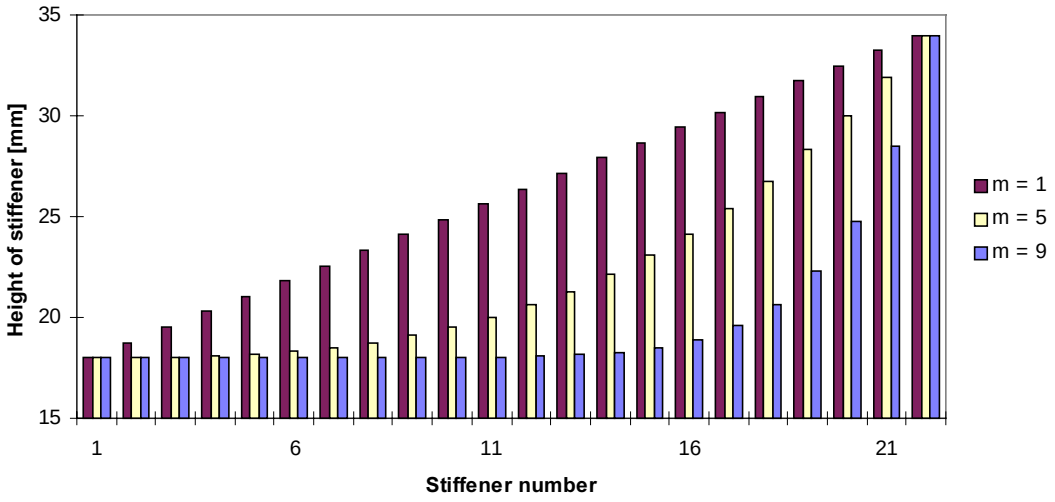

Figure 8.8 Examples of stiffener height distribution on a shell with 22 rings

for an example of height distribution with 22 rings and varying grade number.

8.3.2 Results from different ring-height distributions calculations

As seen in figure 8.9, increasing the grade number will decrease the total weight of the stiffeners. Using a grade number of four reduces the weight of the rings from 76 kg to 63 kg, compered to a linear distribution.

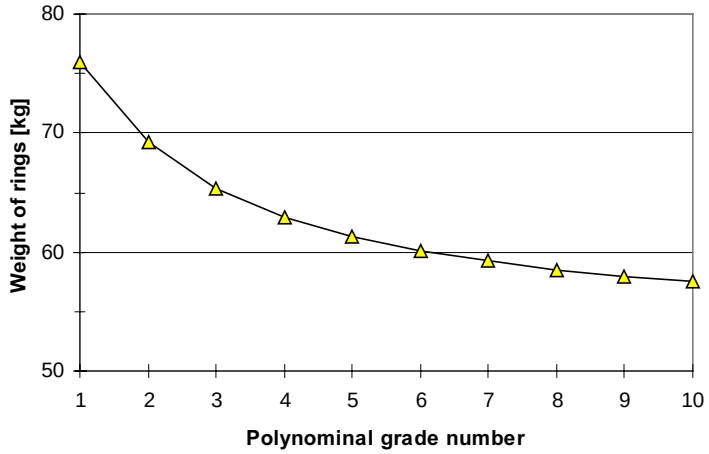

Figure 8.9 Weight reduction with different stiffener height distributions 22 rings

Figure 8.10 shows that mainly the bending frequencies are effected by the ring-height distributions. As the polynomial grade number is increased from one to five, the bending frequencies decrease by about 30 percent and also the fundamental frequency show a small decrease. The membrane frequencies remain almost constant at the same level as without stiffener. So, the use of different ring-height distributions are very effective in reducing ring-weight without reducing the frequencies.

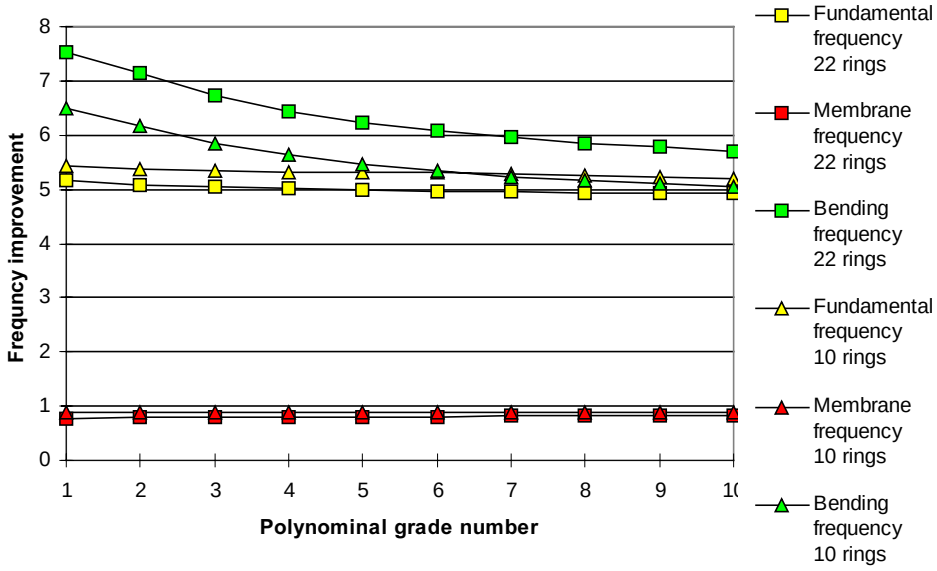

Figure 8.10 Frequency improvement of the Vulcain 2 NE skirt conical shell approximation with varying height distribution from h = 18 to h = 34 mm

8.4 Optimum position of stiffeners

By examining figure 4.2, four different positions with maximum deflection can be detected in the first three meridional modes. The idea is to only add stiffeners at those positions. Also by examining the mode shapes of the real Vulcain 2 NE skirt in Appendix 7, it is possible to measure these positions.

8.4.1 Model of optimum stiffener position

The same model as in chapter 8.1 is used, but the number and sizes of the rings are changed. Using the trial-and-error method, small changes in stiffener location and dimension are tried, until a similar result of the real Vulcain 2 NE skirt is obtained. Finally, a model with seven rings is chosen, where the four deflection maximum points are stiffened with two rings each, except for the one at the large end of the shell which has only one ring. This leads to a 75 percent weight reduction compared to the real Vulcain 2 NE skirt.

8.4.2 Results from Mathematica calculations of optimum stiffener positions

As seen in figure 8.11, the model with 7 rings has almost the same frequencies in both the membrane and in the bending area. However, small changes in stiffener location

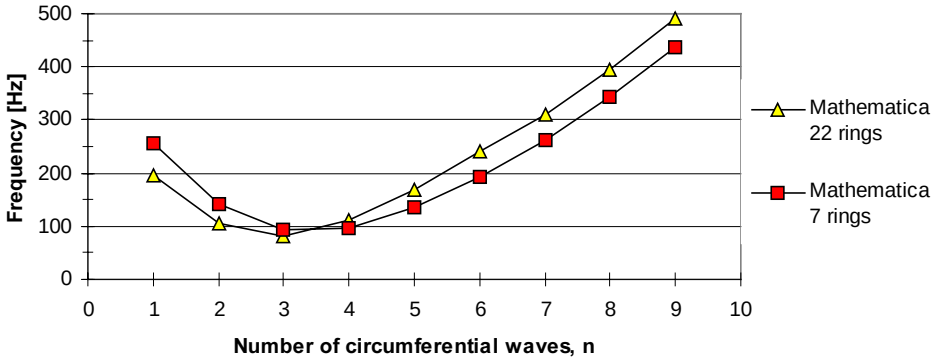

Figure 8.11 Comparison between real Vulcain 2 NE skirt conical shell approximation model and simplified skirt model in Mathematica (m = 1)

and dimensions can result in large frequency changes, so it is perhaps not likely that a optimisation on a conical shell will give good result on a shell with curvature.

8.4.3 ANSYS model of optimum stiffener position

The results from the conical calculations seem almost to good to be true and calculations using ANSYS are made to verify if the results are as promising as they appear. The model is shown in figure 8.12 and uses 4800 elements with 80 elements distributed around the circumference.

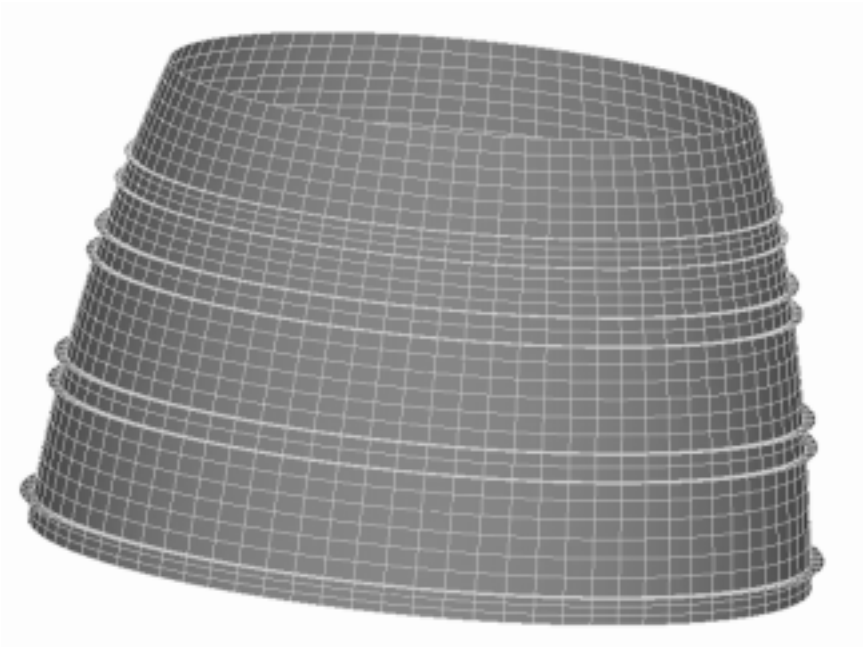

Figure 8.12 Model used to test optimum stiffening of Vulcain 2 NE skirt in ANSYS

8.4.4 Results from ANSYS calculations of optimum stiffener positions

Unfortunately, figure 8.13 shows that the optimum stiffening does not work as well as in the conical shell model. The membrane frequencies and the fundamental frequency are almost the same, but large losses of stiffness in the bending area result in lower bending frequencies. However, the idea of only adding stiffeners at selected positions

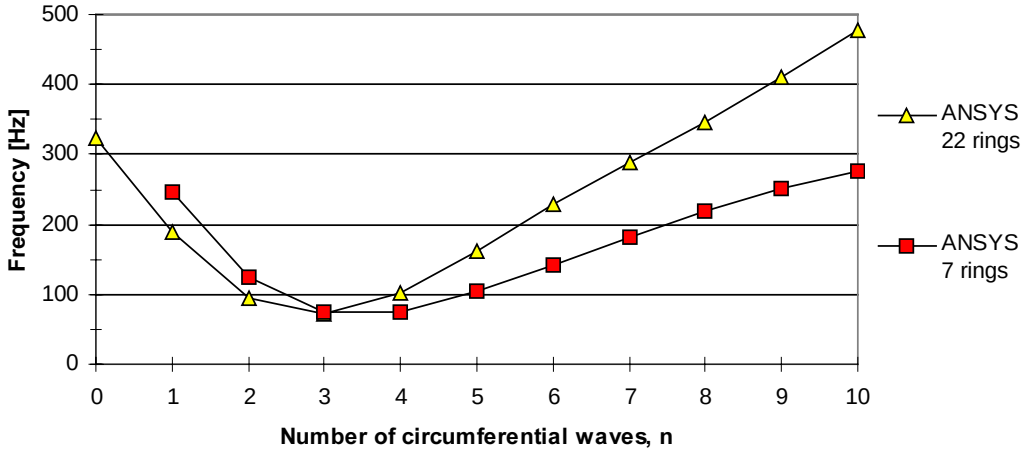

Figure 8.13 Comparison between real Vulcain 2 NE skirt model and simplified skirt model in ANSYS (m = 1)

can probably result in better results than this. More time is needed for optimising the positions for real model. Of course, there are not only natural frequencies constraints on the nozzle, for instance, thermal expansion requires that the stiffeners are placed at correct places so that the nozzle contour will remain according to specifications under hot running conditions. But still, weight reduction is of great interest.

8.5 Influence of different boundary conditions

It is not always that the shell contains ideal boundary conditions. Often, it is partly clamped at the smaller radius, by for instance a number of bolts, or as in the case of the subscale nozzle, it is bolted at three different positions. In the case of the Vulcain 2 NE skirt, it is far from being ideally clamped at the smaller radius. The TEG manifold can perhaps be approximated with a number of bolts.

8.5.1 ANSYS model with different boundary conditions

Calculations are made on the conical approximation of the Vulcain 2 NE skirt in ANSYS, but with no stiffeners. To incorporate the stiffening effect of the stiffeners the thickness is 5 times thicker. The boundary condition at the smaller radius is varied. Out of 256 nodes, 8 and 16 nodes are restrained. Three small sections (about 10°) with seven nodes each symmetrically placed are also restrained. The clamped boundary condition is obtained by restraining all displacement and one rotation.

8.5.2 Results from ANSYS calculations with different boundary conditions

Removing the rotation constraint is of little importance. From figure 8.14 is appears as the bending frequencies are almost the same, independent of the boundary conditions. However, the membrane frequencies are strongly dependent upon the boundary conditions. The more deviation from the ideal clamped boundary condition, the lower the membrane frequencies become and consequently also the fundamental frequency.

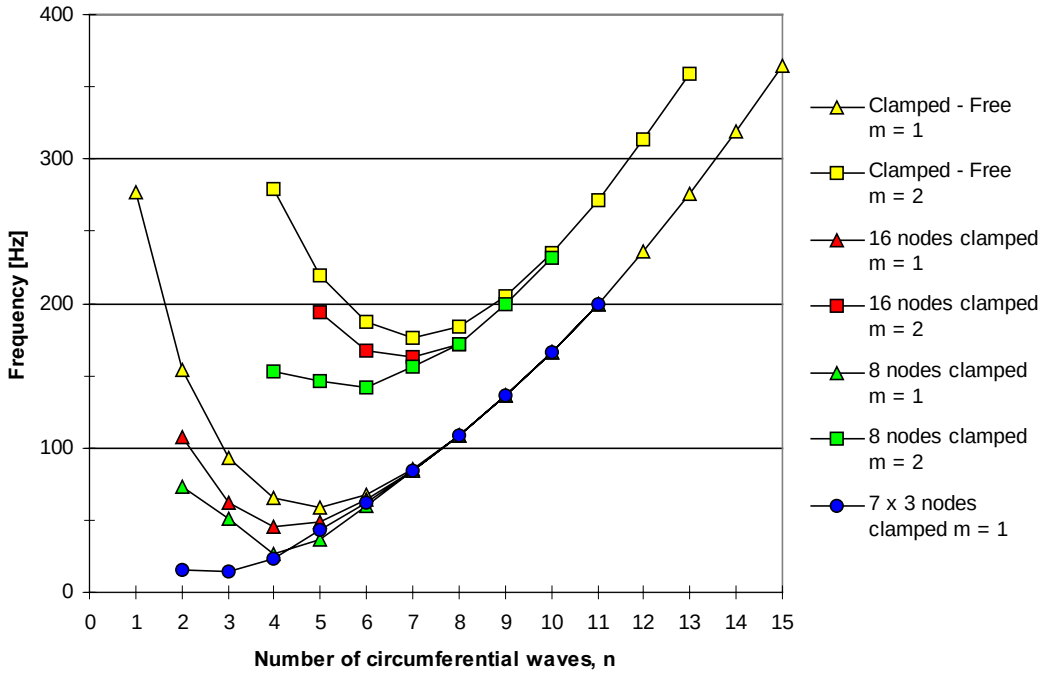

Figure 8.14 Natural frequencies of Vulcain 2 NE skirt conical shell approximation without stiffeners and increased plate thickness with different boundary conditions

9 Conclusions

The analytical method of calculating natural frequencies of ring-stiffened conical shells that have been developed, has proven to be very fast and to have enough accuracy. The errors are of the order of three percent in the six lowest frequencies for a conical shell without stiffeners. It can also be used on shells with a slight curvature, but then the errors can be substantial. The calculations on the Vulcain 2 NE skirt took about eleven hours in ANSYS, but only a few minutes with the developed method. Another great advantage is that pre-processing and post-processing can be reduced to a minimum. It is also strongly advised that the natural frequencies should always be grouped and plotted according to their wave-numbers. It is then possible to draw conclusions about the membrane and bending stiffness and what should be done to increase the frequencies in either area. A much better understanding of the vibration characteristics is obtained and extrapolation of results are also much easier to do.

From the study on how stiffener dimensions and numbers effect the natural frequencies of the Vulcain 2 NE skirt, it can be said that more stiffeners than five to ten do not effect the membrane and fundamental frequency. More stiffeners than fifteen have little influence on the bending frequencies. The stiffener height has the largest impact on the frequencies. Large weight reductions can be accomplished by having stiffeners with varying height. A suggested optimal position of stiffeners has been proposed for the conical shell approximation of the Vulcain 2 NE skirt, where the number of stiffeners is reduced from 22 to 7, while still having almost the same frequencies but with a weight reduction of the stiffeners with almost 75 percent. The commercial price on satellite launchers today is about 12$ per gram, so a weight reduction on the nozzle of ten kilograms could save up to 120 000$. However, the nozzle must also be designed with more than natural frequencies constraint and for nozzles operating at sea-level the buckling strength is often the limitation. Thermal expansion does also require that the stiffeners are placed at correct places so the nozzle contour will remain according to specifications under hot running conditions.

Even if the analytical method has been derived for a conical shell, it is not at all impossible to implement shells with curvature. Caution has to be taken when the energy expressions of the stiffeners are modified and a more detailed study on the derivation of stiffener energy should be done. Also another method of solution, like for instance the finite element method should be implemented and also different boundary conditions should be allowed. This could lead to an extremely fast and accurate method for calculating the natural frequencies for any shell of revolution.

10 References

[1] H. Kraus 1967 *Thin Elastic Shells* (Wiley). New York.

[2] W. Soedel 1993 *Vibration of shells and plate* (Marcel Dekker). New York.

[3] A.W. Leissa 1973 *Vibration of Shells* (NASA SP-288). Washington, D.C.: U.S. Govornment Printing Office.

[4] I.H. Shames and C.L. Dym 1985 *Energy and Finite Element Methods in Structural Mechanics* (Taylor & Francis). Bristol.

[5] O.E. Crenwelge and D. Muster 1969 *Journal of the Acoustical Society of America* **46**, 176-185. Free vibration of ring and stringer stiffened conical shells.

[6] Z. Mecitoglu 1996 *Journal of Sound and Vibration* **197**(2), 191-206. Vibration characteristics of a stiffened conical shell.

[7] S.S. Rao and E.S. Reddy 1981 *Computers and Structures* **14**, 103-110. Optimum design of stiffened conical shells with natural frequencies constraints.

[8] T. Irie, G. Yamada and Y. Kaneko 1984 *Journal of Sound and Vibration* **92**, 447-453. Natural frequencies of truncated conical shells.

[9] W. Soedel 1970 *Journal of the Acoustical Society of America* **49**(5), 1535-1541. Similitude Approximtions for Vibrating Thin Shells.

[10] ANSYS 5.4 Online Manual

[11] Mathematica 3.0 Online Manual

[12] T. Gustafsson 1997 *Subscale nozzle. Test and Measurement Plan*. VAC-report NP PE 114 0000 E 2001

[13] T. Gustafsson 1998 *Report on vibration tests performed on a subscale nozzle.* VAC-report NP RE 114 0000 E 2001

[14] S. Knuts 1998 *Vulcain 2 NE Assy Hot and Cold Contour.* VAC-report M2 NT 114 00DR E 2005

Appendix 1 Equations of Donnell - Mushtari

If one limits the arbitrary shell element to be a surface of revolution which is formed by rotating a plane curve about an axis which lies in its plane, it is possible by the use of differential geometry, to derive simplified expressions in curvilinear co-ordinates. But, the geometrical representation will still be rather complex and because of that, the more simplified geometry of a cone or a cylinder is often used. Only the equations for a conical shell will be given here and equations concerning other geometry can be found in [1-2]. Only the compability and the constitutive equations will be stated in the conical shell form.

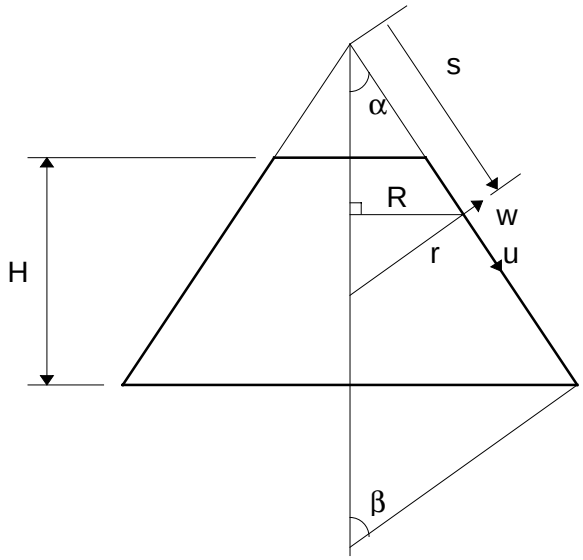

Figure A1.1 Conical shell geometry and co-ordinates

Compability equations

$$
\begin{aligned}
e_s &= \varepsilon_s + z\kappa_s \\
e_\theta &= \varepsilon_\theta + z\kappa_\theta \\
e_{s\theta} &= \varepsilon_{s\theta} + z\kappa_{s\theta}
\end{aligned}
\qquad \textit{(A1.1)}
$$

$$
\begin{aligned}
\varepsilon_s &= \frac{\bar{\partial} u}{\bar{\partial} s} \\
\varepsilon_s &= \frac{u}{s} + \frac{1}{sSin\alpha}\frac{\bar{\partial} v}{\partial\theta} + \frac{w}{sTan\alpha} \\
\varepsilon_{s\theta} &= \frac{1}{sSin\alpha}\frac{\bar{\partial} u}{\partial\theta} + \frac{\bar{\partial} v}{\bar{\partial} s} - \frac{v}{s}
\end{aligned}
\qquad \textit{(A1.2)}
$$

$$
\begin{aligned}
\kappa_s &= -\frac{\partial^2 w}{\bar{\partial} s^2} \\
\kappa_\theta &= -\frac{1}{s^2 Sin^2\alpha}\frac{\partial^2 w}{\partial\theta^2} - \frac{1}{s}\frac{\partial w}{\bar{\partial} s}
\end{aligned}
\qquad \textit{(A1.3)}
$$

$$\kappa_{s\theta} = -\frac{1}{sSin\alpha}\frac{\partial^2 w}{\partial s \partial\theta} + \frac{1}{s^2 Sin\alpha}\frac{\partial w}{\partial\theta}$$

Constitutive equations

$$\sigma_s = \frac{E}{1-\nu^2}(e_s + \upsilon e_\theta)$$
$$\sigma_\theta = \frac{E}{1-\nu^2}(e_\theta + \upsilon e_s) \qquad (A1.4)$$
$$\sigma_{s\theta} = \frac{E}{2(1+\nu)} e_{s\theta}$$

Energy expressions

$$U = \frac{1}{2}\int_V (\sigma_s e_s + \sigma_\theta e_\theta + \sigma_{s\theta} e_{s\theta}) dV \qquad (A1.5)$$

$$T = \frac{1}{2}\int_V \rho(\dot{u}^2 + \dot{v}^2 + \dot{w}^2) dV \qquad (A1.6)$$

where $dV = sSin\alpha \cdot ds d\theta dz$

Boundary conditions

Clamped end: $u = v = w = \partial w/\partial s = 0$ *(A1.7)*

Free end: $N_s = M_s = S_{s_\theta} = V_s = 0$ *(A1.8)*

Simply supported end: $v = w = N_s = M_s = 0$ *(A1.9)*

Where:

$S_{s_\theta} = N_{s_\theta} + M_{s_\theta} / (sTan\alpha)$
$V_s = 1 / (sSin\alpha)\ \partial M_{s_\theta}/\partial\theta$ *(A1.10)*

$$N_s = C(\varepsilon_s + \nu\varepsilon_\theta)$$
$$N_{s\theta} = 4Gh\varepsilon_{s\theta}$$
$$M_s = D(\kappa_s + \nu\kappa_\theta) \qquad (A1.11)$$
$$M_{s\theta} = (Gh^3/6)\kappa_{s\theta}$$

Appendix 2 Beam and ring mode shapes

Clamped - Free beam mode shapes

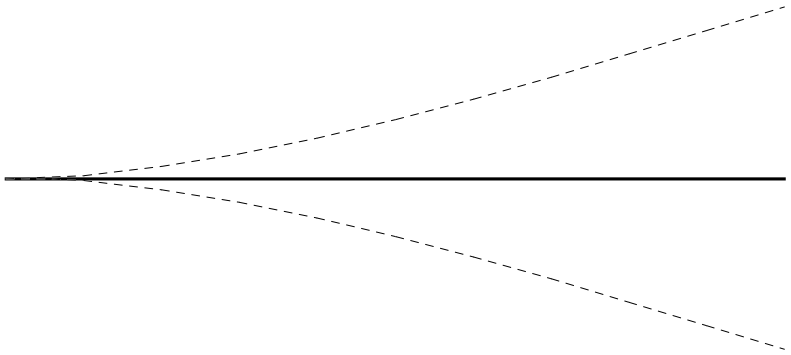

Figure A2.1 Clamped - free beam mode shape, m = 1

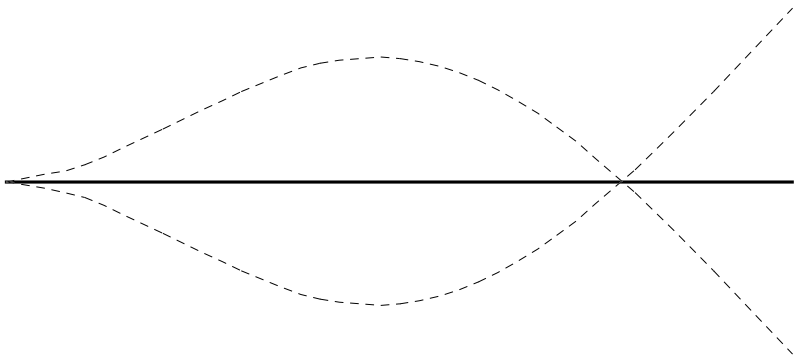

Figure A2.2 Clamped - free beam mode shape, m = 2

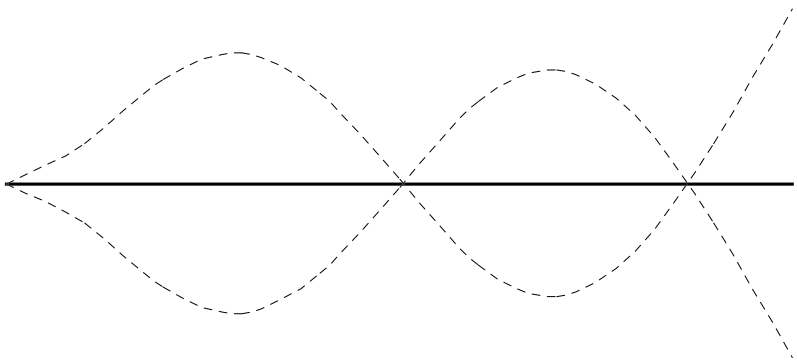

Figure A2.3 Clamped - free beam mode shape, m = 3

Clamped - Clamped beam mode shapes

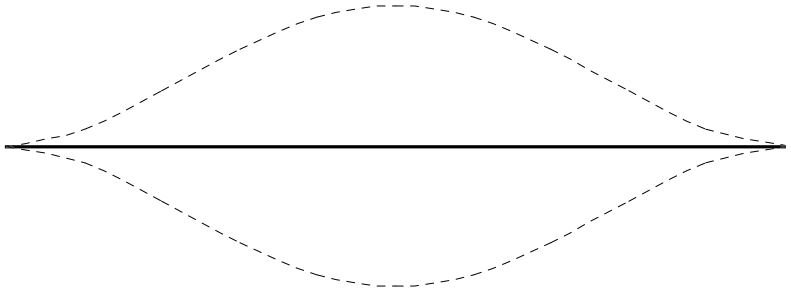

Figure A2.4 Clamped - clamped beam mode shape, m = 1

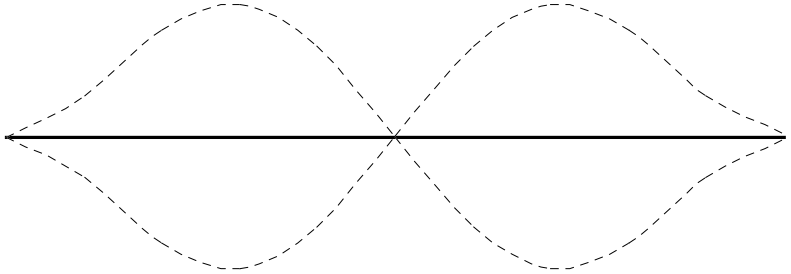

Figure A2.5 Clamped - clamped beam mode shape, m = 2

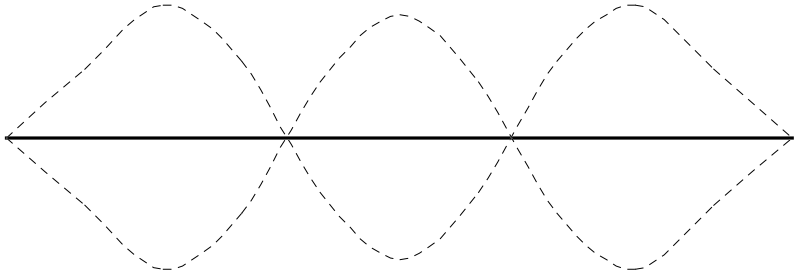

Figure A2.6 Clamped - clamped beam mode shape, m = 3

Circular ring mode shapes

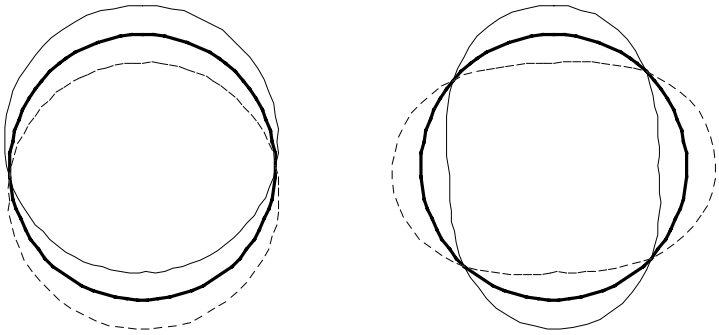

Figure A2.7 Circular ring mode shapes, n = 1 and n = 2

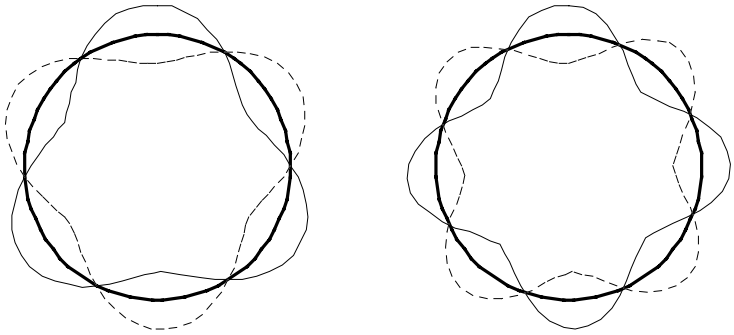

Figure A2.8 Circular ring mode shapes, n = 3 and n = 4

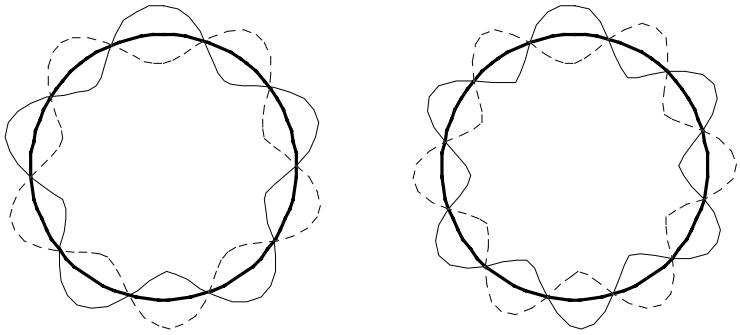

Figure A2.9 Circular ring mode shapes, n = 5 and n = 6

Appendix 3 Conical shell mode shapes

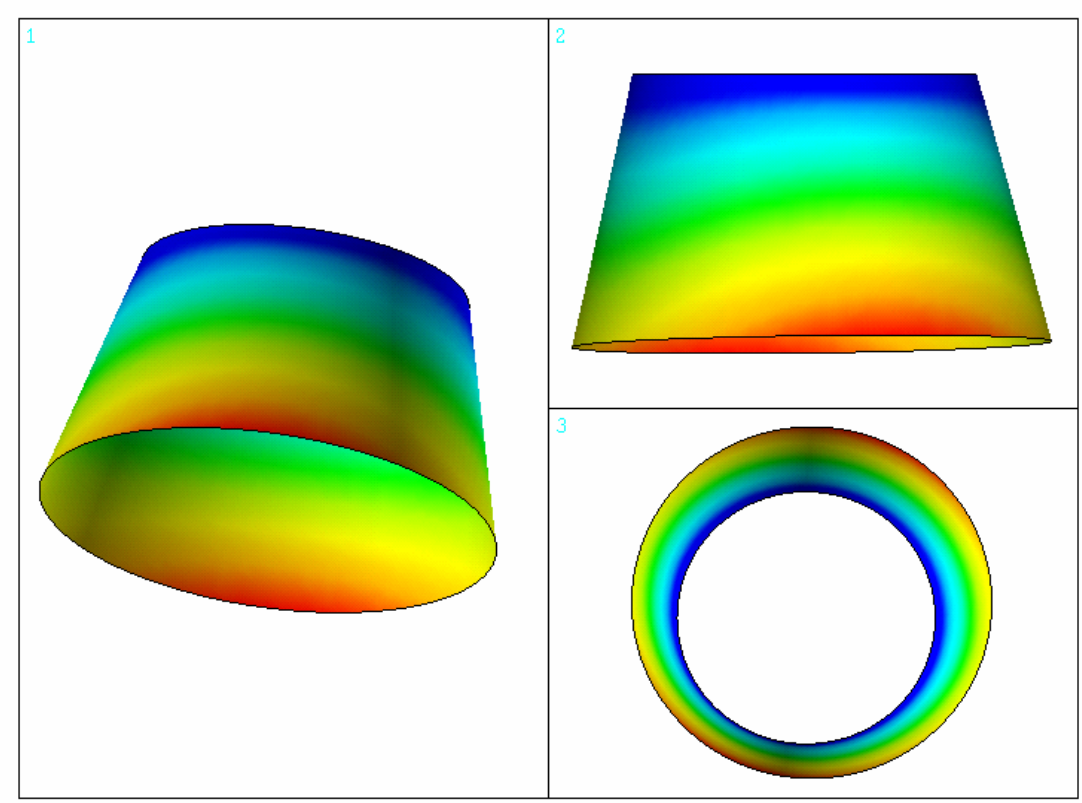

Figure A3.1 Clamped - free conical shell mode shape, f = 277.2 Hz, m = 1, n = 1

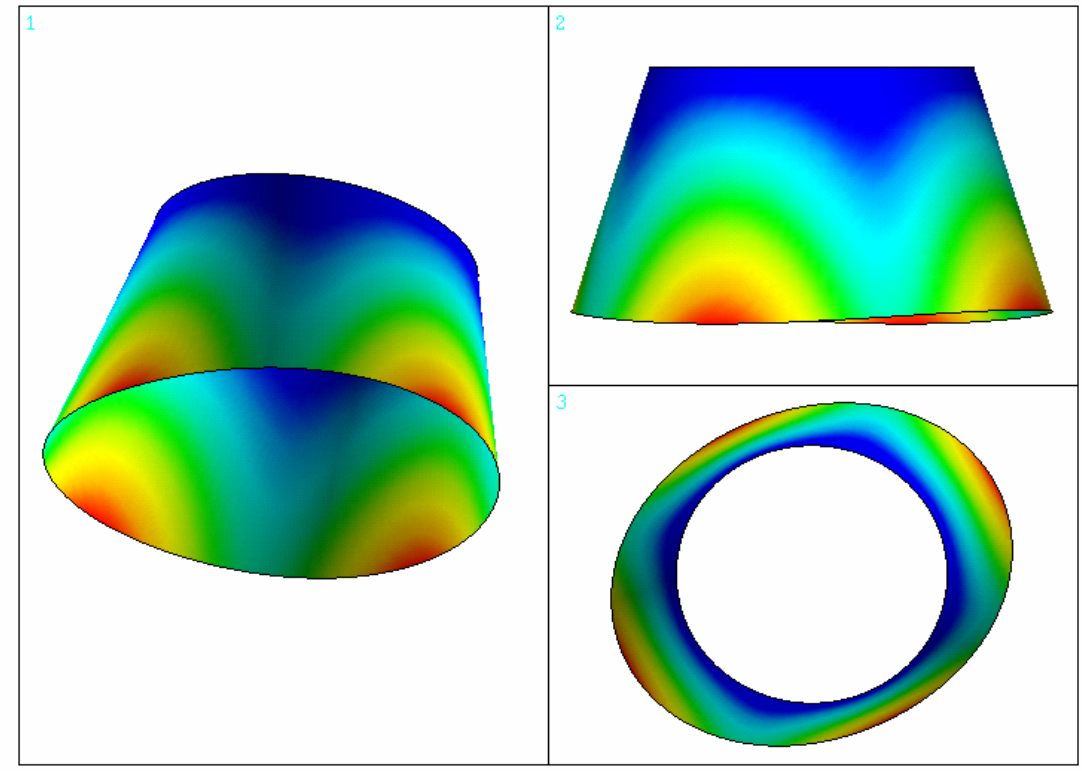

Figure A3.2 Clamped - free conical shell mode shape, f = 153.5 Hz, m = 1, n = 2

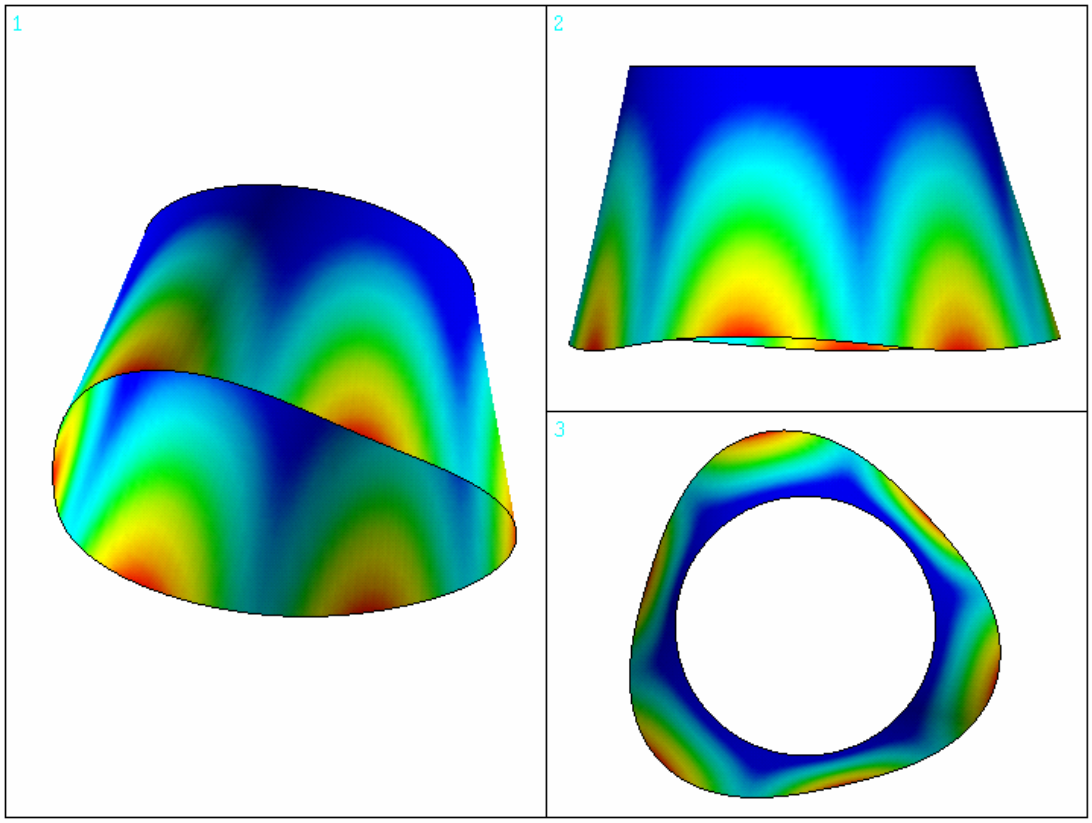

Figure A3.3 Clamped - free conical shell mode shape, f = 93.1 Hz, m = 1, n = 3

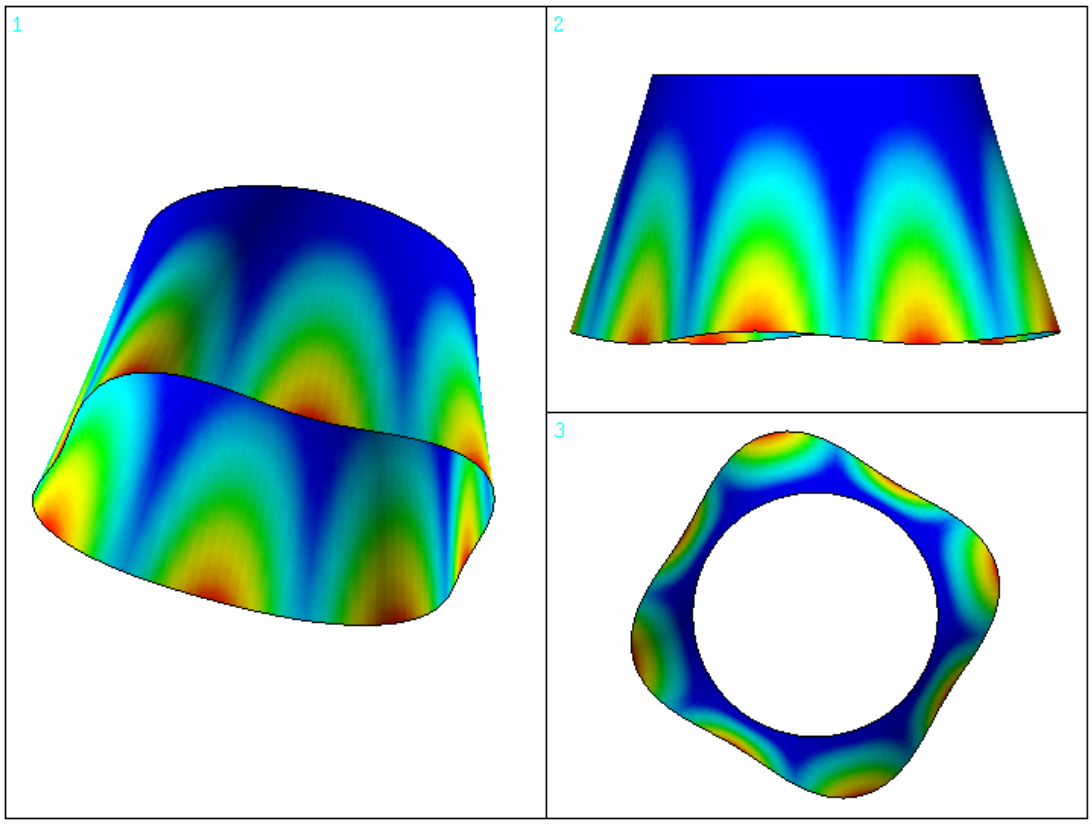

Figure A3.4 Clamped - free conical shell mode shape, f = 65.2 Hz, m = 1, n = 4

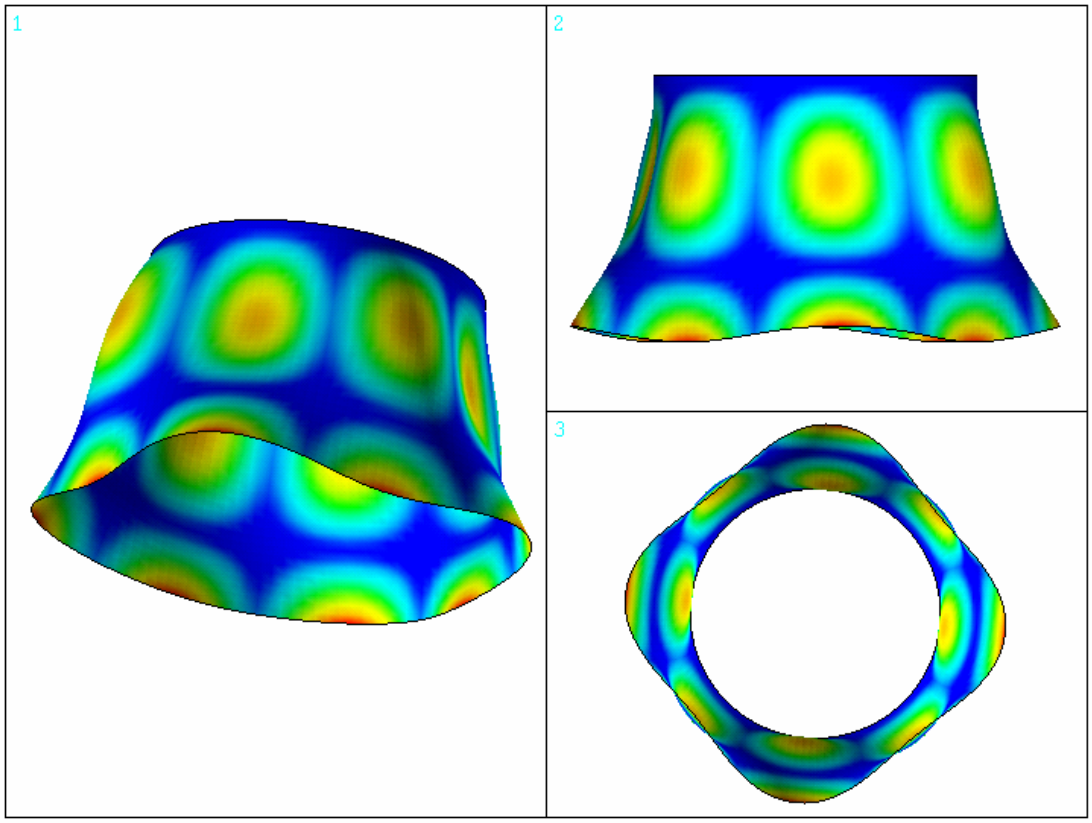

Figure A3.5 Clamped - free conical shell mode shape, f = 278.9 Hz, m = 2, n = 4

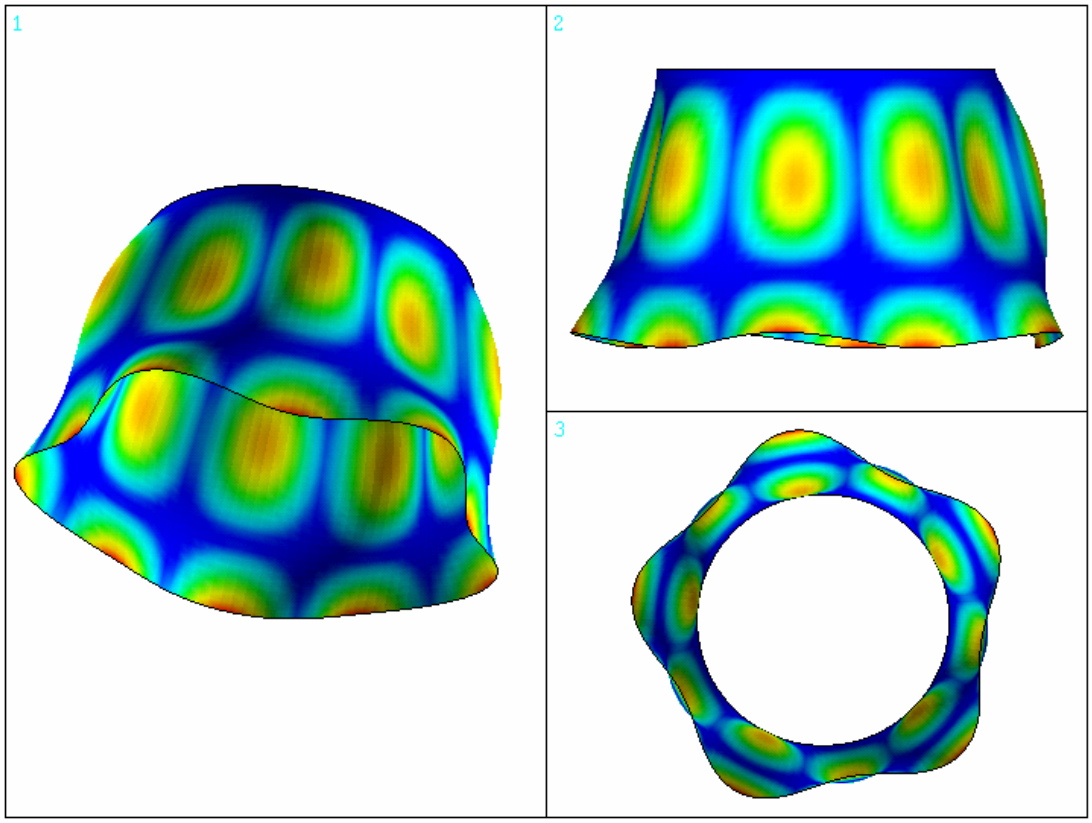

Figure A3.6 Clamped - free conical shell mode shape, f = 219.9 Hz, m = 2, n = 5

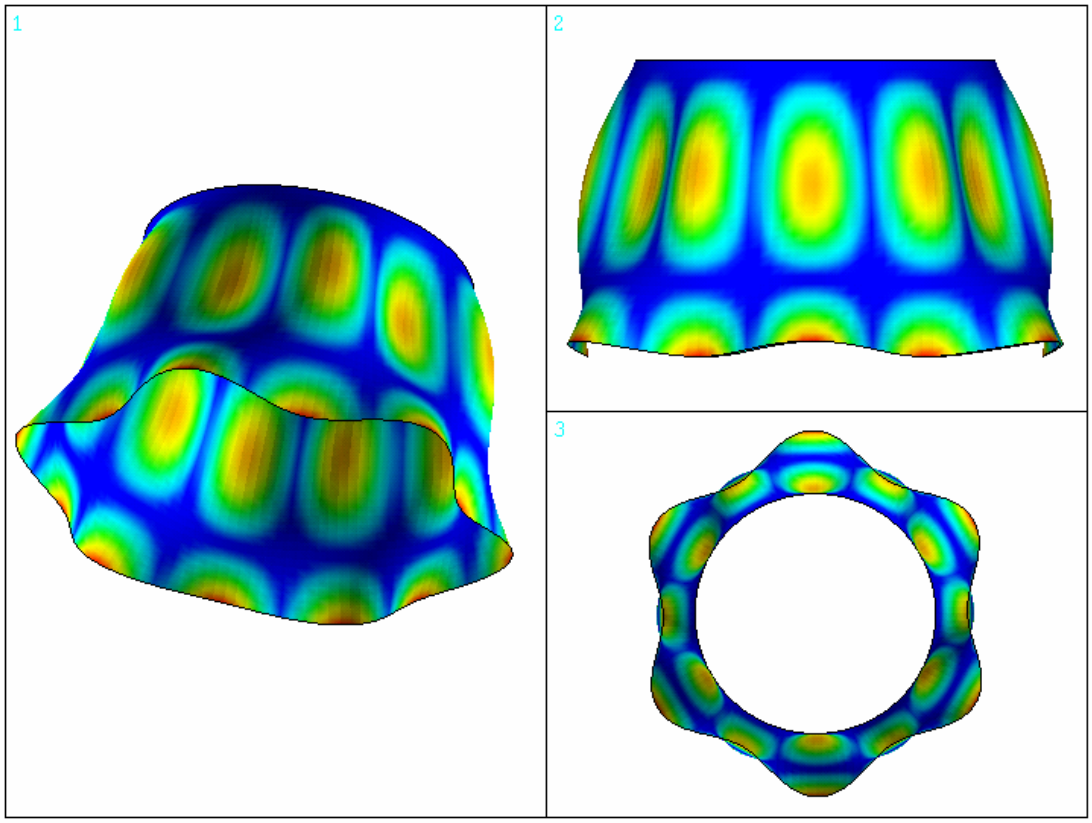

Figure A3.7 Clamped - free conical shell mode shape, f = 187.5 Hz, m = 2, n = 6

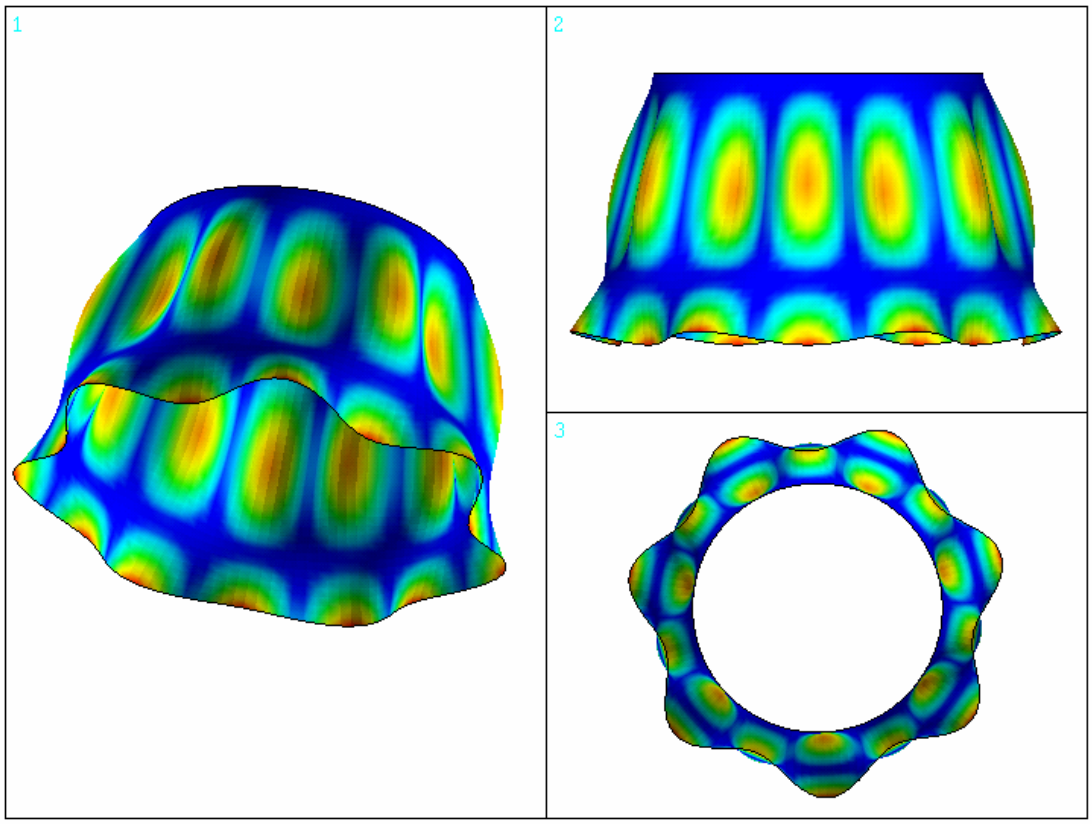

Figure A3.8 Clamped - free conical shell mode shape, f = 176.7 Hz, m = 2, n = 7

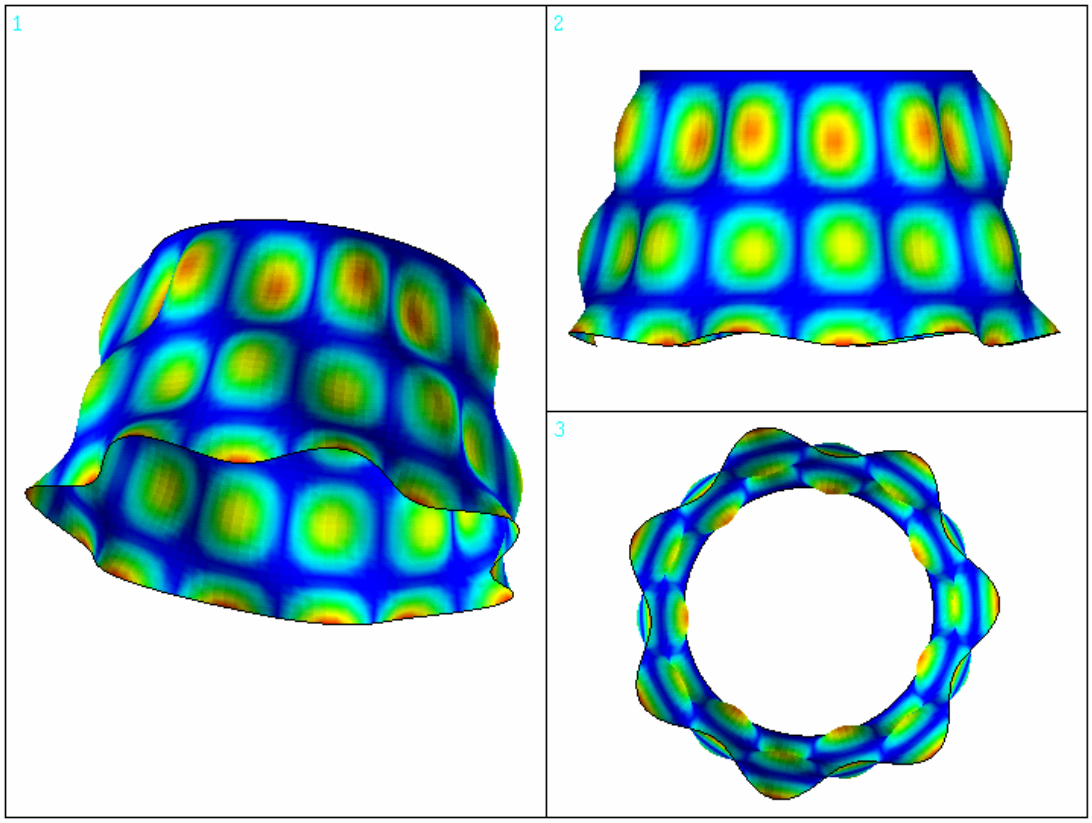

Figure A3.9 Clamped - free conical shell mode shape, f = 336.5 Hz, m = 3, n = 7

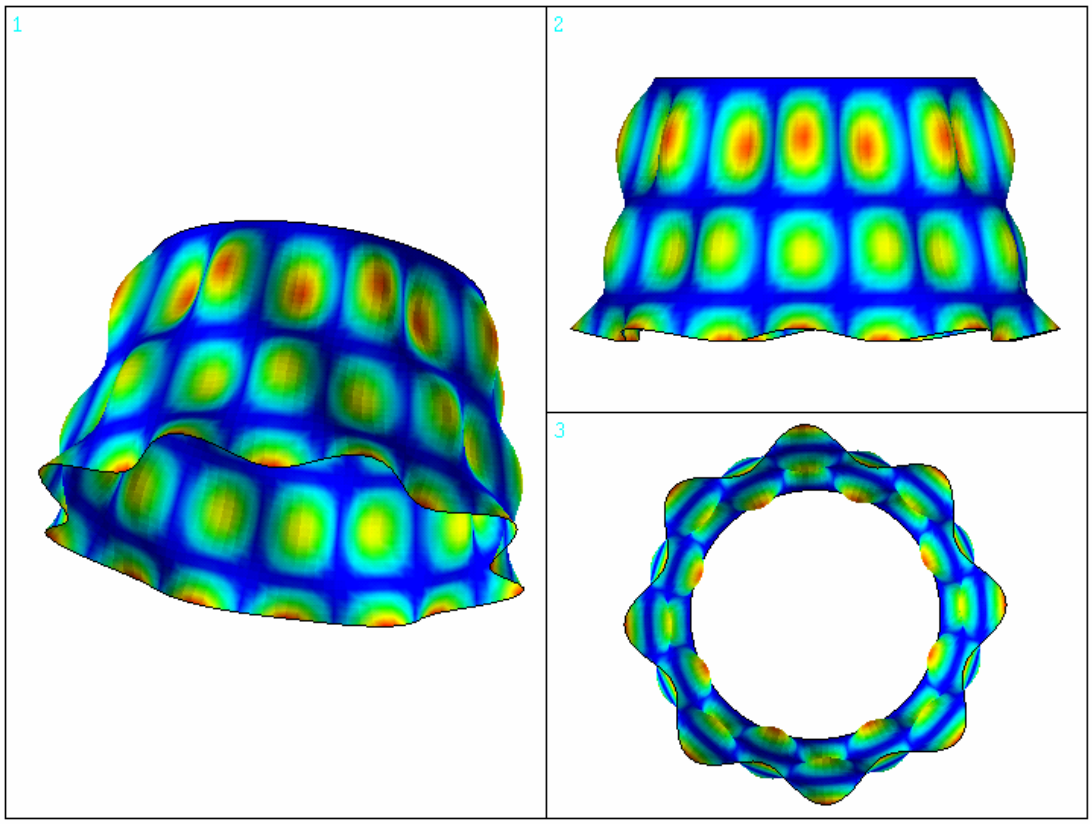

Figure A3.10 Clamped - free conical shell mode shape, f = 316.6 Hz, m = 3, n = 8

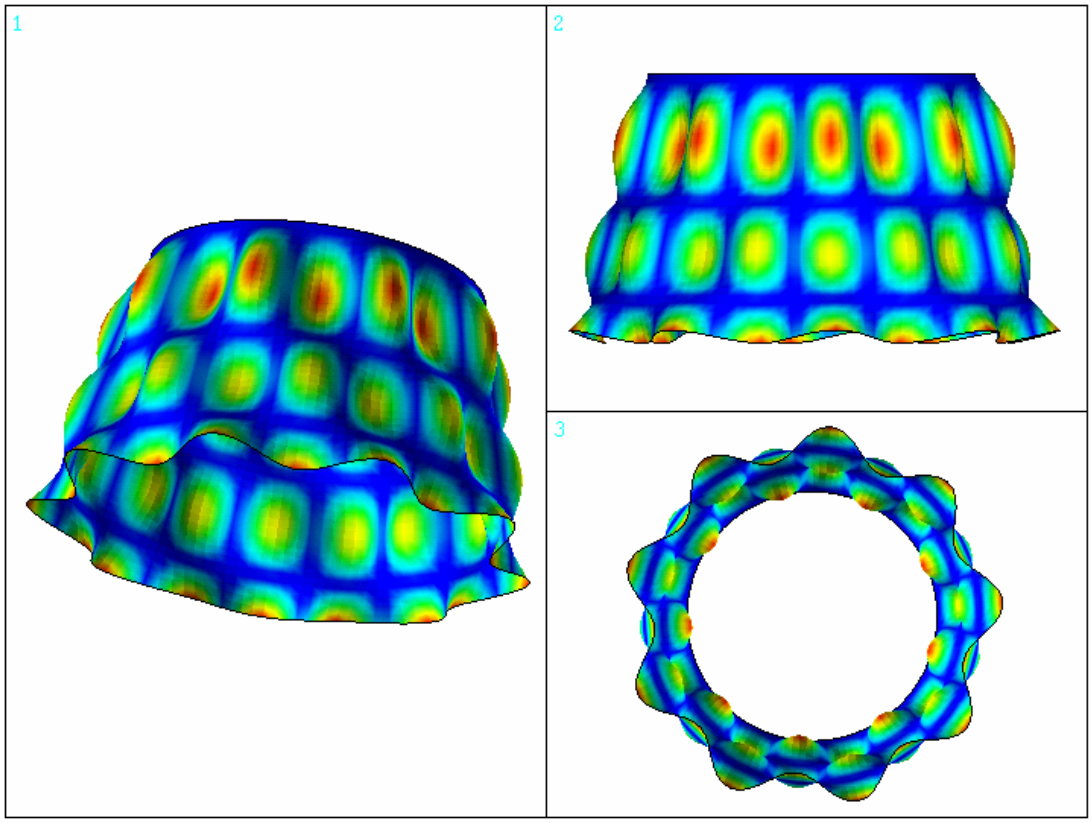

Figure A3.11 Clamped - free conical shell mode shape, f = 314.5 Hz, m = 3, n = 9

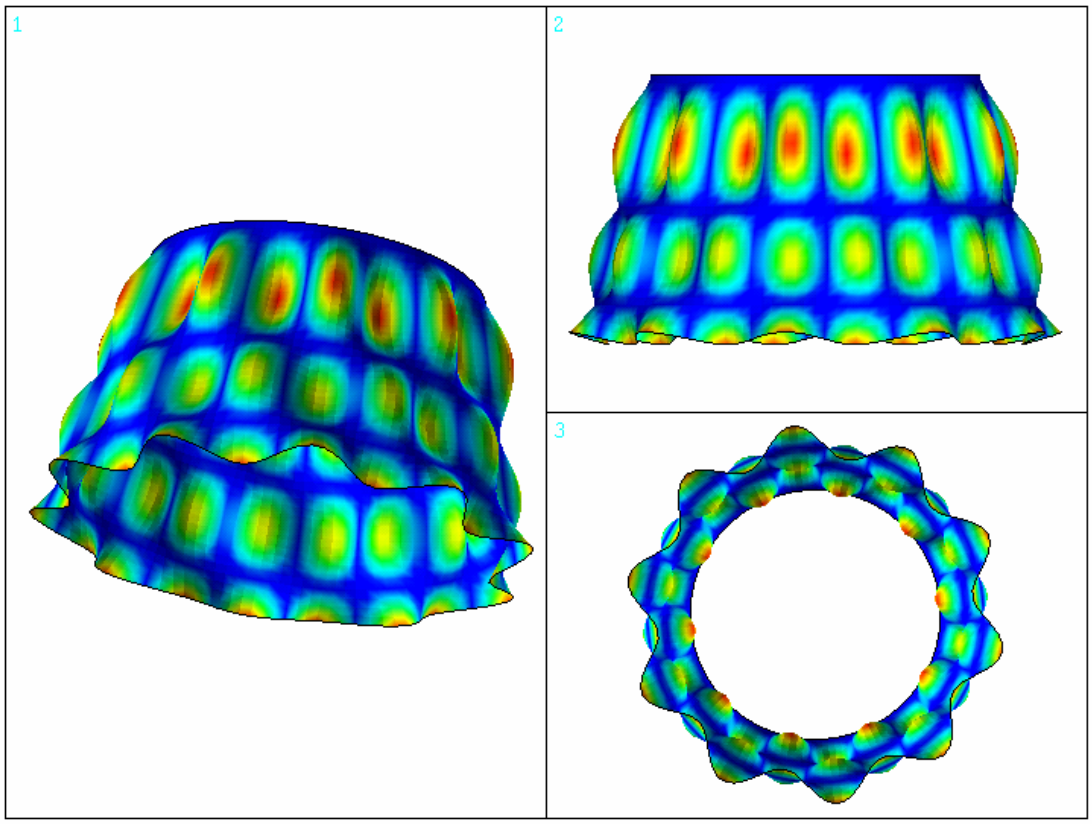

Figure A3.12 Clamped - free conical shell mode shape, f = 328.0 Hz, m = 3, n = 10

Appendix 4 Mathematica program

```
tstart = AbsoluteTime[ ];
Clear[s, B, X, a, b, f, nv, sr, ii, Plist, h, sr, Nr]

R1 = 0.25;
R2 = 1;
L = 1.5;
t = 0.01; (* Model input *)

q = 9; (* Number of unknowns in u,v,w Don' t change !! *)

Ec = 2.08 * 10^11;
ρc = 7850;
ν = 0.3;
Er = 2.08 * 10^11;
νr = 0.3;
ρr = 7850;
Gr = Er / (2 * (1 + νr)); (* Material data *)

α = ArcSin[(R2 - R1) / L];
H = L * Cos[α];
s1 = R1 / Sin[α];
s2 = Sqrt[H^2 + (R2 - R1)^2] + s1; (* Calculate model geometry *)

Nr = 10; (* Number of rings *)
nv = {1, 2, 3, 4, 5, 6, 7, 8, 9}; (* Wanted output *)

sr =
 Table[L / (2 * Nr) + i * L / Nr, {i, 0, Nr - 1}] + s1 ; (* Equaly spaced rings *)
hr = 0.015;   (* ring height, equaly dimensions *)
br = 0.00239; (* ring width, equaly dimensions *)

(*
 gt1 = 1;    (* Grade number for heigh distribution *)
 h1=0.018;   (* Starting height *)
 h2=0.034;   (* Ending height *)
 hr=Table[(h2-h1)/(Nr^gt1-1)*(i^gt1-1)+h1,{i,1,Nr}];

 gt2=1;      (* Grade number for position distribution *)
 d1=0.01*L; (* Starting position *)
 d2=L-0.02; (* Ending position *)
 sr=Table[(d2-d1)/(Nr^(1/gt2)-1)*(i^(1/gt2)-1)+d1,{i,1,Nr}]+s1
*)

C1 = Ec * t / (1 - ν^2);
D1 = Ec * t^3 / (12 * (1 - ν^2)); (* Calculate shell properties *)

sr = {}; (* No stiffeners *)
hr = {};
br = {};

Ar = hr * br;
cr = hr / 2 + t / 2;
Ir = br * hr ^3 / 12;
Jr = br ^3 * hr / 3 * (1 - 0.63 * (br / hr) + 0.052 * (br / hr) ^5);
MRR = Apply[Plus, (sr * Sin[α] + (hr / 2 + t / 2) * Cos[α]) * 2 * Pi * Ar * ρr];
MRS = Pi * (R2 * s2 - R1 * s1) * t * ρc;
ir = Sqrt[Ir / Ar] ;   (* Calculate stiffener properties *)

(* Printing input to calculation *)
StringForm["n = ``", NumberForm[nv, 4]]
StringForm["s1 = ``", NumberForm[s1, 4]]
StringForm["s2 = ``", NumberForm[s2, 4]]
StringForm["R1 = ``", NumberForm[R1, 4]]
StringForm["R2 = ``", NumberForm[R2, 4]]
StringForm["H = ``", NumberForm[H, 4]]
StringForm["L = ``", NumberForm[L, 4]]
StringForm["α = ``", NumberForm[α * 180 / Pi, 4]]
StringForm["sr = ``", NumberForm[sr, 4]]
StringForm["hr = ``", NumberForm[hr, 4]]
StringForm["br = ``", NumberForm[br, 4]]
StringForm["mc = ``", NumberForm[MRS, 4]]
StringForm["mr = ``", NumberForm[MRR, 4]]
```

```
(* Data used to perform first inegration
 u=(s-s1) * (B[1]/s^2 + B[2]/s + B[3]) * Sin[n*θ];
 v=(s-s1) * (B[4]/s^2 + B[5]/s + B[6]) * Cos[n*θ];
 w=(s-s1)^2 * (B[7]/s^3 + B[8]/s^2 + B[9]/s) * Sin[n*θ];

εs= D[u,s];
 εθ= u/s+D[v,θ]/(s*Sin[α])+w/(Tan[α]*s);
 εsθ=D[u,θ]/(s*Sin[α])+ D[v,s]-v/s;
 κs=-D[w,s,s];
 κθ=-D[w,s]/s-D[w,θ,θ]/(s^2*(Sin[α])^2);
 κsθ=-D[w,s,θ]/(s*Sin[α])+D[w,θ]/(s^2*Sin[α]);

e1 = Integrate[εs^2,{θ,0,2*Pi}]
e2 = Integrate[εθ^2,{θ,0,2*Pi}]
e3 = Integrate[εs*εθ,{θ,0,2*Pi}]
 e4 = Integrate[εsθ^2,{θ,0,2*Pi}]
e5 = Integrate[εθ*κθ,{θ,0,2*Pi}]
k1 = Integrate[κs^2,{θ,0,2*Pi}]
k2 = Integrate[κθ^2,{θ,0,2*Pi}]
k3 = Integrate[κθ*κs,{θ,0,2*Pi}]
 k4 = Integrate[κsθ^2,{θ,0,2*Pi}]
 g1 = Integrate[u^2,{θ,0,2*Pi}]
g2 = Integrate[v^2,{θ,0,2*Pi}]
g3 = Integrate[w^2,{θ,0,2*Pi}]
*)

For[ii = 1, ii <= Length[nv], ii++,
Clear[g1, g2, g3, e2, e5, k2, k4, UR, TR, s, T, U];
n = Part[nv, ii];
```

$$e1 = -\frac{1}{4\,n\,s^6}\left((-s\,B[1] + 2\,s1\,B[1] + s\,s1\,B[2] + s^3\,B[3])^2\,(-4\,n\,\pi + \text{Sin}[4\,n\,\pi])\right);$$

$$e2[s\_] := -\frac{1}{4\,n\,s^8}\,((s - s1)^2\,\text{Csc}[\alpha]^2 (-4\,n\,\pi + \text{Sin}[4\,n\,\pi])\,((s - s1)\,(B[7] + s\,(B[8] + s\,B[9]))\,\text{Cos}[\alpha] + s\,(-n\,(B[4] + s\,B[5] + s^2\,B[6]) + (B[1] + s\,B[2] + s^2\,B[3])\,\text{Sin}[\alpha]))^2);$$

$$e3 = -\frac{1}{4\,n\,s^7}\,((s - s1)\,(-s\,B[1] + 2\,s1\,B[1] + s\,s1\,B[2] + s^3\,B[3])\,\text{Csc}[\alpha] (-4\,n\,\pi + \text{Sin}[4\,n\,\pi])\,((s - s1)\,(B[7] + s\,(B[8] + s\,B[9]))\,\text{Cos}[\alpha] + s\,(-n\,(B[4] + s\,B[5] + s^2\,B[6]) + (B[1] + s\,B[2] + s^2\,B[3])\,\text{Sin}[\alpha])));$$

$$e4 = \frac{1}{4\,n\,s^6}\,((3\,s1\,B[4] - 2\,s\,(B[4] - s1\,B[5]) + s^2\,(-B[5] + s1\,B[6]) + n\,(s - s1)\,(B[1] + s\,(B[2] + s\,B[3]))\,\text{Csc}[\alpha])^2 (4\,n\,\pi + \text{Sin}[4\,n\,\pi]));$$

$$e5[s\_] := -\frac{1}{4\,n\,s^2}\left((s - s1)^3\left(\frac{B[1]}{s^2} + \frac{B[2]}{s} + B[3]\right)\left(-\frac{3\,B[7]}{s^4} - \frac{2\,B[8]}{s^3} - \frac{B[9]}{s^2}\right)(4\,n\,\pi - \text{Sin}[4\,n\,\pi])\right) - \frac{1}{2\,n\,s^2}\left((s - s1)^2\left(\frac{B[1]}{s^2} + \frac{B[2]}{s} + B[3]\right)\left(\frac{B[7]}{s^3} + \frac{B[8]}{s^2} + \frac{B[9]}{s}\right)(4\,n\,\pi - \text{Sin}[4\,n\,\pi])\right) - \frac{1}{4\,n\,s^2}\left((s - s1)^4\left(-\frac{3\,B[7]}{s^4} - \frac{2\,B[8]}{s^3} - \frac{B[9]}{s^2}\right)\left(\frac{B[7]}{s^3} + \frac{B[8]}{s^2} + \frac{B[9]}{s}\right)\text{Cot}[\alpha]\,(4\,n\,\pi - \text{Sin}[4\,n\,\pi])\right) - \frac{1}{2\,n\,s^2}\left((s - s1)^3\left(\frac{B[7]}{s^3} + \frac{B[8]}{s^2} + \frac{B[9]}{s}\right)^2\text{Cot}[\alpha]\,(4\,n\,\pi - \text{Sin}[4\,n\,\pi])\right) +$$

$$\frac{1}{4 s^2}\left((s-s1)^3\left(\frac{B[4]}{s^2}+\frac{B[5]}{s}+B[6]\right)\left(-\frac{3 B[7]}{s^4}-\frac{2 B[8]}{s^3}-\frac{B[9]}{s^2}\right)\text{Csc}[\alpha]\,(4 n\pi-\text{Sin}[4 n\pi])\right)+$$
$$\frac{1}{2 s^2}\left((s-s1)^2\left(\frac{B[4]}{s^2}+\frac{B[5]}{s}+B[6]\right)\left(\frac{B[7]}{s^3}+\frac{B[8]}{s^2}+\frac{B[9]}{s}\right)\text{Csc}[\alpha]\,(4 n\pi-\text{Sin}[4 n\pi])\right)+$$
$$\frac{1}{4 s^3}\left(n\,(s-s1)^3\left(\frac{B[1]}{s^2}+\frac{B[2]}{s}+B[3]\right)\left(\frac{B[7]}{s^3}+\frac{B[8]}{s^2}+\frac{B[9]}{s}\right)\text{Csc}[\alpha]^2\,(4 n\pi-\text{Sin}[4 n\pi])\right)+\frac{1}{4 s^3}$$
$$\left(n\,(s-s1)^4\left(\frac{B[7]}{s^3}+\frac{B[8]}{s^2}+\frac{B[9]}{s}\right)^2\text{Cot}[\alpha]\,\text{Csc}[\alpha]^2\,(4 n\pi-\text{Sin}[4 n\pi])\right)-$$
$$\frac{1}{4 s^3}\left(n^2\,(s-s1)^3\left(\frac{B[4]}{s^2}+\frac{B[5]}{s}+B[6]\right)\left(\frac{B[7]}{s^3}+\frac{B[8]}{s^2}+\frac{B[9]}{s}\right)\text{Csc}[\alpha]^3\,(4 n\pi-\text{Sin}[4 n\pi])\right);$$

$$k1=-\frac{1}{n s^{10}}((6 s1^2 B[7]+3 s s1 (-2 B[7]+s1 B[8])+s^2 (B[7]+s1 (-2 B[8]+s1 B[9])))^2 (-4 n\pi+\text{Sin}[4 n\pi]));$$

$$k2[s\_]:=-\frac{1}{16 n s^{10}}((s-s1)^2 (-(3+2 n^2) s1 B[7]+s (B[7]+2 n^2 B[7]-2 s1 B[8]-2 n^2 s1 B[8])+(-1+2 n^2) s^3 B[9]+s^2 (2 n^2 B[8]-s1 B[9]-2 n^2 s1 B[9])+(-s B[7]+3 s1 B[7]+2 s s1 B[8]+s^3 B[9]+s^2 s1 B[9])\text{Cos}[2\alpha])^2 \text{Csc}[\alpha]^4 (-4 n\pi+\text{Sin}[4 n\pi]));$$

$$k3=\frac{1}{4 n s^{10}}((s-s1)(6 s1^2 B[7]+3 s s1 (-2 B[7]+s1 B[8])+s^2 (B[7]+s1 (-2 B[8]+s1 B[9])))(-(3+2 n^2) s1 B[7]+s (B[7]+2 n^2 B[7]-2 s1 B[8]-2 n^2 s1 B[8])+(-1+2 n^2) s^3 B[9]+s^2 (2 n^2 B[8]-s1 B[9]-2 n^2 s1 B[9])+(-s B[7]+3 s1 B[7]+2 s s1 B[8]+s^3 B[9]+s^2 s1 B[9])\text{Cos}[2\alpha])\text{Csc}[\alpha]^2 (-4 n\pi+\text{Sin}[4 n\pi]));$$

$$k4[s\_]:=\frac{1}{4 s^{10}}(n\,(s-s1)^2 (4 s1 B[7]+s (-2 B[7]+3 s1 B[8])-s^2 (B[8]-2 s1 B[9]))^2 \text{Csc}[\alpha]^2 (4 n\pi+\text{Sin}[4 n\pi]));$$

$$g1[s\_]:=-\frac{1}{4 n s^4}((s-s1)^2 (B[1]+s (B[2]+s B[3]))^2 (-4 n\pi+\text{Sin}[4 n\pi]));$$

$$g2[s\_]:=\frac{(s-s1)^2 (B[4]+s (B[5]+s B[6]))^2 (4 n\pi+\text{Sin}[4 n\pi])}{4 n s^4};$$

$$g3[s\_]:=-\frac{1}{4 n s^6}((s-s1)^4 (B[7]+s (B[8]+s B[9]))^2 (-4 n\pi+\text{Sin}[4 n\pi]));$$

```
(* Shell energy *)
Uc = 0.5 * Sin[α] * s * (C1 * (e1 + e2[s] + 2 * ν * e3 + 0.5 * (1 - ν) * e4) +
     D1 * (k1 + k2[s] + 2 * ν * k3 + 2 * (1 - ν) * k4[s]));
Tc = 0.5 * Sin[α] * s * ρc * t * (g1[s] + g2[s] + g3[s]);

(* Stiffener energy *)
```

```
UR = 0.5 * Sin[α] * (Er * Ar *
      (e2[sr] - 2 * cr * e5[sr] + (ir ^ 2 + cr ^ 2) * k2[sr]) + Gr * Jr * k4[sr]) * sr;
TR = 0.5 * Sin[α] * ρr * Ar * (g1[sr] + g2[sr] + g3[sr]) * sr;

(* Total energy *)
U = Integrate[Uc, {s, s1, s2}] + Apply[Plus, UR];
T = X * Integrate[Tc, {s, s1, s2}] + X * Apply[Plus, TR];

For[i = 1, i <= q, i++, b[i] = D[T - U, B[i]]];
For[j = 1, j <= q, j++,
For[i = 1, i <= q, i++, a[i + (j - 1) * q] = Coefficient[b[j], B[i]]]
];

(* Building matrix *)
lhs = {Table[a[i], {i, q}], Table[a[i + q], {i, q}], Table[a[i + 2 * q], {i, q}]
, Table[a[i + 3 * q], {i, q}],
   Table[a[i + 4 * q], {i, q}], Table[a[i + 5 * q], {i, q}],
Table[a[i + 6 * q], {i, q}],
   Table[a[i + 7 * q], {i, q}], Table[a[i + 8 * q], {i, q}]};

(* Solve[{Det[lhs]==0}] *)
ω = Sqrt[Root[Det[lhs], 1]]; (* Solution to problem *)
f[ii] = ω / (2 * Pi);
Print[f[ii]];
]; (* End For *)

Plist = Table[{Part[nv, i], f[i]}, {i, Length[nv]}];
TableForm[Plist, TableHeadings -> {None, {"n", "f [Hz] "}}]
tused = AbsoluteTime[ ] - tstart (* Evaluation time in seconds *)
```

$n = \{1, 2, 3, 4, 5, 6, 7, 8, 9\}$

$s1 = 0.5$

$s2 = 2.$

$R1 = 0.25$

$R2 = 1$

$H = 1.299$

$L = 1.5$

$\alpha = 30.$

$s_r = \{\}$

$h_r = \{\}$

$b_r = \{\}$

$m_c = 462.4$

$m_r = 0$

103.759

48.8613

41.7304

60.0352

86.0329

118.409

157.497

202.681

253.651

n	f [Hz]
1	103.759
2	48.8613
3	41.7304
4	60.0352
5	86.0329
6	118.409
7	157.497
8	202.681
9	253.651

75.00000

```
Plist = Table[{Part[nv, i], f[i]}, {i, Length[nv]}];
ListPlot[Plist, PlotJoined -> True, AxesOrigin -> {0, 0}];
```

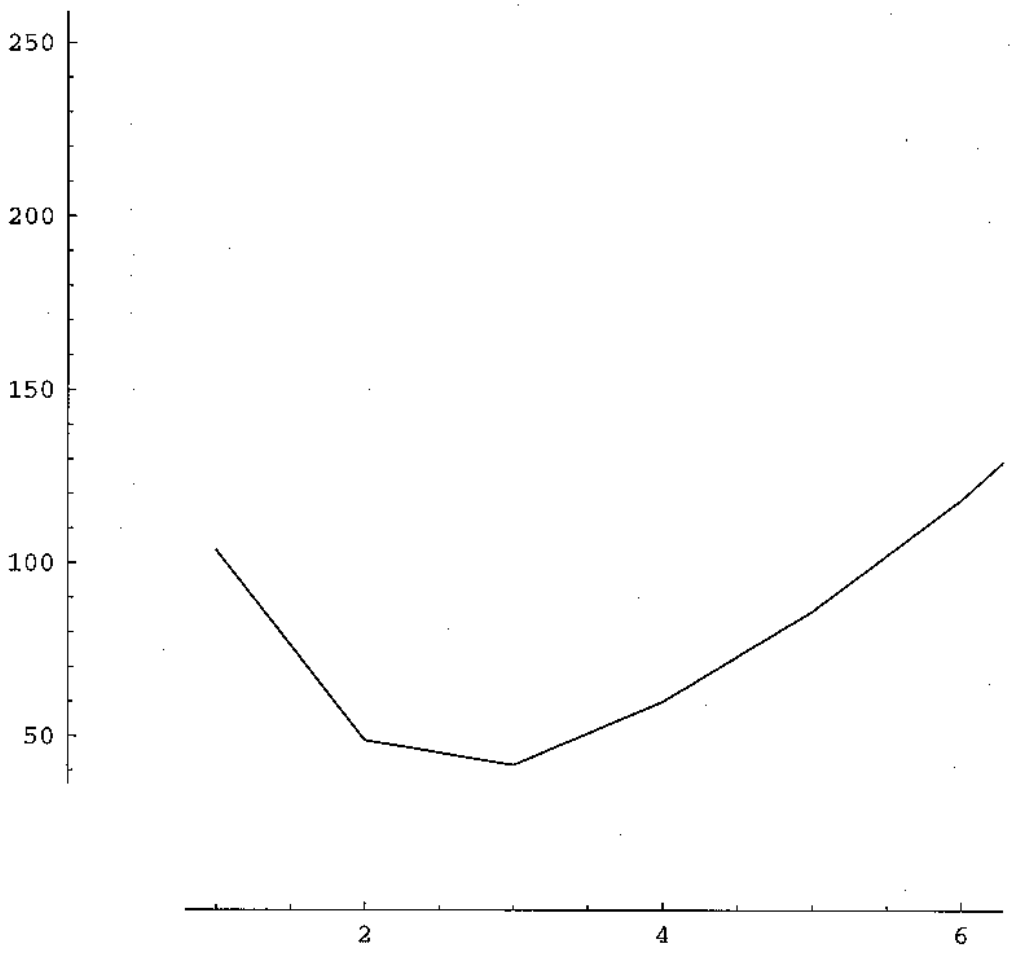

Appendix 5 ANSYS input file - Conical shell

```
/BATCH,LIST
! ******************************************************
! * File for analysing free vibration of a conical shell  *
! * Made by J Bäcklund 980814                             *
! *                                                        *
! ******************************************************
! ##### Units in [N] & [m] ######################################

/TITLE, Free vibration analysis of clamped-free conical shell
/PREP7

! ***** Parameters ********************************
R1 = 0.25  $ R2 = 1
alfa = 30*Pi/180
H = (R2-R1)/TAN(alfa) $ T = 0.01

divR = 8   ! *4 = Number of elements in circumferential direction
divS = 16  ! = Number of elements in meridional direction

!***** Material property
**********************************************
mp,ex,1,2.08e11
mp,dens,1,7850
mp,nuxy,1,0.3

! ***** Define element ******************************
ET,1,SHELL93

! ***** Define Real-constants *****************
R,1,T                 !Thickness of Shell

! ***** Create cone ****************************
CSYS,0
K,1,0,0,0
K,2,0,0,H
K,3,R1,0,0
K,4,R2,0,H
L,3,4
LESIZE,1,,,divS

! ***** Create areas of lines **********************!
AROTAT,1,,,,,,1,2,,,
NUMMRG,KP

CSYS,1
LSEL,S,LOC,z,0
LSEL,A,LOC,z,H
LESIZE,ALL,,,divR

! ***** Mesh *************************
TYPE,1                          !Activates Etype 1
REAL,1
MAT,1
AMESH,1,4

ALLSEL
NUMMRG,NODE

! ***** Boundary conditions ********************************
CSYS,1
NSEL,S,LOC,z,0
```

```
NROTAT,ALL
D,ALL,UX,0.0,,,,UY,UZ,ROTY
NSEL,ALL
FINISH

! ***** Solution ********************************
/SOLU
ANTYPE,modal
MODOPT,subsp,30
SAVE
SOLVE
FINISH

/SOLU
expass,on
mxpand,30,,,yes
solve
finish
```

Appendix 6 Subscale nozzle - Selected mode shapes

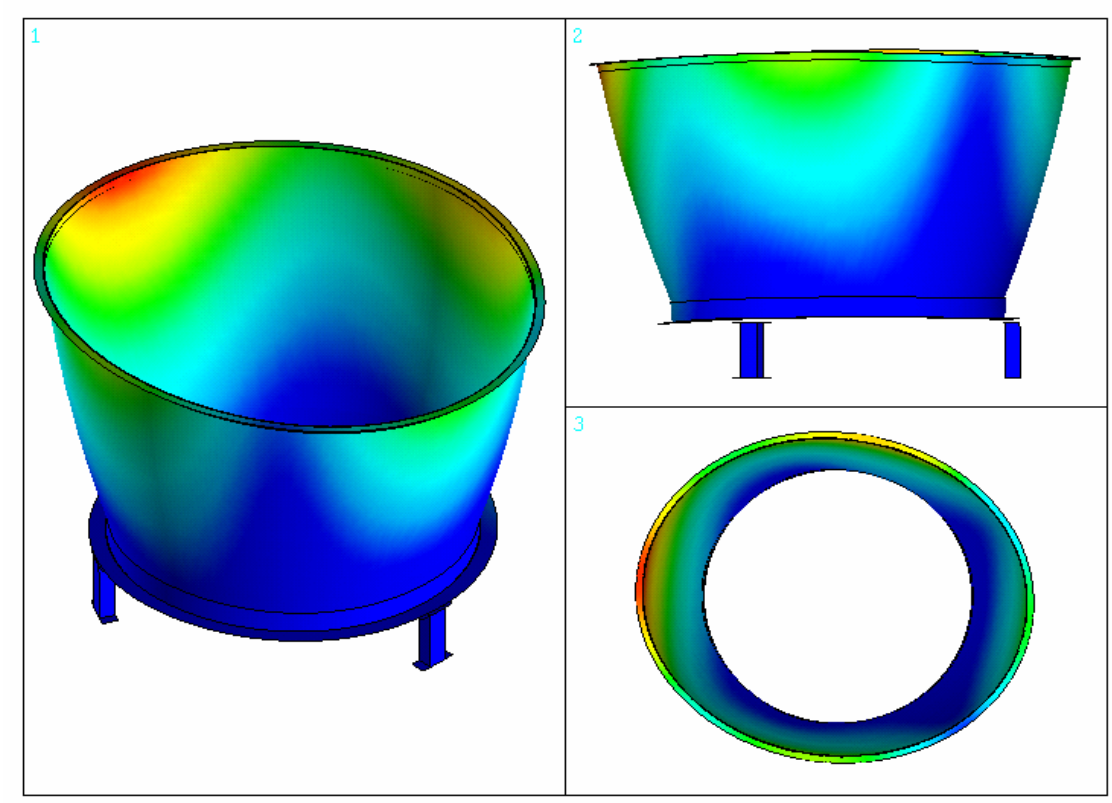

Figure A6.1 Subscale nozzle mode shape, f = 64.6 Hz, m = 1, n = 2

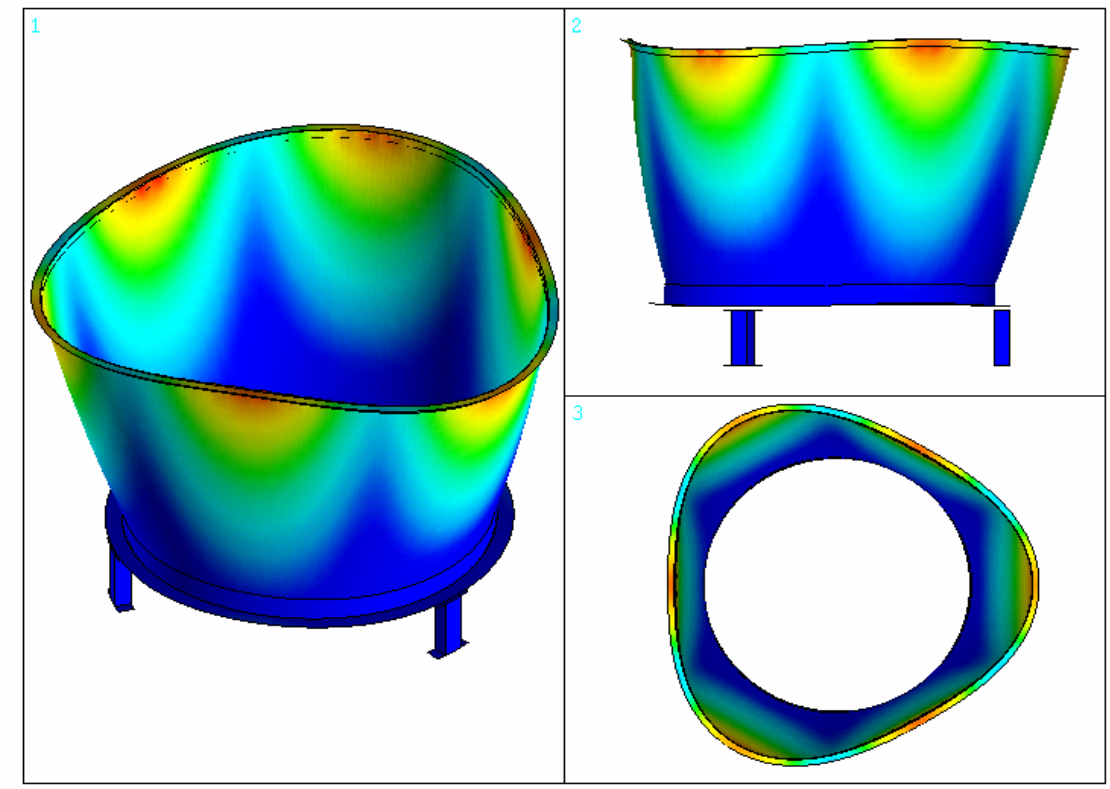

Figure A6.2 Subscale nozzle mode shape, f = 92.2 Hz, m = 1, n = 3

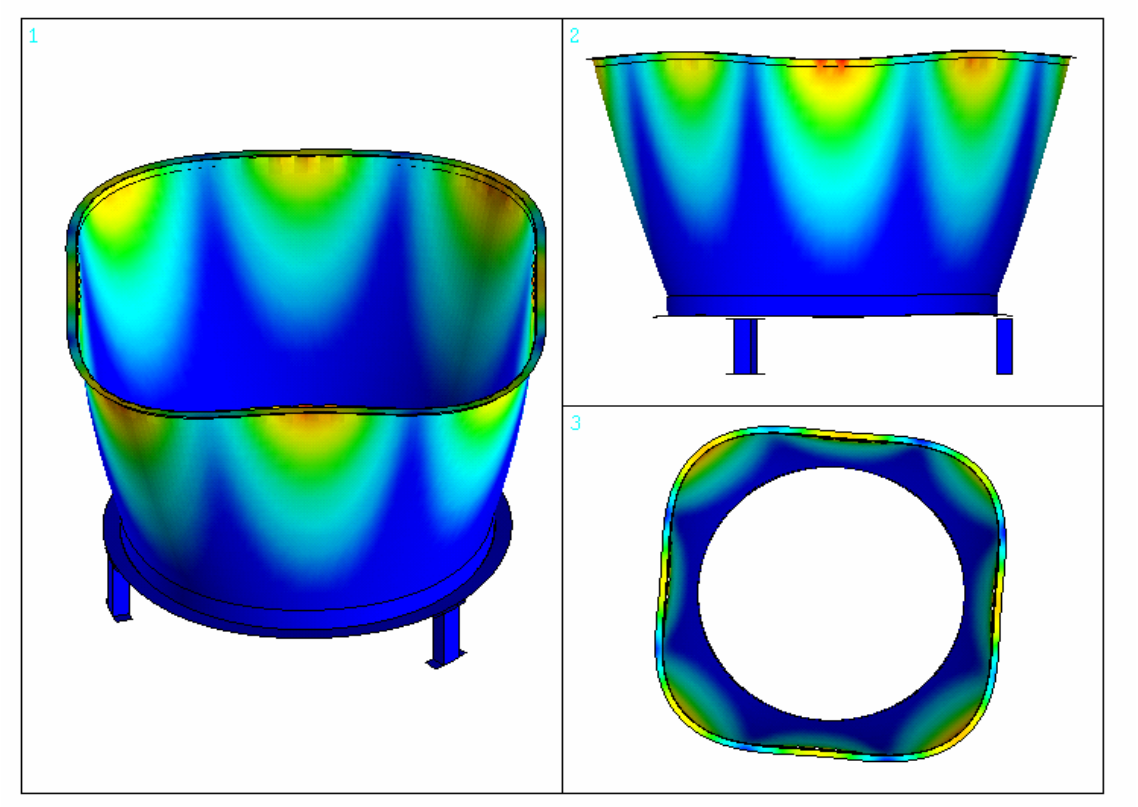

Figure A6.3 Subscale nozzle mode shape, f = 166.1 Hz, m = 1, n = 4

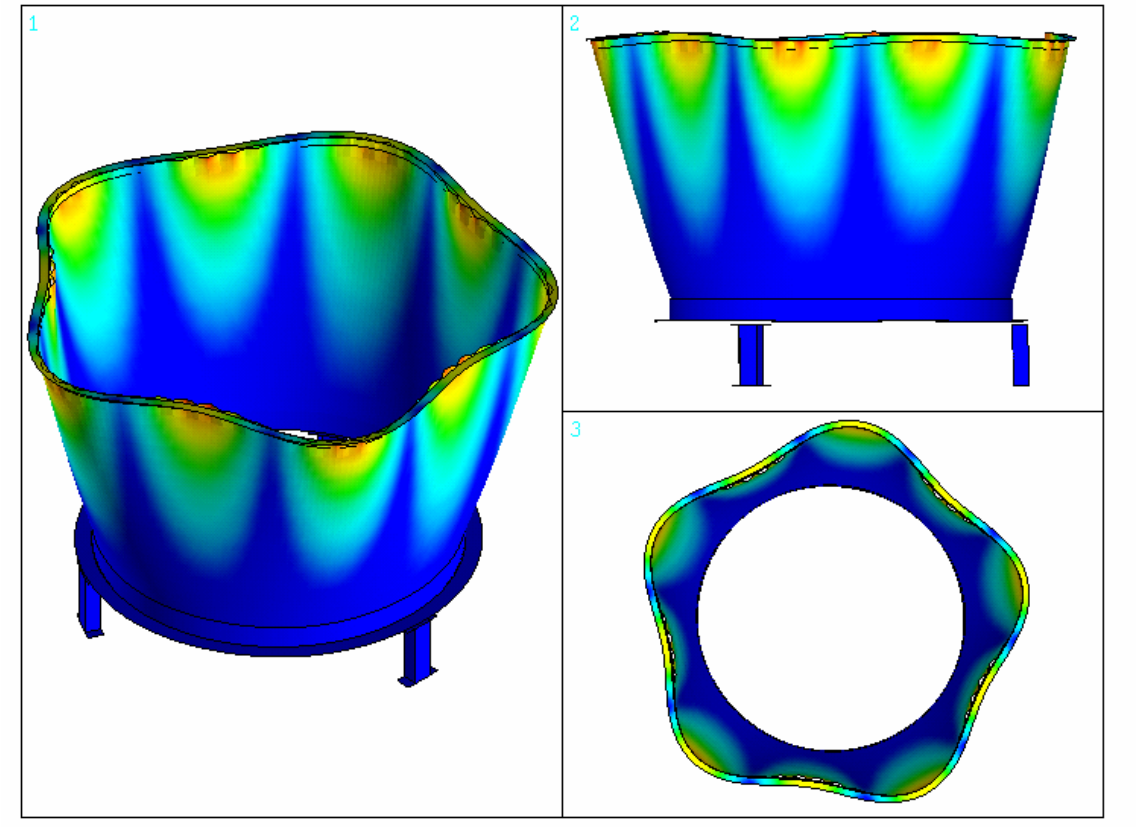

Figure A6.4 Subscale nozzle mode shape, f = 262.5 Hz, m = 1, n = 5

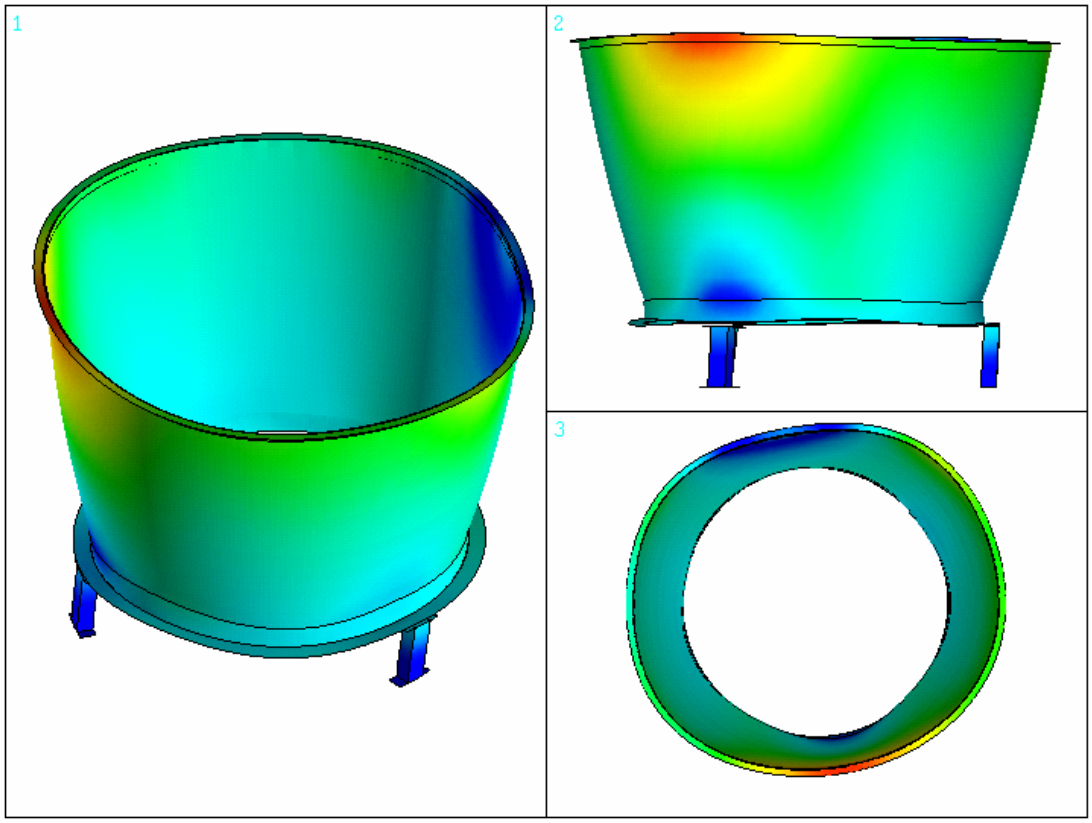

Figure A6.5 Subscale nozzle mode shape, f = 196.4 Hz, non-classified

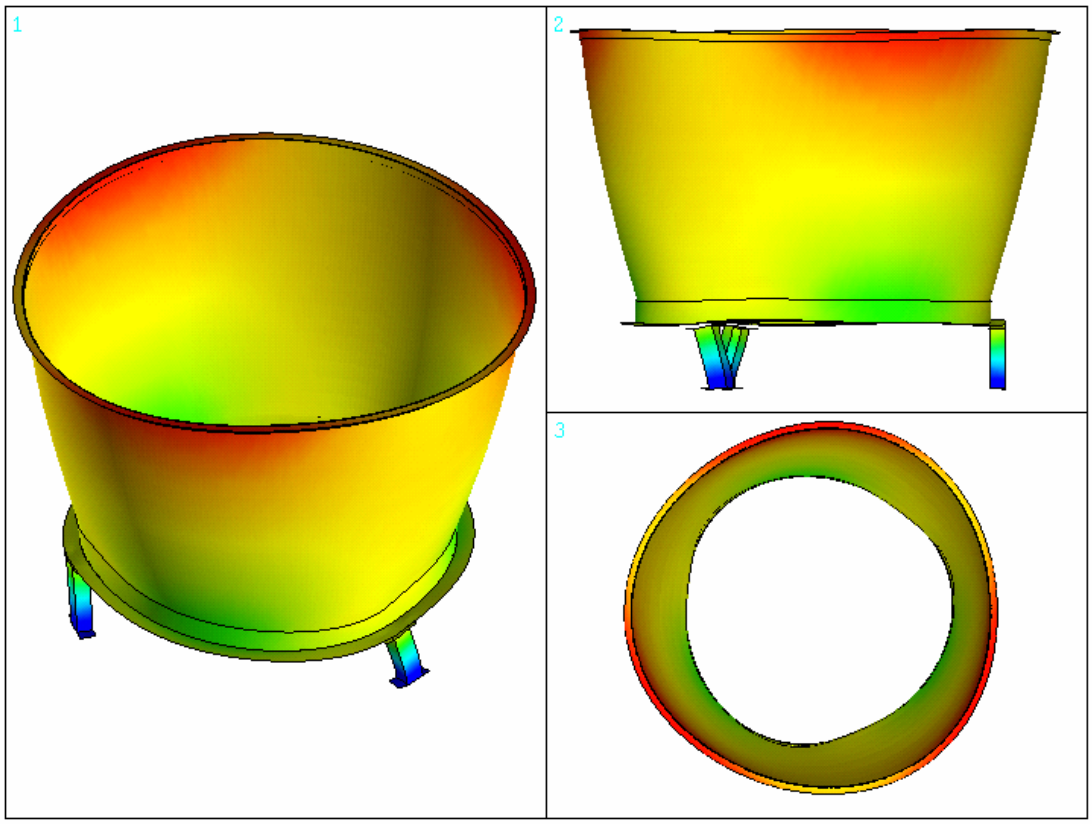

Figure A6.6 Subscale nozzle mode shape, f = 242.3 Hz, non-classified

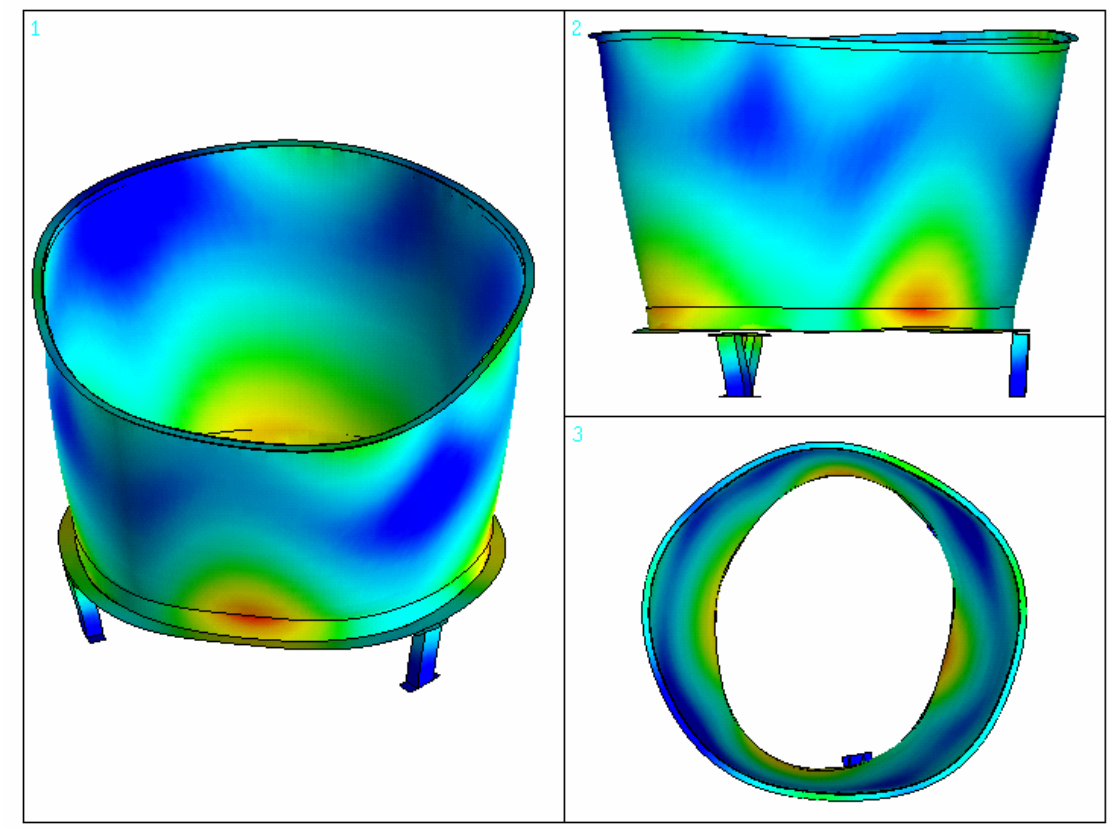

Figure A6.7 Subscale nozzle mode shape, f = 284.0 Hz, non-classified

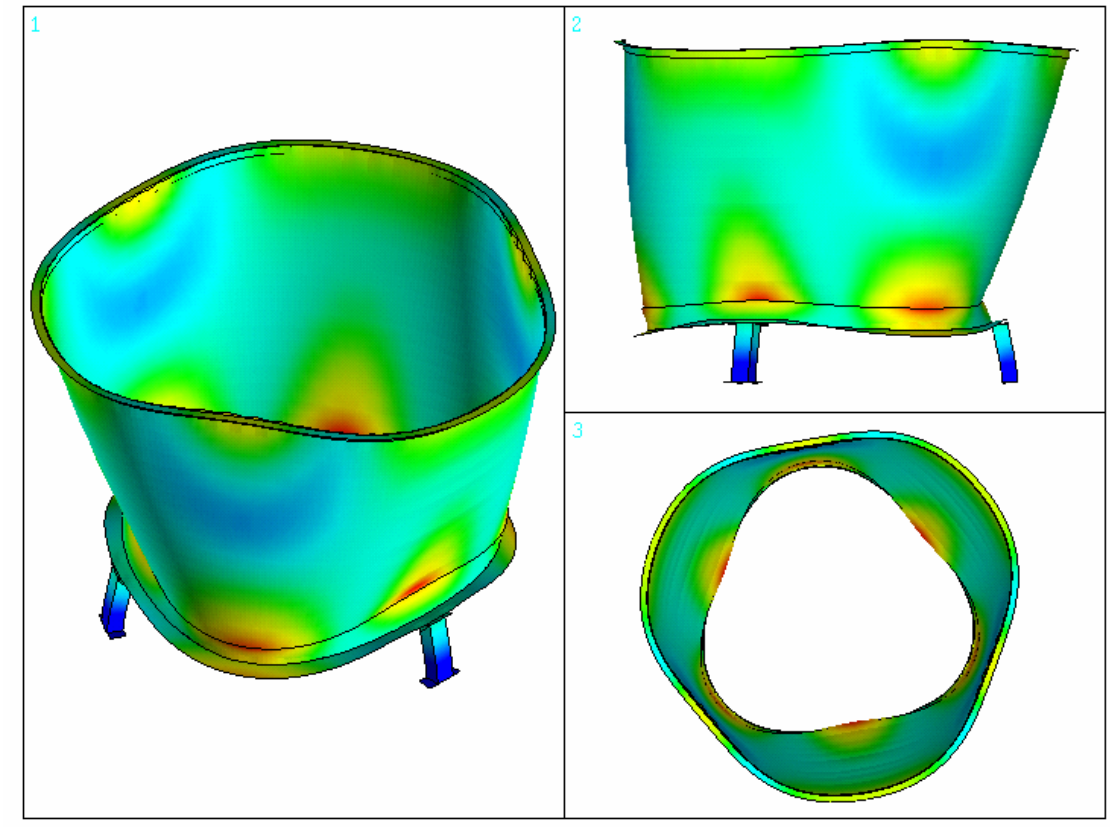

Figure A6.8 Subscale nozzle mode shape, f = 332.4 Hz, non-classified

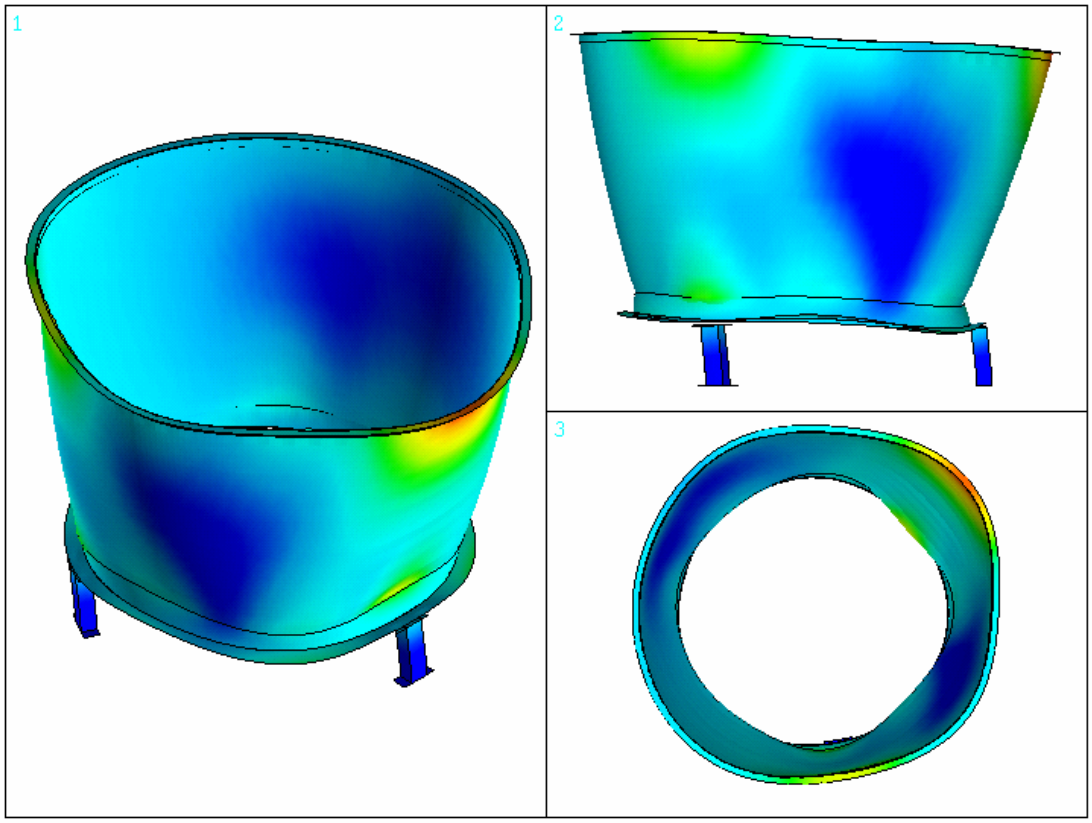

Figure A6.9 Subscale nozzle mode shape, f = 338.9 Hz, non-classified

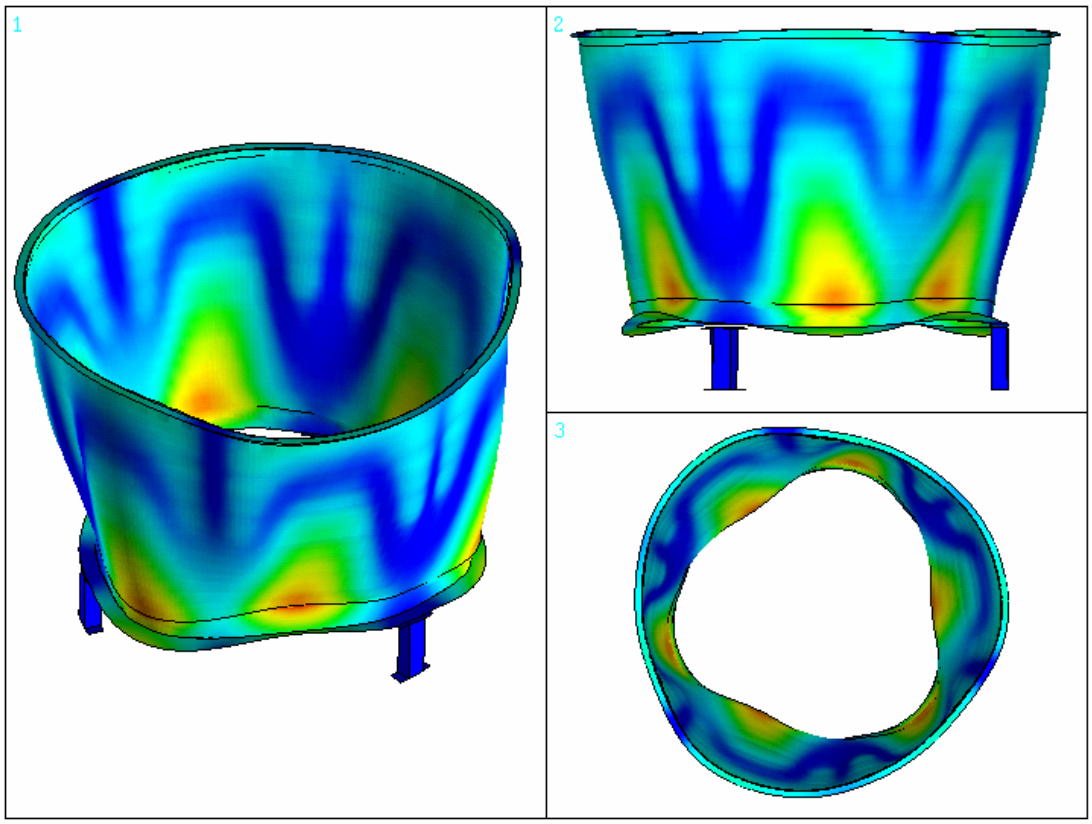

Figure A6.10 Subscale nozzle mode shape, f = 446.2 Hz, non-classified

Appendix 7 Vulcain 2 NE skirt - Selected mode shapes

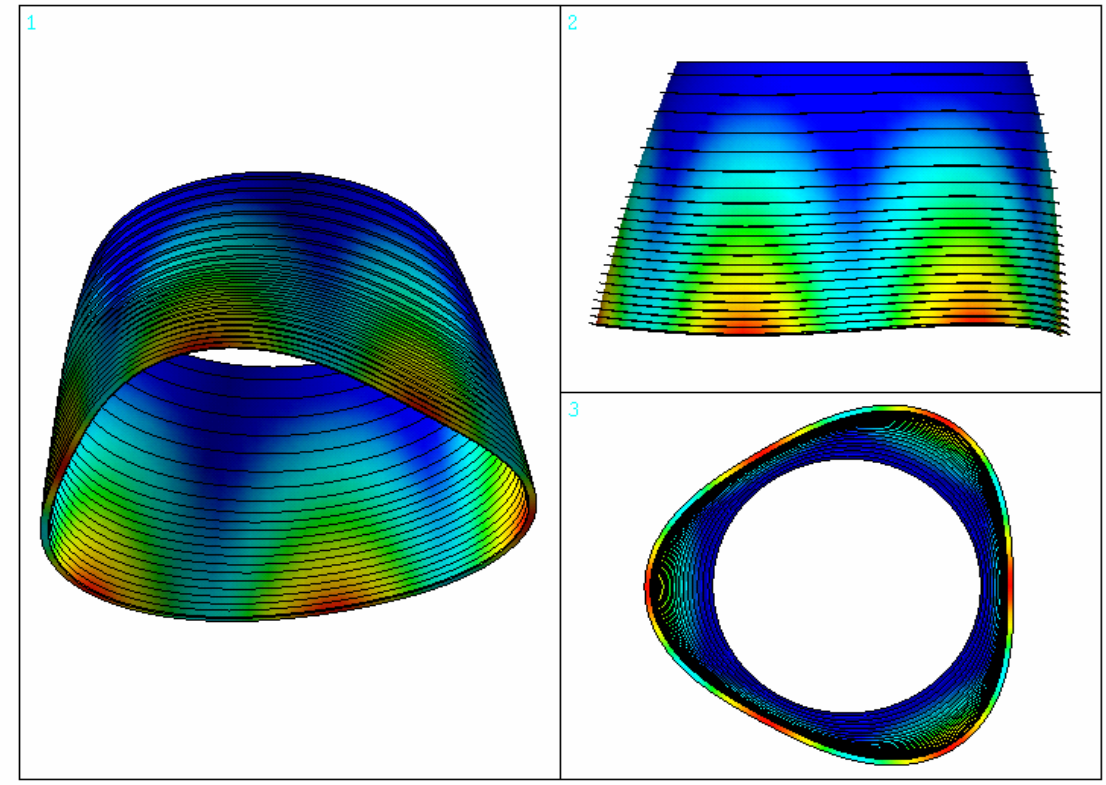

Figure A7.1 Vulcain 2 NE skirt mode shape, f = 71.5 Hz, m = 1, n = 3

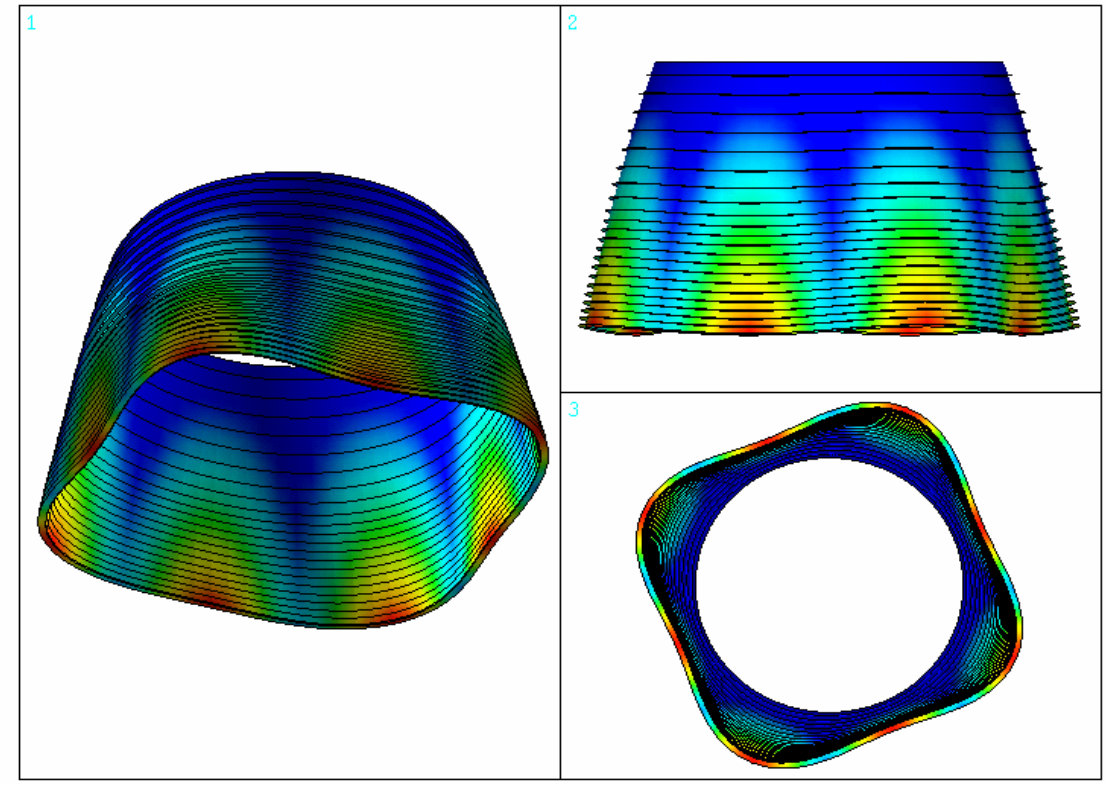

Figure A7.2 Vulcain 2 NE skirt mode shape, f = 103.2 Hz, m = 1, n = 4

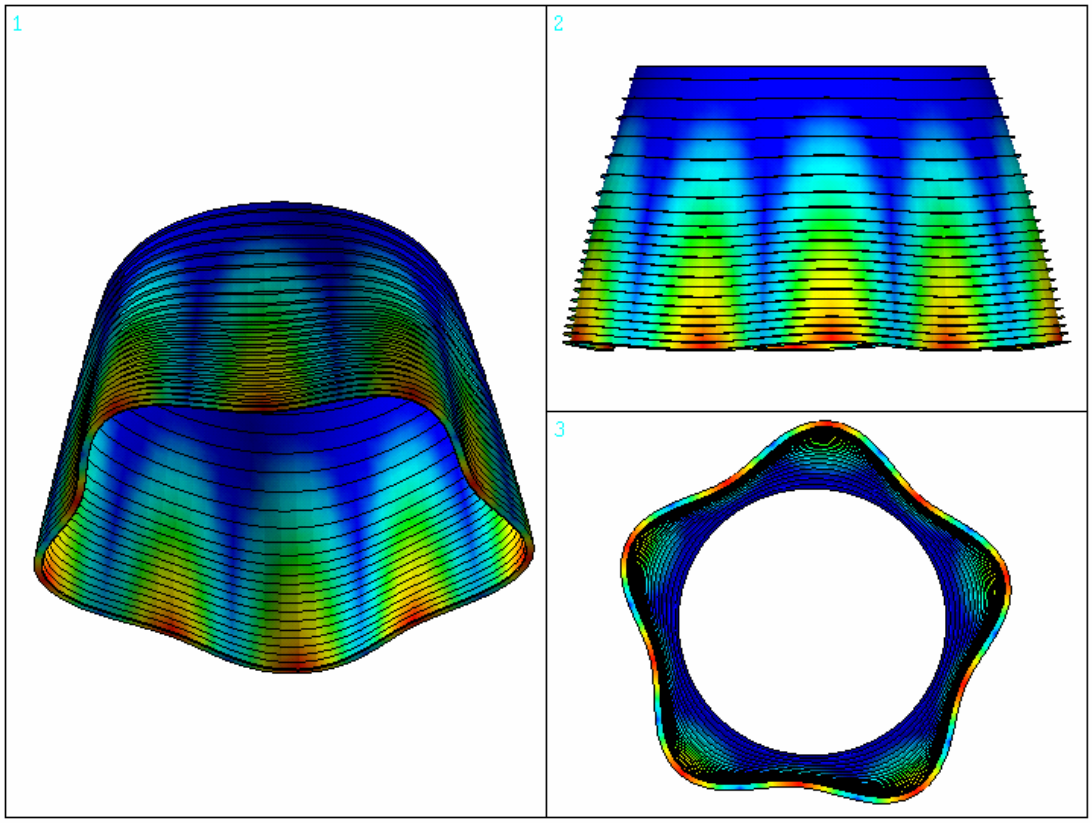

Figure A7.3 Vulcain 2 NE skirt mode shape, f = 161.0 Hz, m = 1, n = 5

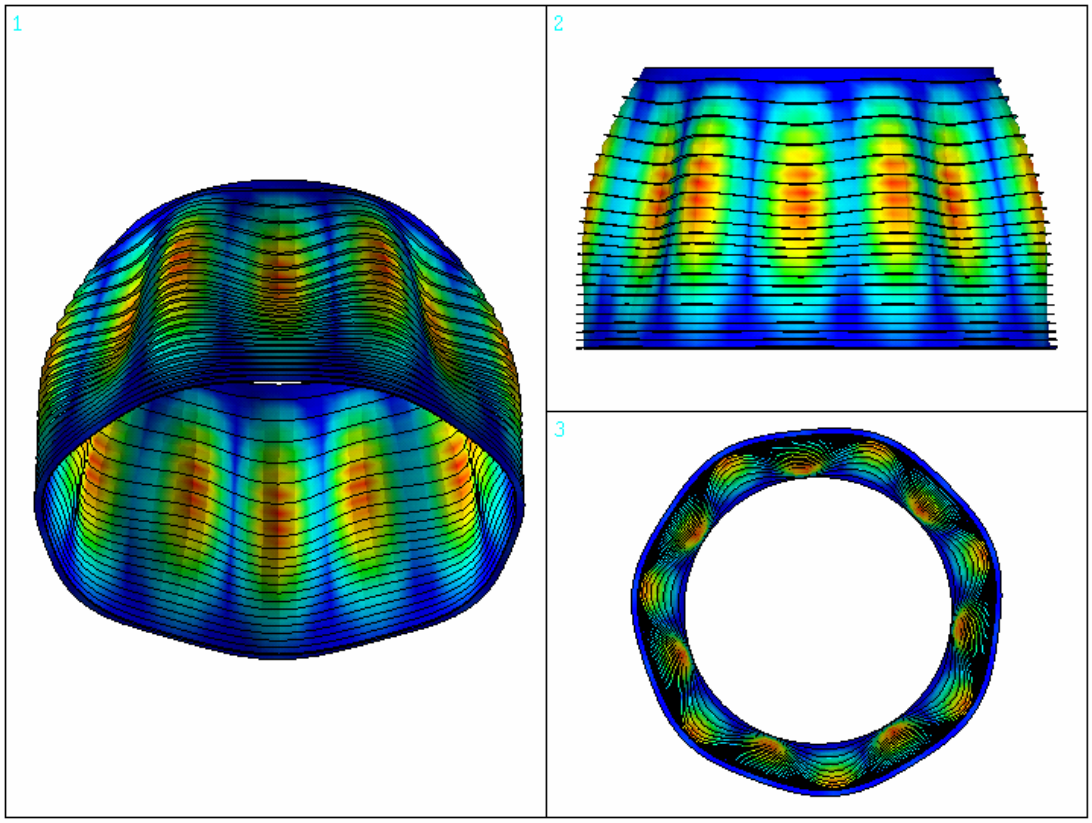

Figure A7.4 Vulcain 2 NE skirt mode shape, f = 288.7 Hz, m = 1, n = 7

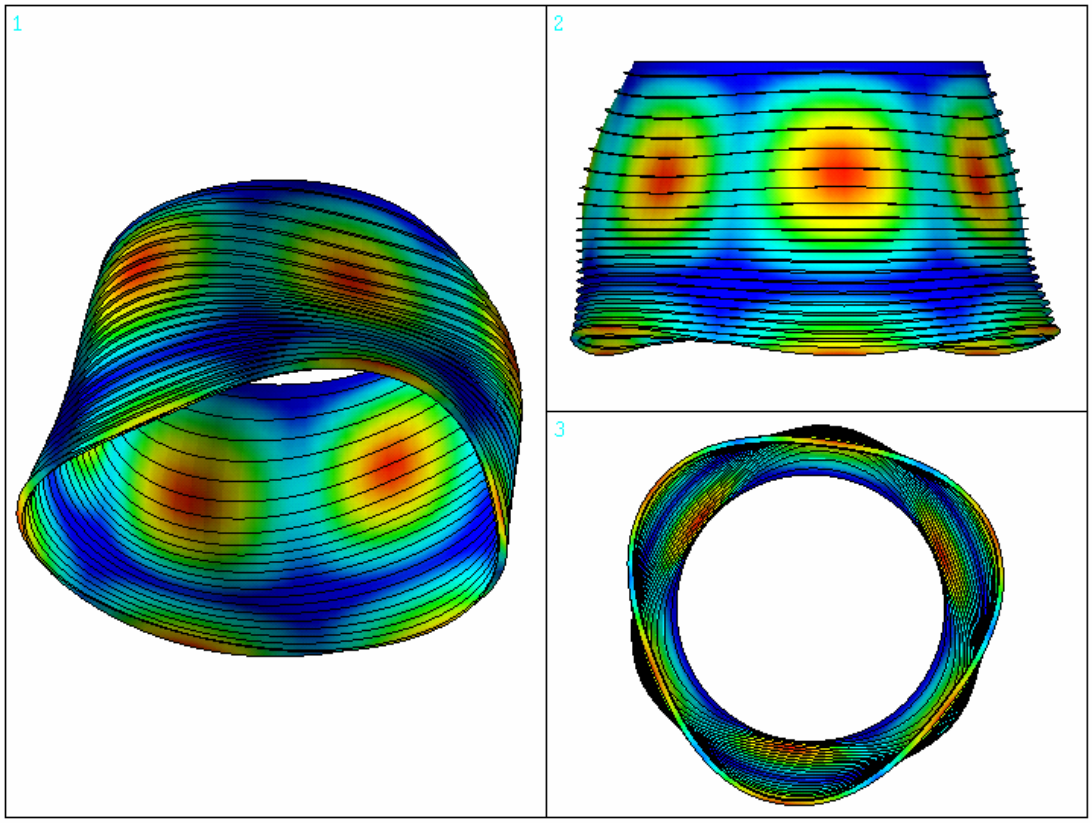

Figure A7.5 Vulcain 2 NE skirt mode shape, f = 355.4 Hz, m = 2, n = 3

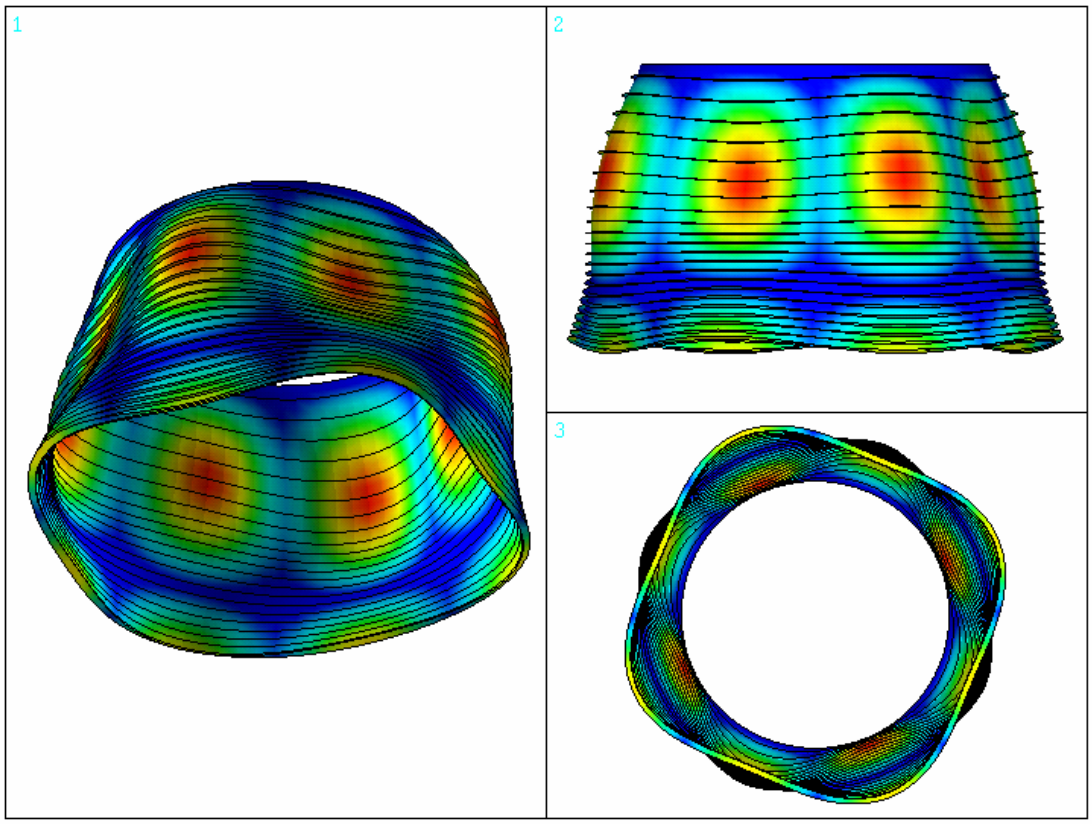

Figure A7.6 Vulcain 2 NE skirt mode shape, f = 292.8 Hz, m = 2, n = 4

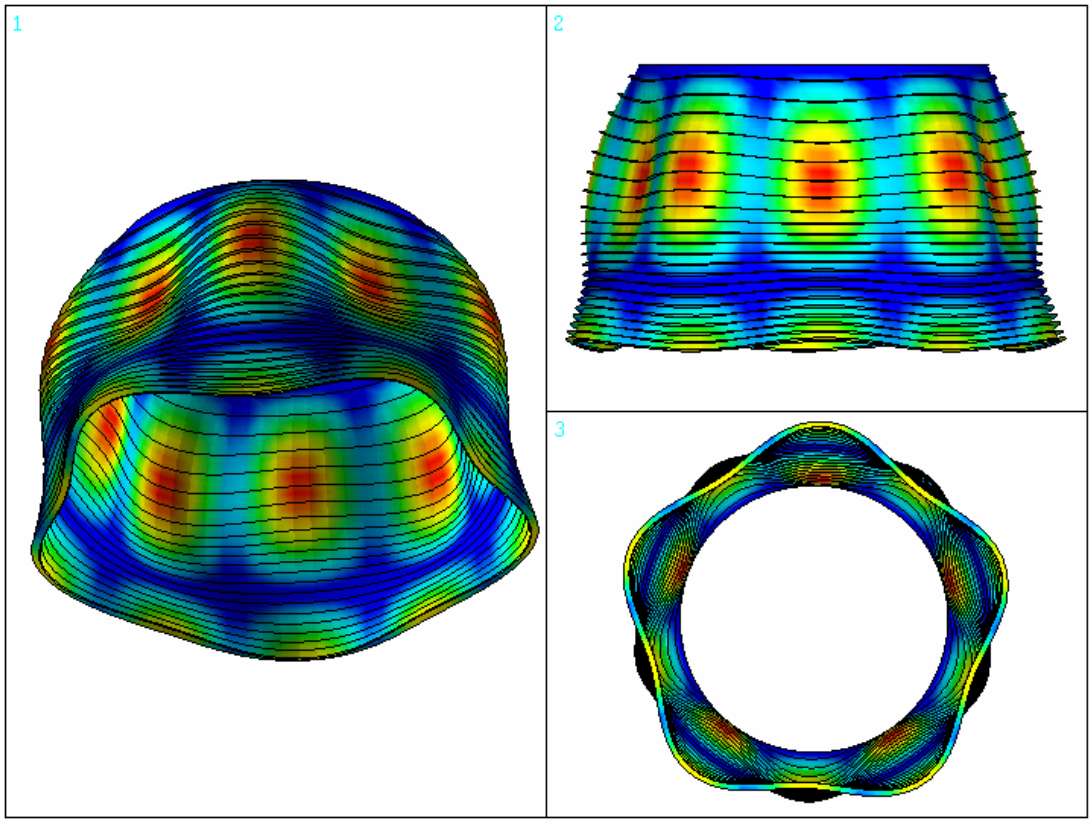

Figure A7.7 Vulcain 2 NE skirt mode shape, f = 268.8 Hz, m = 2, n = 5

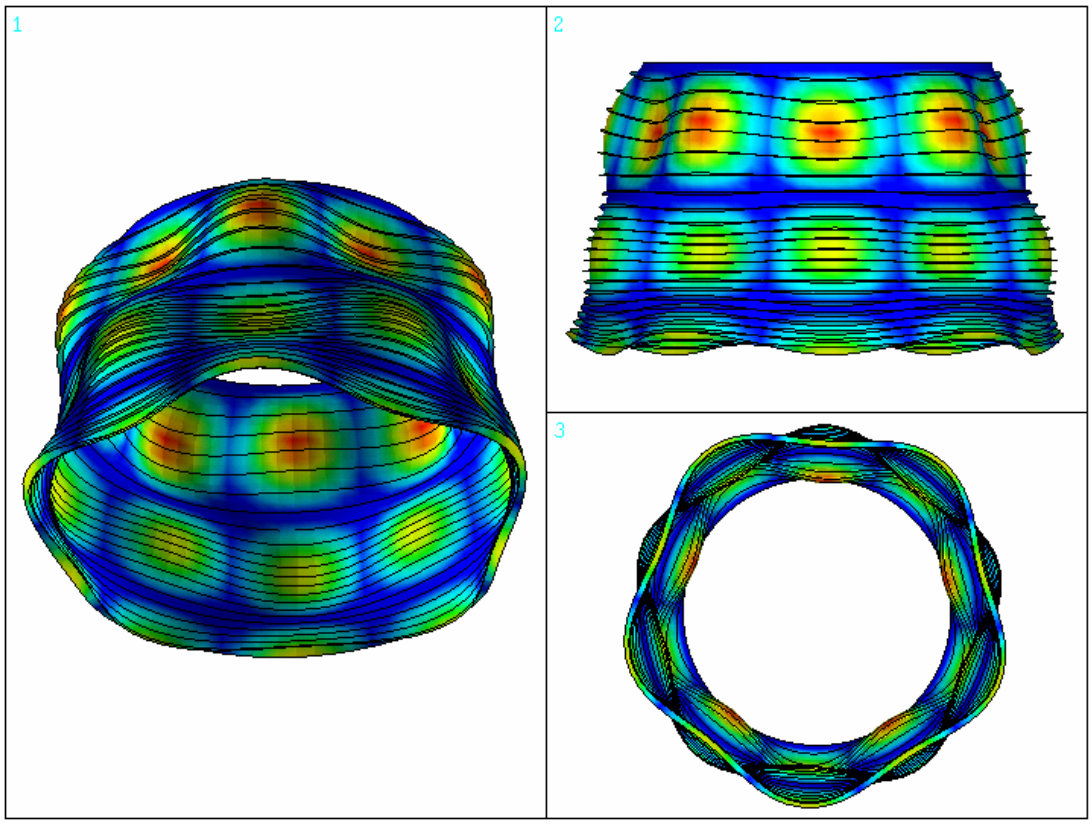

Figure A7.8 Vulcain 2 NE skirt mode shape, f = 428.8 Hz, m = 3, n = 5